

Complex equilibria in strongly alkaline aqueous solutions containing Ca(II), Al(III) and heptagluconate ions

Ph.D. Dissertation



Ákos Buckó

Supervisors: Prof. Pál Sipos
Prof. István Pálinkó

Doctoral School of Chemistry

Department of Inorganic and Analytical Chemistry,
Faculty of Science and Informatics, University of Szeged

Szeged

2021

Table of contents

Introduction	4
Literature review	6
The chemical equilibria of Bayer liquors and its concerns	6
Properties of hydroxycarboxylates in aqueous solutions.....	9
<i>Synthesis of sugar acids</i>	9
<i>The deprotonation of D-gluconate and D-heptagluconate in strongly alkaline medium</i>	10
The interactions of Ca ²⁺ ions with sugar-acids in strongly alkaline aqueous solutions	11
<i>Hydrolytic properties of Ca²⁺ ions</i>	11
<i>Complexation of Ca²⁺ by sugar-acids</i>	12
The complexes of Al ³⁺ ions with sugar-carboxylates	14
Aims of the thesis	16
Experimental Part	17
Reagents and solutions	17
Potentiometry.....	18
Polarimetry.....	20
Nuclear Magnetic Resonance (NMR) Spectroscopy	20
Freezing Point Depression (FPD).....	21
Electrospray Ionization Mass Spectrometry (ESI-MS).....	22
Data evaluation and speciation calculations.....	22
Characterization of the solid samples	22
<i>Synthesis and sample preparation</i>	22
<i>Methods of structural characterization</i>	23
Results and discussion	26
The acid-base properties of D-heptagluconate and D-gluconate.....	26
The calcium complexation properties of D-gluconate and D-heptagluconate ions in alkaline solutions	29
<i>Complexation of Ca²⁺ by gluconate ions in alkaline medium</i>	29
<i>Complexation of Ca²⁺ by heptagluconate ions in alkaline medium</i>	32

Complexation of Al^{3+} by heptagluconate ions in the pH range of 2 – 14	35
<i>The impact of Al^{3+} complexation on the potentiometric titrations and polarimetric data of heptagluconate.</i>	35
<i>Quantitative data analysis based on the potentiometric and polarimetric experiments</i>	36
<i>Model validation and the possible structure of the $\text{Al}_2(\text{OH})_6\text{Hpgl}^-$ complex.</i>	44
<i>NMR study on the structural aspects of the complexation reactions and the possible metal binding sites</i>	48
The structural and thermal analysis of the solid compounds forming in systems containing Ca^{2+} , Al^{3+} and Heptagluconate ions	56
<i>Crystallinity study of the prepared solids and reference compounds.</i>	56
<i>The morphology of precipitates: comparison of binary and ternary solids with the reference compounds.</i>	57
<i>Component quantification and stoichiometric calculation</i>	58
<i>The effect of metal coordination on the infrared and Raman spectra of sodium heptagluconate</i>	60
<i>Thermal analysis of the ternary complexes.</i>	66
Ca^{2+} – Al^{3+} – heptagluconate complexes in the pH range of 8 – 14: Preliminary insights into the solution equilibria and speciation	69
<i>The interpretation of the pH-potentiometric and polarimetric data</i>	69
<i>The effect of ternary complex formation on the ^1H and ^{13}C NMR spectra of heptagluconate.</i> 76	
Equilibria in solutions approaching industrial conditions: The temperature dependence of the calcium complexation properties of D-gluconate	79
<i>Determination of the ionic product of water at various temperatures – validation of the measuring system</i>	79
<i>The Ca^{2+} complexation of gluconate ions in strongly alkaline solutions on elevated temperatures.</i>	81
<i>Characterization of the solid phase forming at high temperature</i>	85
Conclusion	88
Összefoglalás	91
References	94
Acknowledgement	108

Introduction

The interactions between carbohydrate derivatives – such as sugar carboxylates – and metal ions has been extensively studied since the beginning of the last decade due to their numerous biological functions (*e.g.*, in calcium storage [1] and enzymatic reactions [2,3]) as well as widespread applications in different industrial processes. Sugar acids exhibit great affinity towards sequestering various metal ions, owing to the presence of their carboxylic and hydroxy moieties [4].

A renowned member of this group is D-gluconic acid (GlucH, *Figure 1*), which also exists in nature, for instance in fruits or honey. GlucH typically finds application in the food industry as leavening, flavoring or fat absorption reducing agent. Furthermore, the different salts of GlucH also play an important role in various industrial processes. The most widely used sodium-gluconate (NaGluc) has a remarkable affinity towards di- and trivalent metal ions, hence it is employed in bottle washing preparations for removing the accumulated scale from the glass surface. Besides, it is used as an iron sequestrant in the textile industry and as a derusting agent in metallurgy. Also, NaGluc is commonly used as a cement additive as set time retarder, thereby increasing the strength and water resistance of concrete [5]. The outstanding metal-chelating ability of this ligand is also utilized in the pharmaceutical field, mainly during chelation therapy for treating calcium or iron deficiency [6].

In general, owing to the relative abundance and metal-ion-binding ability of these sugar-type compounds, they have a potential impact on the efficiency of a number of industrial processes. For instance, small-molecular-weight organic substances are introduced to the Bayer process by most bauxites, where they are known to affect the solubility of $\text{Ca}(\text{OH})_2(\text{s})$, which is used for NaOH recovery (recausticization) [7,8]. In order to assess the role of these ligands in the solution speciation of various metal ions, a deep understanding of their solution equilibria is indispensable.

The solution chemistry of complex compounds consisting of hydroxy-carboxylates and Group II / Group III metals is well-described in the acidic-to-neutral pH range. In this region, the binding of metal ion typically takes place *via* the $-\text{COO}^-$ group, resulting in the formation of weak mononuclear complexes [9,10]. However, in strongly alkaline media, the deprotonation of (at least one) $-\text{OH}$ group and the simultaneous formation of an alcoholate – being a strong Lewis base – markedly enhances the stability of metal chelates. Furthermore, in alkaline

solutions containing polyhydroxy carboxylates, Ca^{2+} and another tri- or tetravalent metal ions, the formation of heteropolynuclear complexes ($\text{Ca}_p\text{M}_q\text{L}_r^{2p+3q-r}$, where L represents a ligand containing $-\text{OH}$ and $-\text{COO}^-$ groups) has been reported [11,12].

Regarding the Bayer process, apart from the accumulation of organic compounds, Gluc^- is also added intentionally to the spent liquor to drive the reaction towards the formation of CaCO_3 and inhibit the formation of the undesired tricalcium aluminate [8,13]. Even though some structural features of certain $\text{Ca}_p\text{Al}_q\text{L}_r^{2p+3q-r}$ forming under these conditions have been already known from the literature [14] the exact composition and equilibrium properties of these species have remained elusive.

To adequately describe the solution equilibria of such a ternary system, a detailed understanding of the corresponding binary sub-systems is inevitable. Furthermore, the reaction parameters (temperature, ionic strength) should be adjusted to the industrial conditions as close as possible. To this end, in the current work, the effect of both temperature and ionic strength on the speciation in strongly alkaline aqueous solutions containing Ca^{2+} and Gluc^- were studied. In addition, measurements were performed at 25 °C and 1 M ionic strength with the structurally related α -D-heptagluconate (Hpgl^- , *Figure 1*), and the results were compared with those reported earlier for Gluc^- (under the same conditions), which allowed us to assess the effect of the number and configuration of $-\text{OH}$ groups on the complexation of Ca^{2+} ions.

To explore the binding of Al^{3+} ions to polyhydroxy carboxylates, Hpgl^- was used again as complexing agent in a broad range of pH (2–14). Also, the results of the present work with those already existing for Gluc^- were compared. In the next step, based on the results obtained for the binary systems, the speciation of Hpgl^- in the presence of both Ca^{2+} and Al^{3+} ions was investigated in the same pH region. Finally, to gain a comprehensive view on the overall equilibrium including heterogeneous processes, the solid precipitates forming in the ternary and binary systems were also characterized.

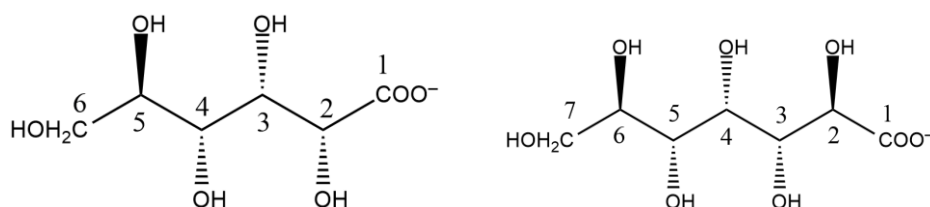


Figure 1 Structural formulae of D-gluconate (left) and D-heptagluconate (right)

Literature review

The chemical equilibria of Bayer liquors and their relevance

Aluminum is the third most abundant of all chemical elements (after oxygen and silicon) as well as the most abundant metal in the Earth's crust, making up more than 8% of its mass [15]. The reason of the substantial accumulation of this particular element in the lithosphere is aluminum's oxide-forming tendency, which bounds it to rocks (feldspars and micas), keeping it relatively close to the surface, while less reactive metals sink to the core [16]. Owing to its strong affinity towards oxygen, aluminum is almost never found in its elemental state, therefore it is the main constituent of a set of different aluminosilicates and aluminum oxides [17].

Despite the occurrence of aluminum in many different minerals, its economically viable sources are almost exclusively bauxite ores, which do not only contain high amounts of aluminum, but the relative ease of their mining also renders bauxite the most important source for alumina production. The importance of this raw material is indicated by the increasing global consumption of bauxite, which exceeded 200 million tons *per annum* in 2007 [18].

Although the known reserves of high-quality bauxite could be sufficient for the next 300 years (based on the average projected growth rate in aluminum use), there is an ever-growing need for the sustainable mining and refinement of this mineral. For instance, the aluminum content of new automobiles was increasing at a rate of 4% every year till 2003, averaging at 130 kg per vehicle. Furthermore, if one considers that typically 4 to 6 tons of bauxite are required to produce one ton of aluminum (which still counts as modest use of mineral resources, compared to other materials,) the growing number of attempts on the improvement of aluminum yield is evident [19].

Nowadays, the principal method of the large-scale alumina production is the renowned Bayer process, invented by Karl Josef Bayer in 1888 [20]. The first step of this process involves the recrystallization of the aluminum content of bauxite, by digesting it in extremely alkaline ($\text{pH} > 14$) aqueous solution of sodium hydroxide at high temperature and pressure ($T = 140\text{--}270\text{ }^\circ\text{C}$, $p < 35\text{ atm}$). Then, the different soluble aluminum-bearing hydroxido complexes are converted to crystalline gibbsite ($\text{Al}(\text{OH})_3(\text{s})$) in a reverse process, which is later calcined to yield alumina ($\text{Al}_2\text{O}_3(\text{s})$).

Although the process itself has been used for more than 120 years now, unexplainable artefacts still occur, partly due to our limited knowledge about Bayer liquors. Therefore, tremendous effort and resources have been put into the investigation of the composition,

structure and stability of the aluminate complexes present in Bayer liquors. However, during the investigation of these solutions one may encounter several obstacles. Apart from the widely known practical difficulties, such as the uncommonly high concentration and alkalinity of the solutions, the interpretation of the experimental data often proves to be challenging, owing to the large number of interrelated experimental parameters. Moreover, a number of macroscopic inhomogeneities as well as precipitates and crystal seeds are present in process liquors, which makes the adequate description of these systems even more difficult.

Besides the heterogeneous nature of the process liquor, most Bayer plants must deal with the control of organic substances, originating from the humic content of Bauxite. According to *Lever*, during the digestion process the humic matter degrades to various lower-molecular-weight compounds, such as benzene carboxylic acids, phenolic acids or aliphatics [21]. It has been shown that a substantial amount of these organic compounds in Bayer liquors can bring about a set of serious process problems, including lower alumina yield, decrement of $\text{Al(OH)}_3(\text{s})$ particle size, lower red mud settling rate or the loss of caustic. These unfavorable impacts prompted scientists to put tremendous effort [21–25] in the in-process identification of these materials, however apart from a few early initiatives [11], the literature on their behavior in solution is sporadic.

For the digestion to be as efficient as possible, the causticity of the process liquor must be maximized. Therefore, lime (slaked lime, Ca(OH)_2) is added to the spent liquor to convert the *in situ* formed sodium carbonate back to sodium hydroxide by the formation of insoluble calcium carbonate. This step is an essential and integral part of most Bayer refineries for their cost-effective operation; hence, lime is one of the primary raw materials for alumina production. Despite the crucial role that calcium plays in an alumina refinery, relatively few in-depth studies have been published on this topic in the literature, albeit at the end of the last century the chemistry of lime in the Bayer process has drawn substantial attention [26–28].

Another scientifically interesting aspect of the chemistry of calcium in Bayer liquors is the formation of different solid phases with aluminate ions and their interconversions [29–32]. According to a recent review by *Rosenberg et al.*, the most stable solid calcium containing compound forming in aluminate solutions is tricalcium aluminate hexahydrate (TCA, $\text{Ca}_3\text{Al}_2\text{O}_6 \cdot 6\text{H}_2\text{O}$), which is formed by the direct reaction of CaO or Ca(OH)_2 with NaAl(OH)_4 [8]. On the one hand, the formation of this precipitate is given its negative impact on the alumina yield, however the presence of TCA may have its advantages, too: the particle size of TCA could be conveniently modified through the adjustment of each component's concentration, which is an important property of filtering agents [33]. Furthermore, TCA can readily bind

silicon through the formation of hydrogarnets ($\text{Ca}_3\text{Al}_2(\text{SiO}_4)_{3-x}(\text{OH})_{4x}$), rendering TCA an excellent silicon-removing agent [33–35].

As reported by *Rosenberg* [8], apart from the formation of TCA, two metastable compounds, the $[\text{Ca}_2\text{Al}(\text{OH})_6]_2 \cdot 1/2\text{CO}_3 \cdot \text{OH} \cdot n\text{H}_2\text{O}$ and the $[\text{Ca}_2\text{Al}(\text{OH})_6]_2 \cdot \text{CO}_3 \cdot n\text{H}_2\text{O}$ layered double hydroxides (LDHs) are also discernible in most Bayer liquors. The formation of LDHs is a critical reaction step in the recausticization of the liquor. Although these intermediate processes first result in a decrease in the concentration of both carbonate and aluminate ions, the latter is recovered due to the decomposition of LDHs above 80°C , yielding calcium carbonate and soluble aluminate [8,36].

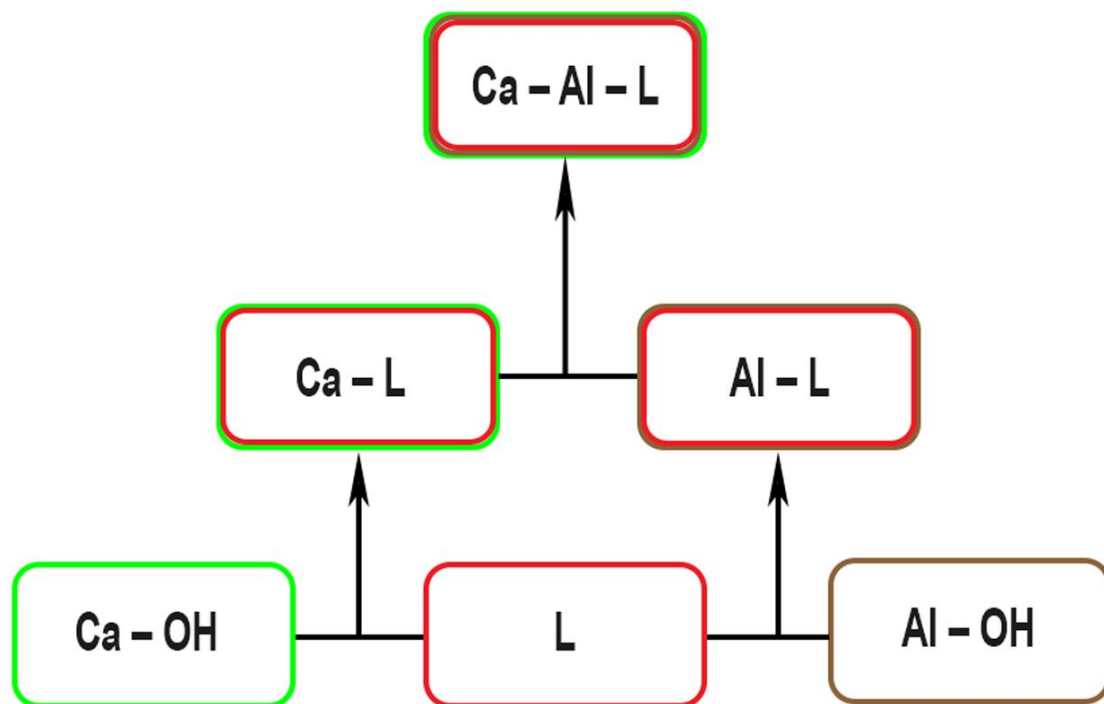


Figure 2 The roadmap for description of chemical equilibria in the $\text{Ca}^{2+} / \text{Al}^{3+} / \text{L}^-$ system. The bottom row refers to the hydrolysis of Ca^{2+} and Al^{3+} , as well as to the acid-base properties of L^- ($=\text{Gluc}^-$ or Hpgl^-), while the second row stands for the corresponding binary systems. The charges are omitted for better representability.

Despite the challenges mentioned above, with due effort and systematic thinking even a complicated equilibrium system, *i.e.*, a highly caustic aluminate solution containing Ca^{2+} ions and low-molecular-weight organics (*Figure 2*), can be appropriately characterized. Besides the mindful planning of instrumentation and experiments, the system needs to be simplified to its most fundamental building blocks, which in turn could be gradually expanded towards more complicated fractions after sound description.

During my work in the *Material and Solution Structure Research Group* we have embarked on the comprehensive characterization of a so-called “synthetic” Bayer liquor, consisting of Ca^{2+} , Al^{3+} , Hpgl^- and OH^- ions, where calcium and heptagluconate ions are to represent the additives and organics present in “real” process liquors. Therefore, in the following pages the literature data for the corresponding subsystems will be reviewed.

Properties of hydroxycarboxylates in aqueous solutions

Synthesis of sugar acids

D-glucose – and aldohexoses in general – can be readily oxidized using only mild oxidizing agents, such as hypobromite or dilute nitric acid, yielding D-gluconic acid (GlucH) [37,38]. Considering that the oxidation step takes place on the pyranose form of glucose, the primary products will be the lactone forms of the corresponding gluconic acid, which are in turn in equilibrium with the open-chain form (see *Figure 3*) [39].

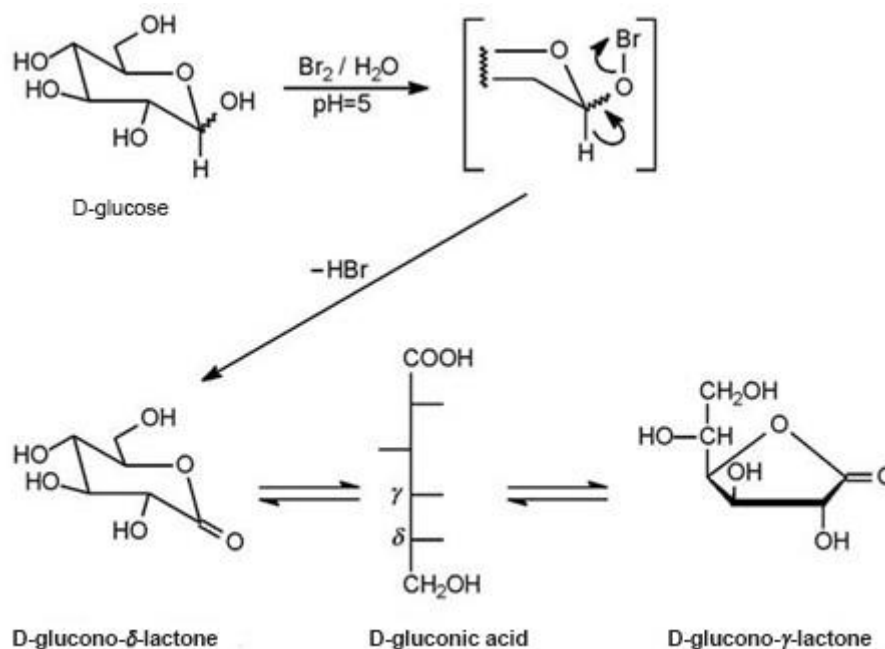


Figure 3 The mild oxidation of D-glucose and its products. In acidic medium, polyhydroxy carboxylates are usually converted to intramolecular five- (γ) or six-membered (δ) cyclic esters, *i.e.*, lactones [39].

Apart from the above chemical route, GlucH can be produced by many different approaches, such as electrochemical [40–43], ultrasound-assisted methods [44–46] or catalytic reactions employing catalysts such as Pt, Rh [43,47–49] and Au/C [50]. However, these methods appear to be less cost-efficient upon comparison with fermentation processes. Therefore, gluconic acid manufacturing predominantly takes place through microbial fermentation [51–57].

To produce sugars that are difficult or impossible to obtain from natural sources, the Kiliani–Fischer synthesis is the most convenient way to elongate their chains to the desired length (see *Figure 4*). It proceeds *via* the synthesis and hydrolysis of a cyanohydrin, thus lengthening the chain of an aldose by one carbon atom, while preserving the configuration of the other chiral carbon atoms. As for the newly inserted carbon, both configurations are generated at the same amount yielding a racemic mixture of the two epimers. This way, one can access any stereoisomer of any chain-length aldose by an appropriate number of iterations of the Kiliani–Fischer synthesis. Nevertheless, while it provides access to every aldose, the process is limited by its own yield, which drops roughly exponentially with each additional iteration [58,59].

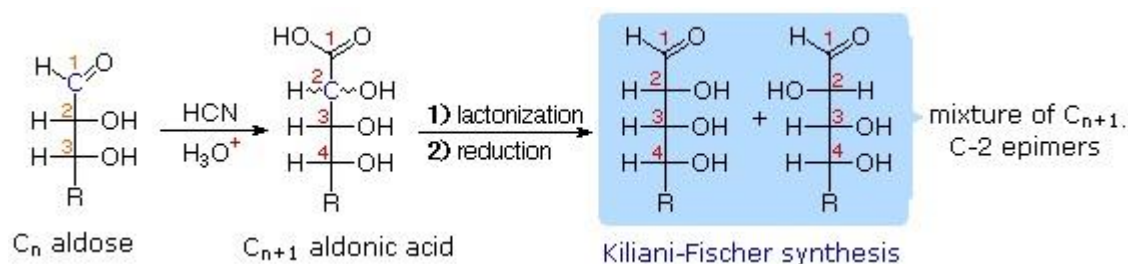


Figure 4 The scheme of the Kiliani–Fischer synthesis performed on aldoses with arbitrary chain-length. The desired stereochemistry and chain-length could be attained by the consecutive iterations of the synthesis [59].

The deprotonation of D-gluconate and D-heptagluconate in strongly alkaline medium

Generally, alcohols are considered weak acids, since the values of pK_a for their acid dissociation reactions range from 16 or 19 (slightly weaker than water, $pK_a = 14$). For instance, $pK_a = 15.5$ for methanol and $pK_a = 16.0$ for ethanol, respectively [60]. Polyhydroxy carboxylates are expected to be stronger acids (*i.e.*, they have lower pK_a) due to statistical reasons: the presence of additional -OH functions increases the probability of proton displacement [61]. The acid dissociation constant for these ligands reads as:



$$K_a = K_p^{-1} = \frac{[LH_{-1}^{2-}][H_3O^+]}{[L^-] \cdot c}, \quad (2)$$

where $L^- = \text{Gluc}^-$ or Hpgl^- , K_p is the protonation constant of LH_{-1}^{2-} and c is the standard molar concentration (1 M).

Owing to the experimental complications caused by the strongly alkaline medium, the main tools for determining the pK_a are pH-potentiometry using glass or H_2/Pt electrodes or NMR spectroscopy. According to an early paper by *Roos and Williams*, the acid dissociation constant of Gluc^- was found to be unrealistically low, $pK_a = 11.18$ (at $t = 37^\circ\text{C}$ and $I = 0.15 \text{ M NaClO}_4$ employing GLE) [62]. Later, a value of $pK_a = 13 \pm 1$ (at $t = 22^\circ\text{C}$ and $I = 0.1 \text{ M NaClO}_4$) was

proposed by *Zhang et al.* based on ^{13}C NMR measurements [63]. More accurate values were obtained for the pH measurement in alkaline solutions by adopting H_2/Pt electrode, which is known to have better performance in such ambience: *Pallagi et al.* obtained $\text{pK}_a = 13.68 \pm 0.03$ for the deprotonation of Gluc^- at $t = 25^\circ\text{C}$ and $I = 1 \text{ M NaCl}$ [64], whereas *Coccioli and Vicedomini* found this value to be $\text{pK}_a = 13.66 \pm 0.24$ at $I = 1 \text{ M NaClO}_4$. Furthermore, they proposed, that GlucH_1^{2-} can also undergo a deprotonation to form GlucH_2^{3-} ; the corresponding pK_a was found to be 14.02 ± 0.3 [65]. The value of 13.92 ± 0.06 was obtained recently by *Kutus et al.* under similar experimental conditions ($t = 25^\circ\text{C}$ and $I = 4 \text{ M NaCl}$), which is in excellent agreement with the previous values, with due consideration on the different ionic strength.

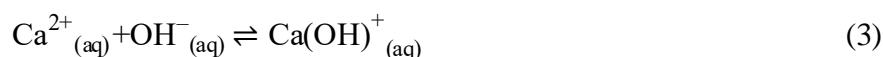
Regarding the structurally similar D-heptagluconate (Hpgl^-), which contains an additional $-\text{CH}_2\text{-OH}$ moiety, the pK_a was reported to be 13.41 ± 0.02 ($t = 25^\circ\text{C}$, $I = 1 \text{ M NaCl}$), determined by pH potentiometric measurements applying H_2/Pt electrode [66]. Its increased acidity may be explained by the statistical effects owing to the additional $-\text{OH}$ functional groups [61].

The interactions of Ca^{2+} ions with sugar acids in strongly alkaline aqueous solutions

Hydrolytic properties of Ca^{2+} ions

The hydrolytic reactions of calcium(II), given the important role of lime in various industrial processes, have been a subject of several studies since the 19th century both on theoretical and experimental basis [67–71]. Besides its central role in the concrete research, hydrometallurgy or scale formation, the hydrolysis of calcium(II) is of paramount significance in the Bayer process, upon carbonate removal [8,72]. Despite the effort made to elucidate these equilibria, the speciation of $\text{Ca}(\text{II})$ in these strongly caustic solutions is still not completely understood. The difficulty of such studies stems from the behavior of calcium in aqueous solutions: calcium, as any other alkaline earth metal ions, only exists as a divalent cation in aqueous solutions. With the increasing atomic number, the size of the alkaline earth cations also increases, which in turn decreases their effective charge and causes the O-H bonds of the coordinated water molecules to be less acidic. Since the calcium ion is significantly bigger, than the magnesium ion, it does not hydrolyze until $\text{pH} \approx 13$, which makes the employment of the conventional glass electrodes problematic [73–75].

According to Kolthoff, the existence of $\text{Ca}(\text{OH})^+$ species was necessary to assume in addition to the aqua-ion, in order to explain the results of the potentiometric measurements [69]. As for the monohydroxido complex, its formation is described in the following reaction:

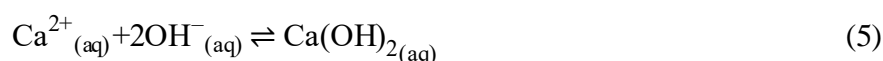


Where the corresponding equilibrium constant is

$$K_{\text{Ca}(\text{OH})^{+}_{(\text{aq})}} = \frac{[\text{Ca}(\text{OH})^{+}_{(\text{aq})}] \cdot c}{[\text{Ca}^{2+}_{(\text{aq})}] [\text{OH}^{-}_{(\text{aq})}]} \quad (4)$$

Using these equations, Kolthoff obtained the value $\log K_{\text{Ca}(\text{OH})^{+}_{(\text{aq})}} = 0.87$ in his work. Later, a plethora of studies attempted to determine the formation constant at $I = 0 \text{ M}$ and $t = 25 \text{ }^{\circ}\text{C}$. Based on potentiometric [76,77], kinetic [78,79] or solubility measurements [80–83], the value of $\log K_{\text{Ca}(\text{OH})^{+}_{(\text{aq})}}$ ranges from 1.0 to 1.6. Furthermore, studies dealing with the determination of $\log K_{\text{Ca}(\text{OH})^{+}_{(\text{aq})}}$ at different ionic strengths and temperatures as well as other works invoking $\text{Ca}(\text{OH})^{+}_{(\text{aq})}$ to interpret various speciation models [64,66,84–90] cemented the existence of this hitherto debated species.

Besides the monohydroxido complex, the existence of the dissolved $\text{Ca}(\text{OH})_{2(\text{aq})}$ has also been proposed in several studies [91,92]. The underlying reaction and equilibrium constant of its formation read as:



$$K_{\text{Ca}(\text{OH})_{2(\text{aq})}} = \frac{[\text{Ca}(\text{OH})_{2(\text{aq})}] \cdot c}{[\text{Ca}(\text{OH})^{+}_{(\text{aq})}] [\text{OH}^{-}_{(\text{aq})}]^2} \quad (6)$$

$$\beta_{\text{Ca}(\text{OH})_{2(\text{aq})}} = \frac{[\text{Ca}(\text{OH})_{2(\text{aq})}] \cdot c^2}{[\text{Ca}^{2+}_{(\text{aq})}] [\text{OH}^{-}_{(\text{aq})}]^2} \quad (7)$$

In several instances, solubility data were also explained through the formation of $\text{Ca}(\text{OH})_{2(\text{aq})}$ in strongly alkaline solutions [86,93,94]. Recently, *Kutus et al.* published a comprehensive study on the formation of the dissolved $\text{Ca}(\text{OH})_{2(\text{aq})}$ in strongly alkaline media. According to their findings, $\text{Ca}(\text{OH})_{2(\text{aq})}$ forms more readily than $\text{Ca}(\text{OH})^{+}_{(\text{aq})}$ in the $\text{pH} > 13$ region, with the former being almost exclusively present in solution at high pH. The authors have also determined the solubility product of the solid $\text{Ca}(\text{OH})_{2(\text{s})}$ as well as the formation constants of the $\text{Ca}(\text{OH})^{+}_{(\text{aq})}$ and $\text{Ca}(\text{OH})_{2(\text{aq})}$ species, to be $K_{\text{sp}} = (8.8 \pm 0.2) \times 10^{-5} \text{ M}^3$, $K_{\text{Ca}(\text{OH})^{+}_{(\text{aq})}} = (1.5 \pm 0.1) \text{ M}^{-1}$ and $\beta_{\text{Ca}(\text{OH})_{2(\text{aq})}} = (4.7 \pm 0.1) \text{ M}^{-2}$, respectively, at $t = 25 \text{ }^{\circ}\text{C}$ and $I = 1 \text{ M}$ (NaCl), expressed in terms of concentration [95].

Complexation of Ca^{2+} by polyhydroxy carboxylates

Generally, sugar-type ligands containing only hydroxyl- or formyl groups form weak complexes with alkaline earth metals, due to the low electron density on the oxygen donor

groups. Consequently, they can hardly displace the strongly-bound water molecules from the first coordination sphere of the metal ions [96].

On the other hand, if one (or more) of the alcoholic groups is deprotonated, the forming alcoholate has a much higher affinity towards binding bi- and trivalent metal ions, owing to its increased basicity. In turn, the metal ion is a strong competitor of H^+ for the alcoholate moiety, which facilitates the deprotonation of the $-OH$ group. In other words, the apparent pK_a of the ligand in its metal-bound form is lower than the pK_a of the free ligands, known as metal-ion-induced deprotonation. If another coordinating group is already present in the ligand, *i.e.*, a carboxylate moiety, if highly stable chelate structures may be formed upon metal-ion binding, which further promote complex formation [97].

The outstanding complexing potential of sugar acids in alkaline aqueous solutions could be easily demonstrated by a simple test-tube experiment: in a solution containing approximately 0.1 M Ca^{2+} ions at $pH \approx 13$, the extensive precipitation of portlandite ($Ca(OH)_2(s)$) is observed. Introducing NaGluc in excess to this suspension, the rapid dissolution of the precipitate occurs, which clearly indicates interaction between the sugar carboxylate and the metal ions.

In an early work of *Mehltretter et al.*, this interaction has already been unfolded, as the authors found that the calcium sequestering capability of Hp gl^- and Gluc $^-$ -containing solutions greatly improved with the increasing pH [98].

Later, a generalized ionization scheme for polyhydroxy carboxylates was proposed by *van Duin et al.*, in order to explain the enhanced complexing ability of this type of ligands. Accordingly, the complexation starts with the deprotonation of the COOH group, which is followed by the subsequent proton displacement of the neighboring α -OH group. Ultimately, the dissociation of another OH group leads to the coordination of metal ion through the forming diolate moiety [99]. Alcoholate – metal ion interactions, being stronger than the ones with hydroxy groups, therefore yield complexes with higher stability.

Concerning the existence of multinuclear complexes of calcium ions with Gluc $^-$, *Sipes* in his PhD thesis proposed the formation of such species with 2:1 metal-ligand stoichiometry [100].

The composition and stability of polynuclear complexes of calcium(II) with various polyhydroxy carboxylates was scrutinized by *Pallagi et al.* Their results, obtained from pH potentiometric measurements, indicated not only the presence of mononuclear calcium complexes but also the simultaneous formation of polynuclear calcium complexes along with the deprotonated Gluc $^-$ and Hp gl^- molecules [64,66]. According to their chemical model for the $Ca^{2+} / Gluc^-$ and $Ca^{2+} / Hpgl^-$ systems, the formation of $CaGluc^+ / CaHpgl^+$, $CaGlucH_{-1}^0 /$

CaHpglH_{-1}^0 , $\text{Ca}_2\text{GlucH}_{-3}^0$ and $\text{Ca}_3\text{Gluc}_2\text{H}_{-4}^0/\text{Ca}_3\text{Hpgl}_2\text{H}_{-4}^0$ species could be observed (in addition to the $\text{Ca}(\text{OH})^+$ complex). The existence of these bi- or trinuclear complexes was supported by EXAFS and ESI-MS measurements as well.

Recently, the equilibria, structure and composition of calcium(II)- gluconate complexes forming in alkaline solutions was summarized by *Kutus et al.* In their review, the following conclusion was drawn: in strongly alkaline aqueous solutions, Ca^{2+} ions tend to form polynuclear species with gluconate and its structurally related peers. These compounds are mainly bi- or trinuclear complexes of surprisingly high stability, and mostly charge-neutral. In these species, the Ca^{2+} ions are simultaneously coordinated by the $\text{COO}^-/\text{C}(2)\text{-O}^-$ and $\text{COO}^-/\text{C}(3)\text{-O}^-$ moieties of Gluc^- , forming Ca-L-Ca-L-Ca chains. They also proposed that the $\text{COO}^-/\text{C}(2)\text{-O}^-$ binding motif seems to be common for the related sugar-carboxylates, while the participation of the $\text{COO}^-/\text{C}(3)\text{-O}^-$ or the $\text{COO}^-/\text{C}(4)\text{-O}^-$ depends on the configuration of the ligand [101].

The hydrolysis of Al^{3+} ions and their complexation by gluconate

Although the thermodynamic properties of the mineral alumina phases are well-described, some controversies still remained regarding the behavior of aqueous aluminum species. This stems from the relatively high charge and small radius of the metal ion, which causes it to hydrolyze and form complexes readily [102].

Aluminum can exist in a large variety of oxide-hydroxide minerals, such as corundum (Al_2O_3 (s)), diaspore ($\alpha\text{-AlO}(\text{OH})$ (s)), boehmite ($\gamma\text{-AlO}(\text{OH})$ (s)) or gibbsite ($\text{Al}(\text{OH})_3$ (s)), which are relevant in the production of alumina, primarily in the strongly alkaline medium. Gibbsite is known to precipitate from oversaturated aluminum containing solutions already at room temperature and it transforms into boehmite at elevated temperature [102–105].

The solubility of various oxide and hydroxide phases is fundamentally important in the high-temperature production of alumina, where the formation of different hydrolysis species can be observed. Among these hydrolysis products forming at high pH, $\text{Al}(\text{OH})_4^-$ is the predominant one, although other hydrolyzed monomeric species, such as $\text{Al}(\text{OH})^{2+}$, $\text{Al}(\text{OH})_2^+$ and $\text{Al}(\text{OH})_3^0$ (aq) are also known to occur. Furthermore, in concentrated aluminum solutions, particularly relevant in various industrial processes, (such as the Bayer process), even polymeric aluminum hydroxides have been identified, e.g. $\text{Al}_2(\text{OH})_2^{4+}$, $\text{Al}_3(\text{OH})_4^{5+}$ or the $\text{Al}_{13}(\text{OH})_{32}^{7+}$ (more precisely $\text{Al}_{13}\text{O}_4(\text{OH})_{24}^{7+}$) species [106].

In his recent review, *Sipos* summarized the qualitative and quantitative description of the speciation of concentrated alkaline aluminate solutions at temperatures up to 100 °C [107]. Besides of the mononuclear aluminate species, such as the well-established Al(OH)_4^- [108–112], the pentacoordinated Al(OH)_5^{2-} [113–115] or the Al(OH)_6^{3-} [116,117], the formation of the oxo-bridged dimeric aluminate species, $(\text{OH})_3\text{Al-O-Al(OH)}_3^{2-}$ [111,118,119] and the existence of various polymeric ones [120–122] were also discussed. The paper concluded that in alkaline aluminate solutions, prevailing under industrial conditions, the predominant aqueous aluminum-bearing species is the pseudo-tetrahedral Al(OH)_4^- ion, which can form stable NaAl(OH)_4^0 ion-pairs, which (depending on the conditions) could be solvent-separated or contact.

In order to assess the chemical composition of real Bayer liquors, the effect of organic contaminants and additives needs to be understood first. Even though there are some initiatives to clarify the equilibria of these systems, the available literature is rather scarce.

The complex equilibria of the $\text{Al}^{3+} / \text{Gluc}^-$ system was extensively studied in the pH range of 2 to 10. In an early publication *Motekaitis and Martell* proposed the formation of three mononuclear species: AlGluc^{2+} , Al(OH)Gluc^+ and $\text{Al(OH)}_3\text{Gluc}^-$. They assumed a “2,4,6” coordination scheme, where the ionized hydroxyl oxygens (located on the C2, C4 and C6 carbon atoms) point towards the aluminum ion, concluding that the existence of 2:1 is sterically possible [123].

Escandar et al. assessed the speciation *via* including the Al(OH)Gluc^+ and $\text{Al(OH)}_3\text{Gluc}^-$ particles only, however based on the NMR data measured for the aluminum(III) – lactobionic acid systems, they supposed the formation of the $\text{Al(OH)}_4\text{Gluc}^{2-}$ in alkaline medium [124].

Lakatos et al. unveiled the existence of several new complexes from pH = 2–10, such as AlGluc^{2+} , Al(OH)Gluc^+ , $\text{Al(OH)}_2\text{Gluc}^0$, $\text{Al(OH)}_3\text{Gluc}^-$, Al(OH)Gluc_2^0 and $\text{Al(OH)}_2\text{Gluc}_2^-$. Besides, they recognized the role of alcoholate groups during metal chelation and proposed a tridentate $\text{COO}^-/\text{O}^-/\text{O}^-$ coordination mode in the bis-complexes. As for the formation of the deprotonated species, they assumed that the binding of Al^{3+} by the carboxylate group is accompanied by a metal-ion-induced deprotonation of one or two α -OH moieties. According to the data acquired for other hydroxy carboxylates, they proposed that the third deprotonation occurs on one of the coordinated water molecules of Al^{3+} [125].

The formation of the $\text{Al(OH)}_4\text{Gluc}^-$ complex has been reported by *Pallagi et al.* The species is formed in strongly alkaline medium, in a pH-independent process *via* the condensation of

Al(OH)_4^- ion with one or two alcoholic $-\text{OH}$ groups of the ligand. The geometry of the forming complex is tetrahedral, similarly to the bare anion [126].

Aims of the thesis

It has been shown that the presence of organic impurities in Bayer liquors could significantly alter the composition of the process liquor and thereby give rise to numerous process problems, such as lower alumina yield, lower red mud settling rate or even the loss of caustic due to the ion-pairing of organic compounds with sodium. On the other hand, these low-molecular-weight organic compounds play a pivotal role during the regeneration of the spent liquor by inhibiting the formation of undesired Ca-Al by-products through complexation.

As a result of extensive studies conducted on the solution equilibria of sugar-type ligands with Group II/Group III metals, the interactions of Hpgl^- (or Gluc^-) with Ca^{2+} or Al^{3+} ions are largely understood in the pH range of 2 to 11. However, when it comes to the literature of these interactions in hyperalkaline medium ($\text{pH} > 12$), only limited resources are at our disposal. Even less information is available regarding the heteropolynuclear complex formation of these ligands with both Ca^{2+} and Al^{3+} ions as well as the speciation at elevated temperature and ionic strength, which is essential to the cost-effective process design.

Therefore, our main goals in the present work were as follows:

- to compare the acid-base and calcium complexation properties of Hpgl^- with those of Gluc^- by determining the stability constants of their complexes.
- to calculate the stability and composition of aluminate complexes, forming with Hpgl^- in the pH range of 2 to 14.
- to identify the Al^{3+} binding sites of Hpgl^- from acidic to strongly alkaline media to gain insights into the structural features of the forming complexes.
- to investigate the complexation of Ca^{2+} and Al^{3+} ions with Hpgl^- in the pH range of 2 to 14 as well as to characterize the corresponding binary and ternary solid compounds.
- to assess the impact of elevated temperature and ionic strength on the speciation using the $\text{Ca}^{2+} / \text{Gluc}^-$ model system; to calculate the corresponding thermodynamic constants.

Experimental Part

Reagents and solutions

All the materials mentioned throughout this work were used without further purification. The solutions were prepared using deionized water (Merck Millipore Milli-Q®) and the ionic strength (I) was adjusted to 4 M with NaCl (VWR, a. r. grade). Applying such high background electrolyte concentrations was necessary to reduce the effects originating from the variation of the activity coefficients of the solution species and to simulate the reaction conditions prevailing during the Bayer-process.

Sodium α -D-heptagluconate (Sigma-Aldrich, $\geq 99\%$ purity) was purchased as hydrated salt. The water content was determined by weighing the solid before and after heating it at 80 °C for six hours. Additionally, the purity of Hpgl⁻ sodium salt was checked by recording its ¹H and ¹³C NMR spectra. No signals of contaminants which peak area was greater than 1% of the total peak area were found. Sodium D-gluconate (Gluc⁻, Sigma-Aldrich, $\geq 99\%$ purity) was used as received.

1 M NaOH stock solutions were made by gravimetric dilution of a 50 w/w% carbonate-free NaOH solution, which was prepared from NaOH pellets (VWR, a. r. grade) according to the procedure reported in the literature [72]. The required amount of *cc.* NaOH was diluted to 1 dm³ volume and standardized against HCl solution. The stock solutions of acid were made by volumetric dilution of approx. 37 w/w% HCl (a.r. grade, Scharlau) and were standardized with KHCO₃ solution.

Sodium aluminate solutions (≈ 4 M NaAl(OH)₄, ≈ 4 M excess NaOH) were prepared according to procedures described in Ref. [127], *i.e.*, by dissolving aluminum wires (J.M. & Co., 99.99% purity) in a carbonate-free NaOH solution. The concentration of Al(OH)₄⁻ was determined by two methods. First, the metal as well as the filtered stock solution after the dissolution reaction was weighed. To convert the mass to volume, the density of the final solution was determined by a 25 mL pycnometer at (25.0 \pm 0.1) °C. Second, a ≈ 0.02 M NaAl(OH)₄ solution was prepared from the concentrated one and the metal content was determined *via* EDTA titration at pH ≈ 2 . The agreement between the values obtained from the two methods was within 1%.

The stock solutions of calcium chloride were prepared by dissolving calcium chloride dihydrate (Analar Normapur, a. r. grade) in deionized water, while the ionic strength was set to

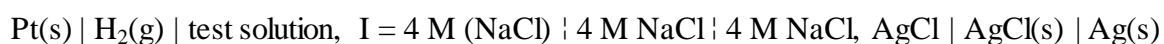
4.0 M (NaCl). The concentration of Ca^{2+} was determined prior to the measurements by EDTA titration.

Table 1. List of compounds used throughout this work

Name	Abbreviation	Purity	Vendor
Sodium D-gluconate	NaGluc	$\geq 99\%$	Sigma–Aldrich
Sodium D-heptagluconate	NaHpgl	$\geq 99\%$	Sigma–Aldrich
Malonic acid	H_2Mal	a. r. grade	Fluka
Calcium D-heptagluconate dihydrate	$\text{Ca}(\text{Hpgl})_2 \cdot 2\text{H}_2\text{O}$	$\geq 98\%$	Sigma–Aldrich
Sodium hydroxide pellets	NaOH	$\geq 98.5\%$	VWR Chemicals
Sodium chloride	NaCl	a. r. grade	VWR Chemicals
Hydrochloric acid solution, 37% w/w	HCl	a. r. grade	Scharlab
Deuterium oxide	D_2O	99.9%	Sigma–Aldrich
Aluminum wires	Al	99.99%	J.M. & Co.
Calcium chloride dihydrate	$\text{CaCl}_2 \cdot 2\text{H}_2\text{O}$	$\geq 99\%$	Sigma–Aldrich

Potentiometry

Potentiometric titrations were performed using an automatic titroprocessor (Metrohm 888 Titrando; tiamo™ 2.5, Metrohm AG, Switzerland) equipped with a SenTix®-62 (from WTW) combined glass (GLE) or a homemade platinized platinum electrode (H_2/Pt); the latter was prepared according to Ref. [128]. In strongly alkaline media ($\text{pH} > 12$), the conventional combined glass electrodes exhibit the so-called alkaline error, during which a part of the H^+ ions in the gel layer of the electrode membrane are replaced by Na^+ ions. As a result, the electrode may eventually respond to Na^+ ions, giving pH values lower than the real values. Therefore, most of the experiments were carried out using platinized platinum electrodes (built in-house). Moreover, the dissolution of CO_2 was minimized by bubbling H_2 into the solution. The electrochemical cell consisted of H_2/Pt and a thermodynamic Ag/AgCl reference electrode was constructed as follows:



The measurements were carried out in a closed custom-made titration vessel, covered with a PTFE lid and externally thermostated to 25.0, 50.0 or 75.0 ± 0.1 °C with a Julabo F12-MB thermostat (with an accuracy of ± 0.1 °C). Throughout the potentiometric measurements with the H_2/Pt electrode, the bubbling H_2 gas was presaturated in a 4 M NaCl humidifier solution to minimize evaporation loss [129]. The perceived decrease was less than 0.1% of the initial solution mass, which was considered insignificant.

The indicator electrodes were calibrated by titrating a weak acid (0.070 M malonic acid, Fluka, a. r. grade) and a strong acid (0.150 M HCl) with ≈ 1 M NaOH solutions by the protocol described in detail in the manual of the pH Cali software [130]. The program is capable of the determination of the electrode intercept, slope and the ionic product of water, taking the pH effect caused by the dissolving CO_2 into account. During the fitting procedure, the $\log K_w$ was fixed to -14.26 [131]. As a result of the calibration, the electrodes were found to be Nernstian at all temperatures in the range of $1.9 < \text{pH}_c < 13.6$ (H_2/Pt) and $1.9 < \text{pH}_c < 10.9$ (GLE), respectively (where pH_c is defined as $-\log ([\text{H}^+]/c^\ominus)$). That is, the relative accuracies of the determined slope values were found to be 0.24%, 0.44% and 0.25% at 25, 50 and 75 °C, while the respective theoretical values are 59.16, 64.12 and 69.08 mV, respectively.

During data acquisition, 70 cm^3 of the samples was titrated with NaOH, HCl or CaCl_2 solutions, depending on the system. The corresponding cell potentials were recorded as follows: to study the protonation of Hpgl^- , the solutions were titrated with 1.0056 M HCl, using GLE. Hereafter for component X, the analytical concentration is denoted as $[\text{X}]_{\text{T},0}$ (at the starting point of a titration) or $[\text{X}]_{\text{T}}$ (for pointwise measurements), while $[\text{X}]$ is referred to as the equilibrium concentration. To avoid the lactonization of the ligand, each solution was measured right after preparation.

The pH effects due to the deprotonation of Hpgl^- and the complexation of Ca^{2+} with L^- (where L^- was Gluc^- or Hpgl^-) occurring in the strongly alkaline pH range were followed with a platinized platinum (H_2/Pt) electrode. Each solution contained $[\text{NaOH}]_{\text{T},0} = 0.005$ M and was titrated with ≈ 1 M NaOH. The complexation of Hpgl^- with Al^{3+} as well as the interactions in solutions containing Ca^{2+} , Al^{3+} and Hpgl^- were investigated by titrations in the pH range of 2–14. The titrant was 1.0056 M HCl, whose ionic strength was set to 5 M (NaCl) to avoid the decrease in background electrolyte concentration caused by neutralization. Due to the rather slow kinetics known for Al(III) in acidic medium, the titrations were started from the strongly alkaline pH range using $[\text{NaOH}]_{\text{T},0} = 0.050\text{--}0.200$ M. During the experiments, a minimum and maximum waiting time was set for each data point to check if the displayed cell potentials show time-dependence. The measured value was accepted if the signal drift did not exceed the maximum tolerance interval (± 0.3 mV) after the minimum waiting time. We found that to attain chemical equilibrium in the entire pH range, the minimum waiting time must be 20 minutes. The CaCl_2 -concentration dependent titrations for the $\text{Hpgl}^-/\text{OH}^-$ and $\text{Al}^{3+}/\text{Hpgl}^-/\text{OH}^-$ systems were performed by changing the titrant to ≈ 1 M CaCl_2 and employing various $[\text{NaOH}]_{\text{T},0}$. Each solution was titrated until the appearance of a white precipitate.

Polarimetry

The optical rotation of the samples was measured using a Lippich-type polarimeter (Krüss P-1000, A. KRÜSS Optronic GmbH, Hamburg, Germany) equipped with a LED light source. The degrees of rotation (α) were measured at the sodium D line (589 nm) using polarimeter tubes with 200 mm path length at room temperature (23 ± 2) °C and at $I = 4$ M (NaCl). The reading accuracy of the instrument was $\pm 0.05^\circ$.

To observe the metal-ligand interactions in the binary systems, solution series with constant $[\text{Hpgl}^-]_{\text{T}}$ and varying $[\text{Ca}^{2+}]_{\text{T}}$ or $[\text{Al}(\text{OH})_4^-]_{\text{T}}$ were measured. A NaOH-concentration dependent series contained $[\text{Hpgl}^-]_{\text{T}} = [\text{Al}(\text{OH})_4^-]_{\text{T}}$ with $[\text{OH}^-]_{\text{T}}$ varying from 0.025 to 0.500 M.

For the ternary $\text{Ca}^{2+}/\text{Al}^{3+}/\text{Hpgl}^-$ system, solutions with $[\text{Hpgl}^-]_{\text{T}}/[\text{Al}(\text{OH})_4^-]_{\text{T}} = 2$ were assembled, while $[\text{Ca}^{2+}]_{\text{T}}$ was gradually increased from 0 to the value of $[\text{Al}(\text{OH})_4^-]_{\text{T}}$. Systems comprising of $\text{Ca}^{2+}/\text{Hpgl}^-$ and $\text{Ca}^{2+}/\text{Al}^{3+}/\text{Hpgl}^-$ contained 0.250 M excess NaOH, while for the $\text{Al}^{3+}/\text{Hpgl}^-$ system $[\text{NaOH}]_{\text{T}}$ was set to 0.200 M.

Nuclear Magnetic Resonance (NMR) Spectroscopy

^1H and ^{13}C NMR spectra were recorded with a Bruker Avance III HD 500 MHz NMR spectrometer equipped with a 5 mm inverse broadband probe head (CryoProbe™ Prodigy) furnished with z-oriented magnetic-field-gradient capability. The magnetic field was stabilized by locking it to the ^2D signal of the solvent prior to spectral acquisition. During the ^{13}C NMR acquisitions the proton decoupler was turned on. The temperature was maintained at (25 ± 1) °C.

To quantify the deprotonation of gluconate, samples of solutions with 0.200 M $[\text{Gluc}^-]_{\text{T}}$ and with varying concentrations of $[\text{NaOH}]_{\text{T}}$ (0–2.989 M) were placed into PTFE liners, which were subsequently inserted into quartz tubes containing D_2O . By this approach, the use of D_2O does not alter the activity of H^+ . For each sample, 512 scans were recorded to obtain the ^{13}C NMR spectra. For the data to be comparable to those from the potentiometric titrations, the ionic strength of the samples was set to 4 M with NaCl.

The Hpgl^- containing samples were prepared by adding 10 % (V/V) D_2O to the solutions. The ^1H peaks of Hpgl^- were assigned according to earlier results published in the literature [66], while that of the ^{13}C nuclei was performed by recording a ^1H – ^{13}C heteronuclear single quantum correlation spectrum for a 0.500 M NaHpgl solution (*Figure 5*).

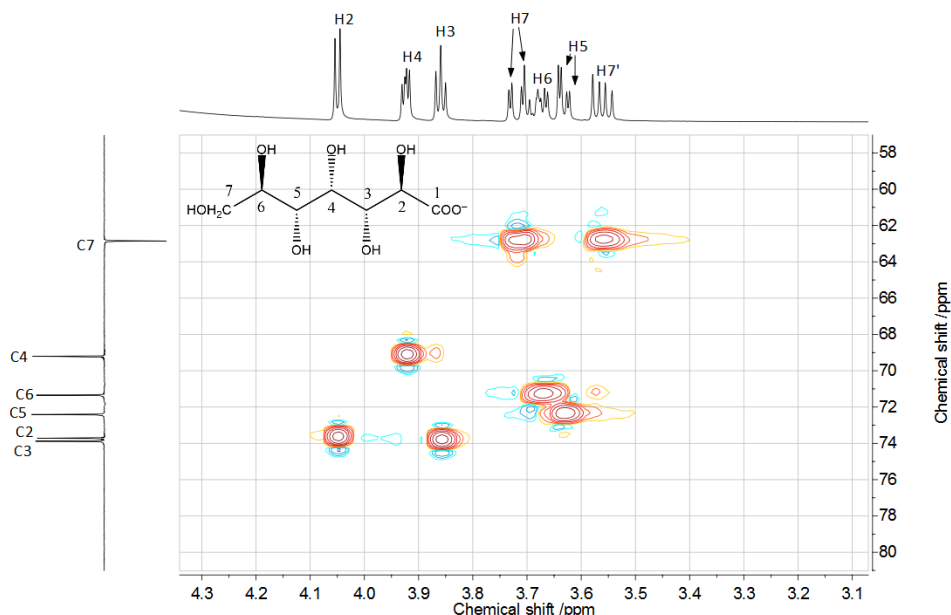


Figure 5 ^1H - ^{13}C heteronuclear single quantum correlation spectrum for a 0.500 M NaHpgl solution

The pH of solutions containing Hpgl^- ions were set using GLE, which was calibrated with dilute buffers (by WTW). Due to the fact that the activity coefficient of H^+ in the buffers differs from that in the samples, the pH adjusted here is regarded as nominal, directly recorded from the pH meter (pH_{nom}). The difference between pH and pH_c is the Irving or A factor [132], which encapsulates the effects originating from the difference in the activity coefficient of H^+ and in the liquid junction potential. To minimize A , no background electrolyte was added to the samples.

Generally, 128 and 1024 interferograms were collected to obtain the ^1H and ^{13}C NMR spectra of Hpgl^- containing samples, although for solutions with $\text{pH} = 4$ and 12, the ^{13}C NMR spectra with 8096 scans were also recorded. The spectra were baseline-corrected and normalized for comparison.

Freezing Point Depression (FPD)

Freezing point depression was measured with a Testo 735 digital precision thermometer using a probe with an accuracy of ± 0.05 °C. The change of temperature was monitored and recorded in every second during the measurements. The accepted temperature value was calculated as the 30s moving average of temperature values after the onset of freezing. The coolant was a mixture of water, ice and $\text{MgCl}_2 \cdot 6\text{H}_2\text{O}$.

Electrospray Ionization Mass Spectrometry (ESI-MS).

The mass spectra of solutions containing $[\text{Hpgl}^-]_{\text{T}} = [\text{Al}(\text{OH})_4^-]_{\text{T}} = 0.001 \text{ M}$ at $\text{pH}_{\text{nom}} = 7$ and 12 were recorded in negative mode using a Micromass Q-TOF Premier (Waters MS Technologies, Manchester, UK) mass spectrometer equipped with an electrospray ion source. The samples were introduced into the MS by applying direct injection method: the built-in syringe pump of the instrument with a 25 mL Hamilton syringe was used. The electrospray needle was adjusted to 3 kV and N_2 was used as nebulizer gas. The theoretical mass spectra were calculated using the Masslynx software [133].

Data evaluation and speciation calculations

The general complexation reaction between Ca^{2+} , $\text{Al}(\text{OH})_4^-$ and L^- ions as well as the corresponding stability product, β_{pqrs} , read as:



$$\beta_{pqrs}^{\emptyset} = \frac{\{\text{Ca}_p\text{Al}_q\text{L}_r(\text{OH})_{4q-s}\} \cdot \{\text{H}_2\text{O}\}}{\{\text{Ca}\}^p \cdot \{\text{Al}(\text{OH})_4\}^q \cdot \{\text{L}\}^r \cdot \{\text{H}\}^s} = \frac{[\text{Ca}_p\text{Al}_q\text{L}_r(\text{OH})_{4q-s}]}{[\text{Ca}]^p \cdot [\text{Al}(\text{OH})_4]^q \cdot [\text{L}]^r \cdot [\text{H}]^s} \cdot \frac{\gamma_{\text{Ca}_p\text{Al}_q\text{L}_r(\text{OH})_{4q-s}} \cdot \{\text{H}_2\text{O}\}}{\gamma_{\text{Ca}}^p \gamma_{\text{Al}}^q \gamma_{\text{L}}^r \gamma_{\text{H}}^s} \quad (9)$$

$$\beta_{pqrs} = \beta_{pqrs}^{\emptyset} \cdot \Gamma^{-1}, \quad (10)$$

where $p, q, r \geq 0$. In this respect, the calculated stability constants include the activity of water $\{\text{H}_2\text{O}\}$. The stability constants, freezing point depression and the molar rotation of the individual species as well as the limiting chemical shifts of Gluc^- and its two- and three-fold deprotonated forms were calculated with the PSEQUAD software [134]. Throughout the fitting procedure, $\log\beta_{pqrs}$ was refined by the minimization of the so-called fitting parameter (FP):

$$\text{FP} = \sqrt{\frac{\sum_{i=1}^n (Y_{i,\text{calc}} - Y_{i,\text{meas}})^2}{n-k}}, \quad (11)$$

where $Y_{i,\text{calc}}$ and $Y_{i,\text{meas}}$ represent the calculated and measured i^{th} data, while n refers to the number of measured data and k to the number of fitted parameters.

The speciation calculations were performed with the aid of the MEDUSA [135] software. In the $\text{Al}(\text{III})$ -containing systems, $\text{Al}(\text{OH})_4^-$ was set as the primary species, therefore, $[\text{Al}(\text{III})]_{\text{T}} = [\text{Al}(\text{OH})_4^-]_{\text{T}}$.

Characterization of the solid samples

Synthesis and sample preparation

During several titrations performed for the $\text{Ca}^{2+}/\text{Gluc}^-$ and the $\text{Ca}^{2+}/\text{Al}(\text{OH})_4^-/\text{Hpgl}^-$ systems, the appearance of a white precipitate was observed. The binary calcium- or aluminum-

containing solids were precipitated from solutions consisted of $[\text{Gluc}^-]_{\text{T},0} = 0.150 \text{ M}$, $[\text{Ca}^{2+}]_{\text{T},0} = 0.100 \text{ M}$, $[\text{OH}^-]_{\text{T},0} = 0.005 \text{ M}$; $[\text{Hpgl}^-]_{\text{T},0} = 0.200 \text{ M}$, $[\text{Ca}^{2+}]_{\text{T},0} = 0.135 \text{ M}$, $[\text{OH}^-]_{\text{T},0} = 0.250 \text{ M}$ and $[\text{Hpgl}^-]_{\text{T},0} = 0.146 \text{ M}$, $[\text{Al}(\text{OH})^-]_{\text{T}} = 0.292 \text{ M}$, $[\text{OH}^-]_{\text{T}} = 0.146 \text{ M}$, respectively. As for the ternary compounds, solid samples were obtained by titrating various $\text{Al}(\text{OH})_4^-$ and Hpgl^- containing solutions with 0.9923 M CaCl_2 ($I = 4 \text{ M NaCl}$). The identifiers of the solid samples and the corresponding solution compositions at the onset of precipitation are listed in *Table 2*.

Each sample was filtered through a hydrophilic PVDF $0.45 \mu\text{m}$ porous size membrane filter and rinsed with boiling deionized water to remove NaCl traces from the surface. Prior to the measurements, the solids were dried in a desiccator.

Table 2 The list of the prepared solid precipitates and the analytical concentrations of the solutions at which the precipitates appeared. Here, L^- refers to the ligand, gluconate (Gluc^-) or heptagluconate (Hpgl^-).

Sample ID	$[\text{Ca}^{2+}]_{\text{T}} / \text{M}$	$[\text{Al}(\text{OH})^-]_{\text{T}} / \text{M}$	$[\text{L}^-]_{\text{T}} / \text{M}$	$[\text{OH}^-]_{\text{T}} / \text{M}$
Ca-Gluc	0.084	—	0.126	0.004
Ca-Hpgl	0.135	—	0.200	0.250
Al-Hpgl	—	0.292	0.146	0.146
CaAl-Hpgl-1	0.055	0.095	0.095	0.236
CaAl-Hpgl-2	0.120	0.088	0.176	0.220
CaAl-Hpgl-3	0.122	0.132	0.175	0.220
CaAl-Hpgl-4	0.063	0.047	0.094	0.235
CaAl-Hpgl-5	0.322	0.169	0.338	0.169
CaAl-Hpgl-6	0.197	0.081	0.160	0.042
CaAl-Hpgl-7	0.200	0.120	0.160	0.042
CaAl-Hpgl-8	0.175	0.165	0.165	0.044

Methods for the structural characterization of these solids

X-ray diffractograms were recorded with a Rigaku MiniFlex Type II. X-ray diffractometer with 3° $2\theta/\text{min}$ sampling rate, using $\text{CuK}\alpha$ radiation ($\lambda=0.15406 \text{ nm}$) at 40 kV , 30 mA . After processing, the diffractograms were smoothed with a 15 points adjacent-average algorithm and their intensities were normalized.

The morphology of the binary and ternary precipitates was investigated by a Hitachi S-4700 scanning electron microscope at various magnifications and acceleration voltages. The elemental distribution in the solids was analyzed by energy-dispersive X-ray spectroscopy using a Röntec QX2 spectrometer mounted on the microscope and equipped with Be window.

The thermal properties of the samples were investigated with a Setaram Labsys derivatograph operating under a constant flow of air at $5^{\circ}\text{C}\cdot\text{min}^{-1}$ heating rate. For the analysis, 25–30 mg portions of the solids were placed into high-purity alpha-alumina crucibles.

The infrared spectra of the samples at room temperature were recorded using a Bio-Rad Digilab Division FTS65A/896 FT-IR Spectrometer with a Harrick's Meridian™ SplitPea Single Reflection Diamond ATR accessory. The measurements were performed in the range of $4000\text{--}400\text{ cm}^{-1}$ at 4 cm^{-1} optical resolution and 128 interferograms were averaged to achieve good signal to noise ratio. Raman spectra were obtained between 100 cm^{-1} and 3500 cm^{-1} with 2 cm^{-1} resolution using a Thermo Scientific Raman DXR microscope at room temperature. A diode-pumped, frequency-doubled Nd:YAG laser ($\lambda = 760\text{ nm}$) was used as a light source at 15 mW maximum laser power. All spectra were analyzed (including deconvolution, peak fitting, etc.) with the aid of the Thermo Galactic Inc. GRAMS/AI version 7 software [136].

The total concentrations of Ca^{2+} and Al^{3+} ions were determined with a Thermo Scientific iCAP 7400 ICP-OES DUO spectrometer with radial plasma viewing. $\approx 25\text{ mg}$ portions of each sample were dissolved in $5\text{ cm}^3 \approx 2\text{ M}$ hydrochloric acid and diluted to 1:10 ratio with deionized water. An ICP Multielement standard solution IV (CertiPUR®) was used for the calibration along with internal magnesium standard.

The spectra of heptagluconate were recorded with a Specord 210 plus double beam UV-vis spectrophotometer at $(25.1 \pm 0.1)^{\circ}\text{C}$, in the wavelength range of $185\text{--}500\text{ nm}$ with 0.1 nm resolution. The optical path length of the quartz cuvette was 1 cm . Minute amounts of each sample ($\approx 50\text{ mg}$) were dissolved in $\approx 2\text{ M HCl}$ and measured right after their preparation. This approach was necessary to minimize the gradual shift in the absorbance caused by the lactonization of Hpgl^{-} in strongly acidic medium [137]. Also, the absorbance readings were taken at the isosbestic point at 218 nm , which is invariant of the progress of lactonization (see *Figure 6a*). The calculation of concentrations in the samples was based on the calibration curve recorded for a solution series with known concentrations of Hpgl^{-} ($0.001\text{ M} - 0.010\text{ M}$) at $\approx 2\text{ M HCl}$ (*Figure 6b*), applying Beer's law.

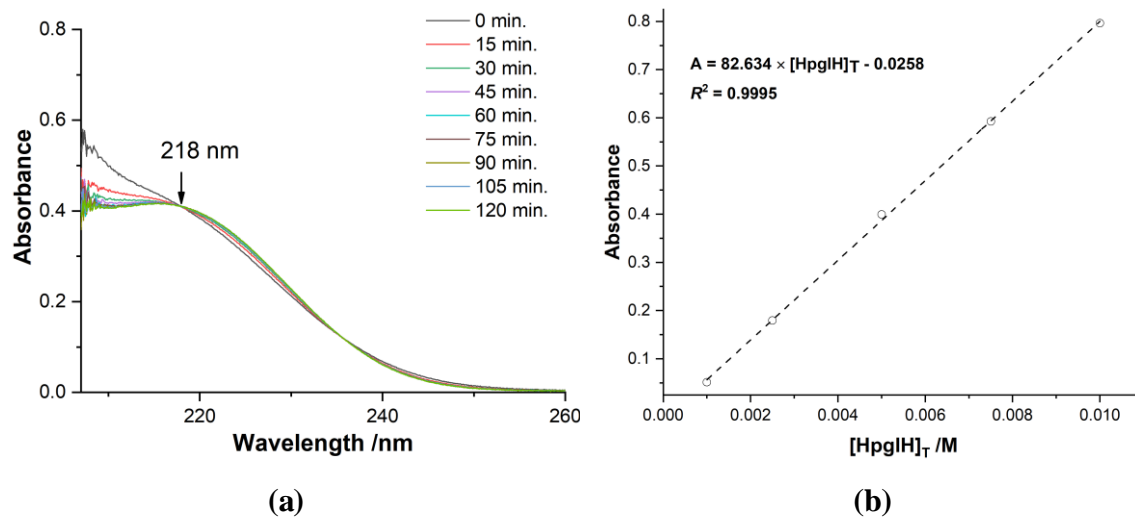


Figure 6 Time-dependency of the UV-vis spectra ($[\text{NaHpgl}]_T = 0.005 \text{ M}$, $[\text{HCl}]_T = 2.008 \text{ M}$, (a)) and the obtained calibration curve of heptagluconic acid (b). The result of linear fitting is depicted as dashed line.

Results and discussion

The acid-base properties of D-heptagluconate and D-gluconate

The acid-base equilibria of D-gluconate and D-heptagluconate were investigated by pH potentiometric titrations as well as ^1H and (only in the case of Gluc^-) ^{13}C NMR spectroscopic measurements.

The carboxylate group of Hpgl^- , as it is common for any other hydroxycarboxylates, undergoes protonation yielding heptagluconic acid (HpglH) [101]:



$$K_p = \beta_{0011} = \frac{[\text{HpglH}] \cdot c}{[\text{Hpgl}^-][\text{H}_3\text{O}^+]} \quad (13)$$

where K_p is the protonation constant of the anion. Note that according to *Equation 9*, $K_p = \beta_{0011}$. To investigate the protonation of Hpgl^- , potentiometric measurements were performed at $[\text{Hpgl}^-]_{\text{T}} = 0.050 \text{ M}$ and 0.200 M , whereas the ionic strength was set to $I = 4 \text{ M}$ (NaCl). The two sets of experimental data were fitted simultaneously, while the ionic product of water was fixed at 14.26 [131]. Fitting the potentiometric curves (*Figure 7*) resulted in an excellent agreement between the measured and calculated data ($\text{FP} = 0.40 \text{ mV}$) and yielded $\log K_p = 3.64$. This value agrees well with the one reported in Ref. [138], with due account to the different ionic strength.

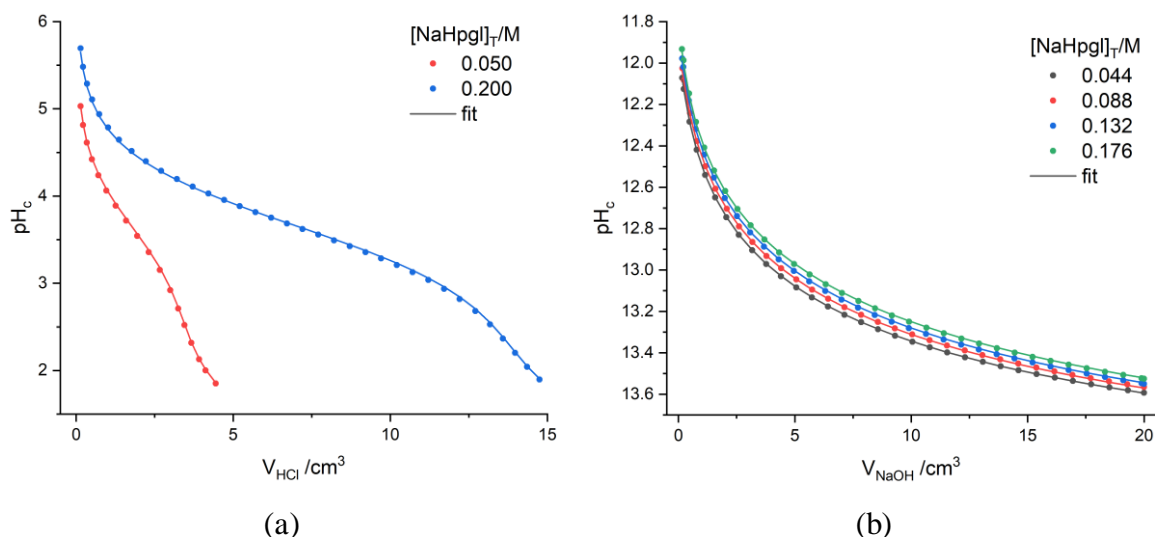


Figure 7 Measured pH_c values as a function of added titrant volume in solutions consisting of heptagluconate and HCl (protonation experiments, Figure 7a) or NaOH (deprotonation experiments, Figure 7b). Experimental conditions: $t = (25 \pm 0.1) \text{ }^\circ\text{C}$ and $I = 4 \text{ M}$ (NaCl); the initial compositions are shown in the legend. Symbols represent the measured data, whereas solid lines are the results of the fits based on the calculated stability constants discussed in the text and provided in Tables 3 and 4.

On the other hand, a much lower value has been determined by ^1H NMR spectroscopy [66], which may be originated from the improper calibration of the glass electrode. For Gluc^- , $\log K_p$ was reported to be 3.73 [97]. Nevertheless, we have found good agreement with the reported values, determined at the same ionic strength.

Table 3 Protonation constants $\log K_p$, of Gluc^- and Hpgl^- , organized by reaction and background electrolyte. Data corresponds to $t = 25^\circ\text{C}$. The triple standard errors are included in parentheses.

Reaction	Background electrolyte	$\log K_p$	Ref.	Method
$\text{Gluc}^- + \text{H}_3\text{O}^+ \rightleftharpoons \text{GlucH} + \text{H}_2\text{O}$	4 M NaCl	3.73(5)	[97]	GLE
$\text{Hpgl}^- + \text{H}_3\text{O}^+ \rightleftharpoons \text{HpglH} + \text{H}_2\text{O}$	4 M NaCl	3.64(1)	[137]	GLE / POL
	0.1 M NaNO_3	3.38(2)	[139]	GLE
	1 M NaCl	2.49(2)	[66]	GLE / ^1H NMR

In strongly alkaline medium, the OH group(s) of hydroxycarboxylates undergoes deprotonation [66]:



$$K_a = \beta_{001-1} = \frac{[\text{LH}^{2-}_1][\text{H}_3\text{O}^+]}{[\text{L}^-] \cdot c} \quad (15)$$

where K_a is the deprotonation constant of the ligand ($\text{L}^- = \text{Hpgl}^-$ or Gluc^-).

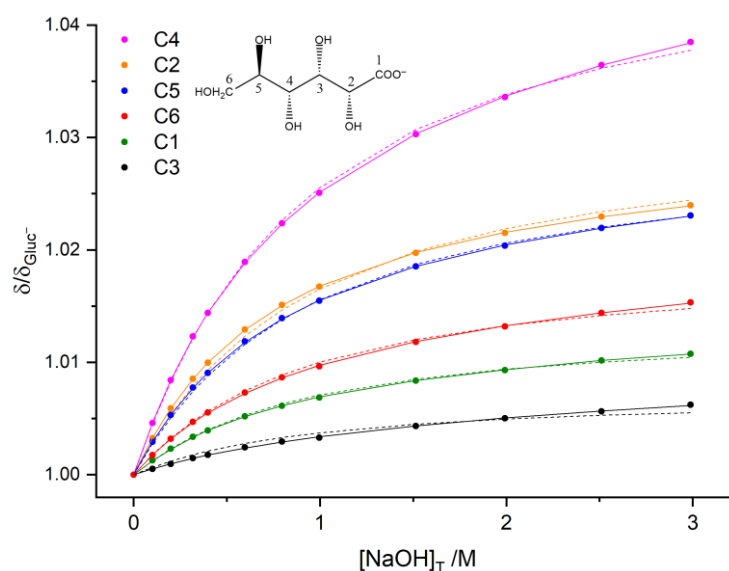
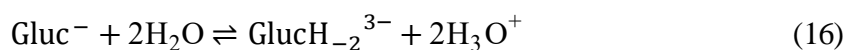


Figure 8 Observed (symbols) and calculated (lines) ^{13}C NMR chemical shifts of gluconate-containing species as a function of $[\text{NaOH}]_T$. Experimental conditions: $t = 25^\circ\text{C}$, $I = 4\text{ M}$ (NaCl); $[\text{NaGluc}]_T = 0.200\text{ M}$, $[\text{NaOH}]_T = 0\text{--}2.989\text{ M}$. The calculations were performed by fitting the first (dashed line) or the first and second (solid line) deprotonation constants of Gluc^- . For better visualization, the chemical shifts were normalized to those of 0.200 M NaGluc. The appropriate nuclei and their numbering are indicated in the legend.

First, the deprotonation of Gluc^- was investigated by using ^{13}C NMR spectroscopy and pH potentiometry. The ^{13}C NMR measurements were performed with a solution series containing $[\text{NaGluc}]_{\text{T}} = 0.200 \text{ M}$ and $[\text{NaOH}]_{\text{T}} = 0\text{--}2.989 \text{ M}$. The addition of NaOH caused systematic variations in the chemical shifts (*Figure 8*), indicative of the deprotonation of the OH groups of Gluc^- .

Fitting the experimental data assuming one deprotonation step yielded $\log \beta_{001-1}$ ($= \log K_{\text{a}}$) $= -14.16$ with the fitting parameter (FP) being 0.025 ppm. However, using this constant, systematic errors are seen between the observed and calculated chemical shifts (*Figure 8*), which suggests a further chemical equilibrium. Therefore, a second deprotonation of the anion was considered.



$$\beta_{001-2} = \frac{[\text{GlucH}_{-2}^{3-}][\text{H}_3\text{O}^+]^2}{[\text{Gluc}^-] \cdot c^2} \quad (17)$$

This assumption significantly decreased the value of FP to 0.003 ppm and yielded $\log \beta_{001-1} = -13.90$ and $\log \beta_{001-2} = -28.82$. That is, the two stepwise deprotonation constants of Gluc^- were found to be $\text{p}K_{\text{a},1} = 13.90$ and $\text{p}K_{\text{a},2} = 14.92$. In earlier publications $\log \beta_{001-1}$ was reported to be -13.68 at 1 M NaCl [64], whereas at 1 M NaClO_4 , $\log \beta_{001-1}$ and $\log \beta_{001-2}$ were found to be -13.66 and -27.68 , respectively [65]. The difference between the literature data and our results stems probably from the different ionic strength and/or the different background electrolyte.

Considering that GlucH_{-2}^{3-} is formed to a rather low extent (only $\approx 30\%$) at the highest pH and that the chemical shifts of GlucH_{-1}^{2-} and GlucH_{-2}^{3-} are very similar, the formation of GlucH_{-2}^{3-} needs further affirmation. Hence, as an independent method, matrix rank analysis [140] was used to determine the number of spectroscopically different gluconate-containing species. In principle, this method is applicable to any ‘absorbance-type’ quantities for which the experimental signal is linearly proportional to the concentration of the ‘absorbing species’. For the present system, the observed chemical shift can be described as follows:

$$\delta = \delta_{\text{Gluc}^-} \frac{[\text{Gluc}^-]}{[\text{Gluc}^-]_{\text{T}}} + \delta_{\text{GlucH}_{-1}^{2-}} \frac{[\text{GlucH}_{-1}^{2-}]}{[\text{Gluc}^-]_{\text{T}}} + \delta_{\text{GlucH}_{-2}^{3-}} \frac{[\text{GlucH}_{-2}^{3-}]}{[\text{Gluc}^-]_{\text{T}}} \quad (18)$$

Equation 18 shows that the observed chemical shift (δ) is linearly proportional to the free concentration of a certain species and the proportionality coefficient is the ratio of the limiting chemical shift of the species and $[\text{Gluc}]_{\text{T}}$ (0.200 M). In this respect, the chemical shift can be regarded as an ‘absorbance-type’ quantity. For this system, the analysis yielded three linearly independent species attesting the formation of GlucH_{-1}^{2-} and GlucH_{-2}^{3-} .

The deprotonation constants of both Hpgl^- and Gluc^- were determined by pH potentiometric titrations as well. Since a maximum of $[\text{NaOH}]_{\text{T}} = 0.26 \text{ M}$ was employed during the titrations, only the first deprotonation step was expected to occur. Our results obtained from potentiometry verified this assumption, as one deprotonation constant was sufficient to describe the titration curves adequately. For Gluc^- , $\log \beta_{001-1}$ was determined to be -14.08 , which is in line with those obtained from NMR spectroscopic experiments (-13.90), with due account to the different experimental method. Regarding Hpgl^- , the fit yielded $\log K_{\text{a}} = -13.81$ (FP = 0.25 mV , *i.e.*, $0.004 \text{ pH}_{\text{c}}$ units); the simulated titration curves are depicted in *Figure 7b*. The thus obtained agrees fairly well with the one obtained at $I = 1 \text{ M NaCl}$ [66] (considering the effect of different ionic strength).

Table 4 Deprotonation constants, $\log K_{\text{a}}$, determined for Gluc^- and Hpgl^- , organized by the reaction and background electrolyte concentration, corresponding to $t = 25 \text{ }^\circ\text{C}$. The triple standard errors are included in parentheses.

Reaction	Background electrolyte	$\log K_{\text{a}}$	Ref.	Method
$\text{Gluc}^- + \text{H}_2\text{O} \rightleftharpoons \text{GlucH}_{-1}^{2-} + \text{H}_3\text{O}^+$	4 M NaCl	$-14.08(3)$	p.w.	H_2/Pt POT
	4 M NaCl	$-13.90(3)$	p.w.	^{13}C NMR
	1 M NaCl	$-13.68(3)$	[64]	H_2/Pt POT
	1 M NaClO_4	$-13.66(24)$	[65]	H_2/Pt POT
$\text{Gluc}^- + 2\text{H}_2\text{O} \rightleftharpoons \text{GlucH}_{-2}^{3-} + 2\text{H}_3\text{O}^+$	4 M NaCl	$-14.72(5)$	p.w.	H_2/Pt POT
	1 M NaClO_4	$-14.02(30)$	[65]	H_2/Pt POT
$\text{Hpgl}^- + \text{H}_2\text{O} \rightleftharpoons \text{HpglH}_{-1}^{2-} + \text{H}_3\text{O}^+$	4 M NaCl	$-13.81(1)$	p.w.	H_2/Pt POT
	1 M NaCl	$-13.41(2)$	[66]	H_2/Pt POT

The calcium complexation properties of D-gluconate and D-heptagluconate ions in alkaline solutions

Complexation of Ca^{2+} by gluconate ions in alkaline medium

The interactions between calcium ions and Gluc^- in alkaline medium ($[\text{NaOH}]_{\text{T}} = 0.005\text{--}0.267 \text{ M}$) were investigated by systematic potentiometric titrations using H_2/Pt electrode. All the measurements were performed in ligand excess, specifically by varying the ratio of $[\text{Ca}^{2+}]_{\text{T}}:[\text{Gluc}^-]_{\text{T}}$ between 1:1.32 and 1:40. The obtained titration curves are shown in the order of increasing $[\text{Gluc}^-]_{\text{T}}$ and $[\text{Ca}^{2+}]_{\text{T}}$ in *Figure 9a*.

At relatively low metal and ligand concentrations, a minor shift in the fashion of the titration curves can be observed indicating the formation of mononuclear complexes. Upon increasing $[\text{Ca}^{2+}]_{\text{T}}$ and $[\text{Gluc}^-]_{\text{T}}$, these shifts gradually become more pronounced, resulting in a noticeable change in the shape of the titration curves at the same metal-to-ligand ratios. The detected

changes in the curvature are very similar to those previously observed at 1 M ionic strength [64], therefore the formation of multinuclear species can be inferred.

To reinforce our assumption, calcium(II)-dependent titrations were performed with solutions containing $[\text{NaGluc}]_{\text{T},0} = 0.1\text{--}0.2$ M and $[\text{NaOH}]_{\text{T},0} = 0.1$ M. Upon addition of 1 M CaCl_2 to these solutions, a continuous decrease in the pH was seen (*Figure 9b*). Although the dilution could give rise to a 0.08 decrease in the measured pH, the observed changes were one order of magnitude higher (*ca.* 1–1.3 units), corresponding unambiguously to the formation of deprotonated Ca(II) gluconate complexes, which is indeed accompanied by such a decrease in pH_c .

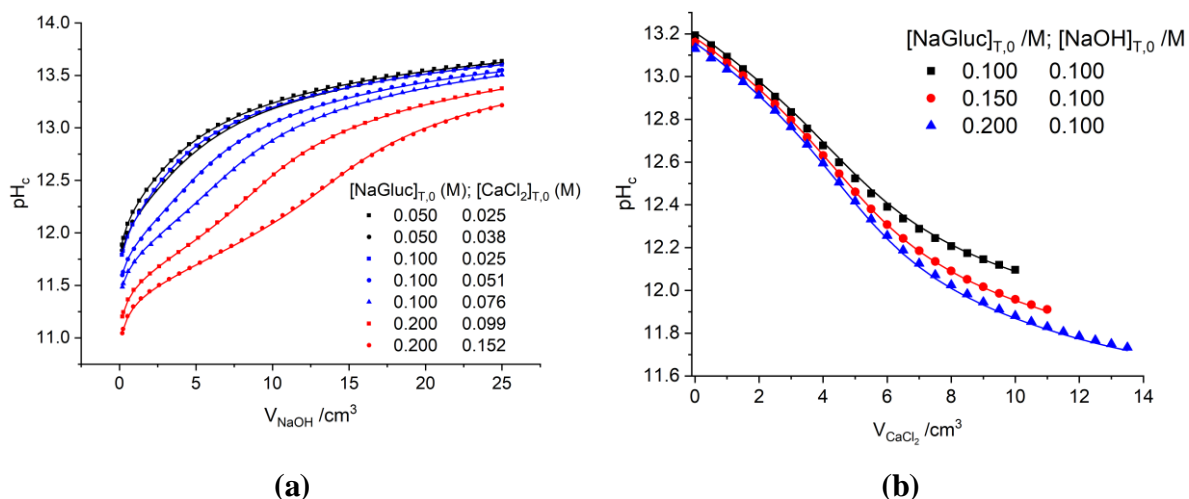


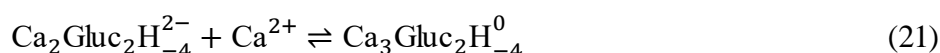
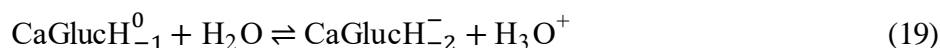
Figure 9 Measured (symbols) and calculated (lines) pH for gluconate in the presence of CaCl_2 and NaOH. Experimental conditions: $t = 25$ °C, $I = 4$ M (NaCl); (a) $[\text{NaGluc}]_{\text{T},0} = 0.050\text{--}0.200$ M, $[\text{CaCl}_2]_{\text{T},0} = 0.025\text{--}0.152$ M, $[\text{NaOH}]_{\text{T},0} = 0.005$ M, Titrant: 1 M NaOH; (b) $[\text{NaGluc}]_{\text{T},0} = 0.100\text{--}0.200$ M, $[\text{NaOH}]_{\text{T},0} = 0.100$ M, Titrant: 1 M CaCl_2 . Symbols represent the measured data, whereas solid lines are the results of the fits based on the speciation model provided in *Table 6*.

To extract the stoichiometry and stability constants of the various Ca^{2+} complexes, the measured titration datasets were simultaneously fitted by fixing pK_w to 14.26 and $\log \beta_{001-1}$ to -13.81 . The formation constants of $\text{Ca}(\text{OH})^+$ and $\text{Ca}(\text{OH})_2^0$, *i.e.*, $\log \beta_{100-1}$ and $\log \beta_{101-2}$, were taken from Ref. [95], while pK_w was fixed at 14.26 [131].

Fitting the titration data assuming only the formation of the CaGlucH_{-1}^0 mononuclear complex yielded $\text{FP} = 14.7$ mV. To further decrease the average error between the measured and calculated values, *ca.* 50 additional species were tested. By the inclusion of the $\text{Ca}_3\text{Gluc}_2\text{H}_{-4}^0$ complex in the model, FP dropped to 2.4 mV. However, the possible formation of this major trinuclear species is not unprecedented: earlier, its formation has been reported not only in the presence of D-gluconate [64], but also with the structurally similar D-heptagluconate

[66] and L-gulonate [141], too, at $I = 1$ M. A significant reduction in the value of FP could be achieved by assuming the formation of a third species, which can be either CaGlucH_{-2}^{-} (FP = 0.86 mV) or $\text{Ca}_2\text{Gluc}_2\text{H}_{-4}^{2-}$ (FP = 0.70 mV). Previously, $\text{Ca}_2\text{GlucH}_{-3}^0$ was reported to form at $I = 1$ M NaCl [25]. On the other hand, $\text{Ca}_2\text{GlucH}_{-3}^0$ is interchangeable with $\text{Ca}_2\text{Gluc}_2\text{H}_{-4}^{2-}$ yielding the same FP, therefore the formation of both species at $I = 1$ M NaCl could be inferred, even though they are indistinguishable by potentiometry.

Considering the possibility, that both CaGlucH_{-2}^{-} and $\text{Ca}_2\text{Gluc}_2\text{H}_{-4}^{2-}$ may be present at $I = 4$ M, the formation of $\text{Ca}_3\text{Gluc}_2\text{H}_{-4}^0$ could be described as follows:



By this proposed scheme, CaGlucH_{-2}^{-} seems to dimerize yielding $\text{Ca}_2\text{Gluc}_2\text{H}_{-4}^{2-}$. Since the latter species provided slightly lower FP, it was chosen for the final chemical model. The respective $\log\beta_{\text{pqrs}}$ constants are presented in *Table 6*.

Regarding these complexes, $\text{Ca}_3\text{Gluc}_2\text{H}_{-4}^0$ is the predominant one above $\text{pH} = 12.5$ at $[\text{NaGluc}]_{\text{T}} = 0.050$ M and $[\text{CaCl}_2]_{\text{T}} = 0.025$ M (see *Figure 10*, solid lines). Increasing $[\text{NaGluc}]_{\text{T}}$ to 0.2 and $[\text{CaCl}_2]_{\text{T}}$ to 0.150 M, respectively, the formation of this trinuclear complex is even more pronounced (dashed lines). The binuclear species becomes dominant above pH_c 13.3 at both compositions.

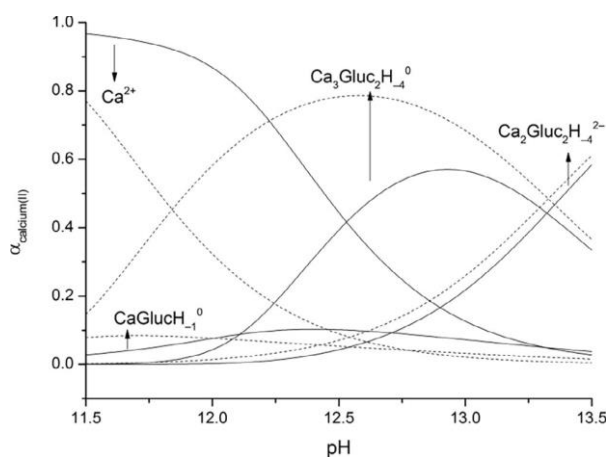


Figure 10 Distribution of calcium(II) among the various aqueous species in the presence of gluconate (Gluc^-) as a function of pH. The calculations correspond to $t = 25$ °C and $I = 4$ M (NaCl); solid lines: $[\text{NaGluc}]_{\text{T}} = 0.050$ M, $[\text{CaCl}_2]_{\text{T}} = 0.025$ M, dashed lines: $[\text{NaGluc}]_{\text{T}} = 0.200$ M, $[\text{CaCl}_2]_{\text{T}} = 0.150$ M. The simulations were performed using the stability constants given in *Table 6*.

Complexation of Ca^{2+} by heptagluconate ions in alkaline medium

The Ca^{2+} complexation properties of D-heptagluconate in alkaline medium were also studied by pH potentiometry and polarimetry at $t = 25\text{ }^\circ\text{C}$ and $I = 4\text{ M NaCl}$. As for potentiometry, both pH- and Ca^{2+} -dependent experiments were carried out using $[\text{NaHpgl}]_{\text{T},0} = 0.04\text{--}0.175\text{ M}$ and $[\text{CaCl}_2]_{\text{T},0} = 0.025\text{--}0.152\text{ M}$ initial concentrations (Figure 11). As expected, the structure of the titration curves greatly resembled to those of D-gluconate due to the structural similarity of the two ligands: heptagluconate only differs from gluconate in an additional $-\text{CH}_2\text{-OH}$ group and thus the same speciation model could be envisaged (Figure 12). Upon fitting the potentiometric data, it was found that assuming the formation of CaHpgl^+ , $\text{Ca}_2\text{Hpgl}_2\text{H}_{-4}^{2-}$, $\text{Ca}_3\text{Hpgl}_2\text{H}_{-3}^+$ and $\text{Ca}_3\text{Hpgl}_2\text{H}_{-4}^0$ provides the best description of the experimental titrations (FP = 0.78 mV). An intriguing aspect of the determined speciation is the presence of $\text{Ca}_3\text{Hpgl}_2\text{H}_{-3}^+$ complex, which could not be detected for gluconate in the present work ($I = 4\text{ M}$) or previously ($I = 1\text{ M}$) [66]. Nevertheless, these results are in line with those reported for heptagluconate [66] and gulonate [142] in $I = 1\text{ M}$ (NaCl) medium.

The difference between the speciation model between Gluc^- and Hpgl^- can be explained by the different arrangements of their OH functions. The C2-OH and C3-OH groups of Hpgl^- and Gul^- are in *erythro*, while the C3-OH and C4-OH moieties are in *threo* position, as compared to Gluc^- , where the C2-OH and C3-OH groups are also in *threo* position. Consequently, the two ligands possess a different binding motif, even though their relative configuration is very similar [141].

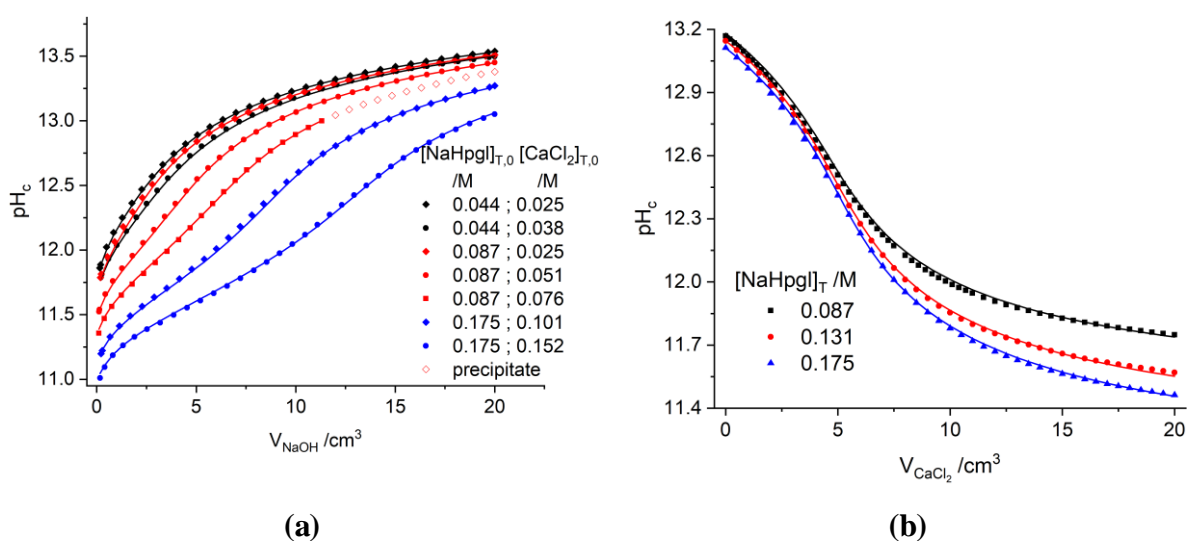


Figure 11 Measured (symbols) and calculated (lines) pH for heptagluconate in the presence of CaCl_2 and NaOH . Experimental conditions: $t = 25\text{ }^\circ\text{C}$, $I = 4\text{ M}$ (NaCl); (a) $[\text{NaHpgl}]_{\text{T},0} = 0.050\text{--}0.200\text{ M}$, $[\text{CaCl}_2]_{\text{T},0} = 0.025\text{--}0.152\text{ M}$, $[\text{NaOH}]_{\text{T},0} = 0.005\text{ M}$, Titrant: 1 M NaOH ; (b) $[\text{NaHpgl}]_{\text{T},0} = 0.100\text{--}0.200\text{ M}$, $[\text{NaOH}]_{\text{T},0} = 0.100\text{ M}$, Titrant: 1 M CaCl_2 . Solid lines were fitted based on the speciation model provided in Table 6.

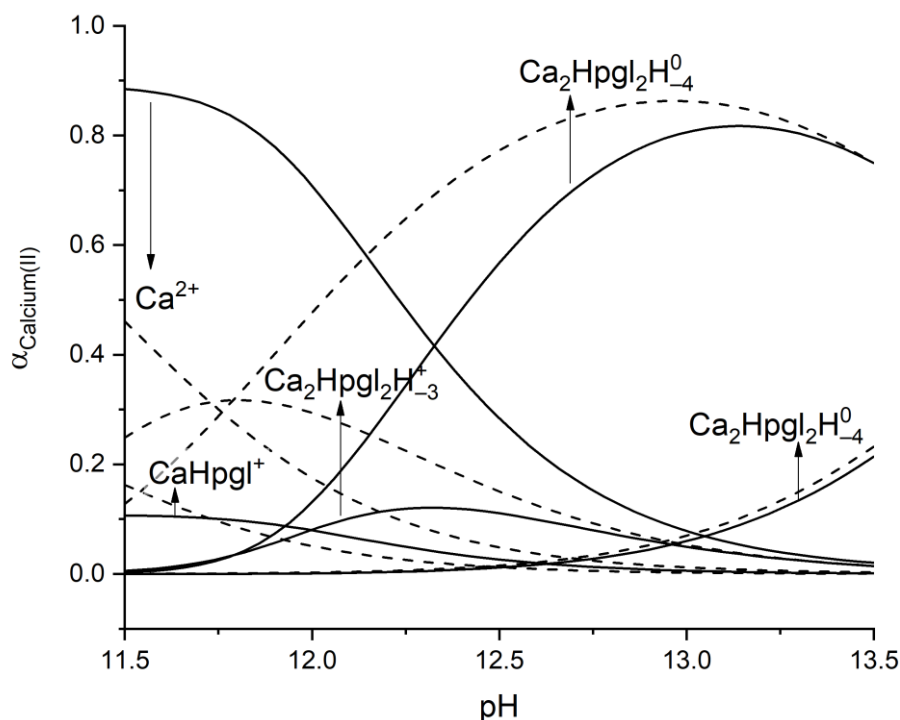


Figure 12 Distribution of calcium(II) among the various aqueous species in the presence of heptagluconate (Hpgl⁻) as a function of pH. The calculations correspond to $t = 25\text{ }^{\circ}\text{C}$ and $I = 4\text{ M}$ (NaCl); solid lines: $[\text{NaHpgl}]_{\text{T}} = 0.050\text{ M}$, $[\text{CaCl}_2]_{\text{T}} = 0.025\text{ M}$, dashed lines: $[\text{NaHpgl}]_{\text{T}} = 0.200\text{ M}$, $[\text{CaCl}_2]_{\text{T}} = 0.150\text{ M}$. The simulations were performed using the stability constants provided in *Table 6*.

It is known that the association of alkaline earth metal ions may affect the optical activity of the ligand [143]. Therefore, the Ca^{2+} -complexation properties of heptagluconate was also investigated by polarimetry (*Figure 13*) at different ligand concentrations in strongly alkaline medium ($[\text{NaOH}]_{\text{T}} = 0.1\text{ M}$). With increasing concentration of CaCl_2 , the observed optical rotation gradually increased, indicating that upon complexation the optically active species formed have higher specific rotations than the plain ligand. While the direction of these variations is obvious, the magnitude of the increase is rather small, which implies that the adequate determination of formation constants is not possible. However, fitting this data together with potentiometric ones is a reliable way to validate the calculated speciation.

In analogy with Beer's law, the observed optical rotation is linearly proportional to the free concentration of formed complexes, $[\text{Ca}_x\text{Hpgl}_y\text{H}_z]$, (the charges were omitted for simplicity) and the molar optical rotation, $\alpha_{\text{Ca}_x\text{Hpgl}_y\text{H}_z}$:

$$\alpha = \sum \alpha_{\text{Ca}_x\text{Hpgl}_y\text{H}_z} \cdot [\text{Ca}_x\text{Hpgl}_y\text{H}_z], \quad (22)$$

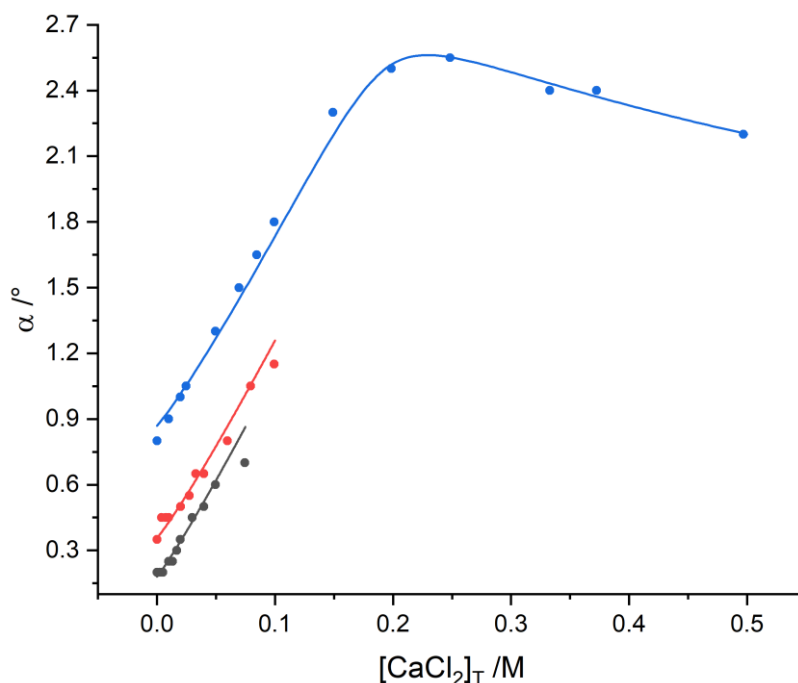


Figure 13 Optical rotation of D-heptagluconate (Hpgl^-) as a function of CaCl_2 concentration. Experimental conditions: $[\text{NaOH}]_{\text{T}} = 0.100 \text{ M}$, $t = (25 \pm 2) \text{ }^\circ\text{C}$ and $I = 4 \text{ M}$ (NaCl); **black curve:** $[\text{Hpgl}^-]_{\text{T}} = 0.100 \text{ M}$, $[\text{Ca}^{2+}]_{\text{T}} = 0\text{--}0.075 \text{ M}$; **red curve:** $[\text{Hpgl}^-]_{\text{T}} = 0.200 \text{ M}$, $[\text{Ca}^{2+}]_{\text{T}} = 0\text{--}0.100 \text{ M}$; **blue curve:** $[\text{Hpgl}^-]_{\text{T}} = 0.500 \text{ M}$, $[\text{Ca}^{2+}]_{\text{T}} = 0\text{--}0.500 \text{ M}$. Symbols refer to the measured data whereas solid lines are the results of the fits based on the speciation model provided in *Table 6*.

Table 5 Specific rotations of the free ligand, the deprotonated ligand and their calcium(II) complexes. The data corresponds to $t = 25 \pm 2 \text{ }^\circ\text{C}$. The triple standard errors are included in parentheses.

Species	$[\alpha]_{\text{D}}^{25} / \text{ }^\circ \cdot \text{cm}^3 \cdot \text{g} \cdot \text{dm}^{-1}$	Species	$[\alpha]_{\text{D}}^{25} / \text{ }^\circ \cdot \text{cm}^3 \cdot \text{g} \cdot \text{dm}^{-1}$
Hpgl^-	3.55 ^a	$\text{Ca}_2\text{Hpgl}_2\text{H}_{-4}^{2-}$	13.62(3.71)
HpglH_{-1}^{2-}	4.84(43)	$\text{Ca}_3\text{Hpgl}_2\text{H}_{-3}^+$	16.25(69)
CaHpgl^+	1.7(1.4) ^b	$\text{Ca}_3\text{Hpgl}_2\text{H}_{-4}^0$	30.50(85)

^a This constant was determined by measuring the optical rotation of a 0.500 M NaHpgl solution

^b This constant was taken from the literature [101] and corresponds to $I = 1 \text{ M}$ (NaCl)

The stability constants and molar optical rotation values were determined by the simultaneous fitting of the polarimetric and potentiometric data with the PSEQUAD software [134], while the molar optical rotations of plain Hpgl^- and its calcium complex, CaHpgl^+ were fixed at $1.6 \text{ }^\circ \cdot \text{dm}^3 \cdot \text{mol}^{-1}$ and $0.9 \text{ }^\circ \cdot \text{dm}^3 \cdot \text{mol}^{-1}$, respectively. The calculation process yielded a reasonably good fit with $\text{FP} = 1.48$, which is still acceptable considering the accuracy of the two methods. At $\text{pH} \approx 13$, where polarimetric measurements were carried out, $\text{Ca}_2\text{Hpgl}_2\text{H}_{-4}^{2-}$ is formed only to an extent of *ca.* 10%. Consequently, the correlation between its stability constant

and the specific rotation is high, hence the larger error of the latter. The results of these calculations are depicted on *Figure 13* and summarized in *Table 6*.

Table 6 Stability products ($\log \beta_{pqrs}$, with triple standard error) of $\text{Ca}_p\text{L}_r\text{H}_s^{(2p-r+s)}$ complexes, where L^- denotes D-gluconate (Gluc^-) or D-heptagluconate (Hpgl^-). The experiments were performed with H_2/Pt electrode, unless indicated differently. Literature sources for the corresponding ligand are included in brackets. Data correspond to $t = 25^\circ\text{C}$.

Reaction	Background electrolyte	Gluc^-	Hpgl^-
$\text{Ca}^{2+} + \text{L}^- \rightleftharpoons \text{CaL}^+$	1 M NaCl	1.08(4) ^a [144]	1.21(12) ^a [66]
	1 M NaCl	0.70(5) [101]	0.85 ^{b,d} [66]
	4 M NaCl		0.42(19)
$\text{Ca}^{2+} + \text{L}^- + \text{H}_2\text{O} \rightleftharpoons \text{CaLH}_{-1}^0 + \text{H}^+$	1 M NaCl	-10.76(3) [64]	-10.65(5) ^c [141]
	4 M NaCl	-11.73(3)	
$2\text{Ca}^{2+} + 2\text{L}^- + 4\text{H}_2\text{O} \rightleftharpoons \text{Ca}_2\text{L}_2\text{H}_{-4}^{2-} + 4\text{H}^+$	1 M NaCl	-44.99(8) ^a [144]	
	4 M NaCl	-46.54(3)	-46.61(25)
$3\text{Ca}^{2+} + 2\text{L}^- + 3\text{H}_2\text{O} \rightleftharpoons \text{Ca}_3\text{L}_2\text{H}_{-3}^+ + 3\text{H}^+$	4 M NaCl		-31.19(19)
$3\text{Ca}^{2+} + 2\text{L}^- + 4\text{H}_2\text{O} \rightleftharpoons \text{Ca}_3\text{L}_2\text{H}_{-4}^0 + 4\text{H}^+$	1 M NaCl	-41.89(8) ^a [144]	-41.64(9) ^c [141]
	4 M NaCl	-43.80(3)	-42.98(11)

^a These constants were determined by Ca-ISE measurements

^b These constants were determined by ^{13}C NMR measurements

^c These constants were determined by the simultaneous fitting of potentiometric and polarimetric data

^d Triple standard error was not reported

To summarize the results, both Gluc^- and Hpgl^- form high stability polynuclear complexes with Ca^{2+} in alkaline solutions. The stability and composition of these complexes are very similar, although the overall speciations are not identical.

Complexation of Al^{3+} by heptagluconate ions in the pH range of 2 – 14

The impact of Al^{3+} complexation on the potentiometric titrations and polarimetric data of heptagluconate

To investigate the interactions between Hpgl^- and $\text{Al}(\text{OH})_4^-$, both potentiometric and polarimetric measurements were carried out. The first method is sensitive to any pH-dependent processes, while the second one report on the formation of complexes where the structural rearrangement of the ligand upon metal-ion binding significantly alters its optical rotation. Given the different sensitivities of the two methods, a simultaneous fit of the titration curves and optical rotations is instrumental to obtain a comprehensive picture on the speciation.

For titrations conducted at $[\text{NaOH}]_{\text{T},0} = [\text{Al}(\text{OH})_4^-]_{\text{T},0} = 0.2 \text{ M}$ (*Figure 14*, black curves), the increase of $[\text{Hpgl}^-]_{\text{T},0}$ was found to exert a considerable impact on the shape of the curves in the pH range of ≈ 10.0 – 13.3 . This shows that the formation of complexes, for which $r/q \geq 2$, (for r and q see *Equation 9* takes place mainly in the alkaline medium. Furthermore, the increase of $[\text{Al}(\text{OH})_4^-]_{\text{T},0}$ at constant $[\text{NaOH}]_{\text{T},0} = [\text{Hpgl}^-]_{\text{T},0} = 0.2 \text{ M}$ (*Figure 14*, blue curves) results in strong aluminate-dependence of the curves below $\text{pH} \approx 10$. This is indicative of the formation of multinuclear species, particularly with $q > 1$. In addition to this, when the $[\text{Al}(\text{OH})_4^-]_{\text{T},0}/[\text{Hpgl}^-]_{\text{T},0} = 2$ (*Figure 14*, curve with blue triangles), the ligand cannot keep Al(III) in the solution phase, leading to the formation of solid phase below $\text{pH} \approx 11.5$. Essentially, the presence of several inflection points in the titration curves suggests overlapping chemical equilibria, where the forming complexes undergo stepwise protonation as HCl is added to the samples.

Upon increasing $[\text{Al}(\text{OH})_4^-]_{\text{T}}$ at constant $[\text{Hpgl}^-]_{\text{T}}$ (*Figure 15*), the optical rotation of the ligand markedly increases, from $\approx 0.5^\circ$ to 2.5° , 5.5° and 11.5° at $[\text{Hpgl}^-]_{\text{T}} = 0.2, 0.4$ and 0.8 M , respectively. The ligand possesses five chiral centers, whose relative spatial arrangement (through the HCCH dihedral angles) determines $[\alpha]_{25}^{\text{D}}$ and hence α through the well-known relationship analogous to Beer's law. Therefore, the marked increase in α is a strong indicator that the conformation of Hpgl^- undergoes variation to a large extent as a token of complexation with aluminate. Furthermore, the fact that α increases steeply and then reaches a plateau (at least for $[\text{Hpgl}^-]_{\text{T}} = 0.1$ and 0.2 M) implies (almost) quantitative complex formation. Another discernible feature is that with the doubling of $[\text{Hpgl}^-]_{\text{T}}$, the maximum value of α increases to the same extent, signaling that the same species is formed, independently of the concentration of the ligand. The minimum of the optical rotation appearing upon increasing $[\text{NaOH}]_{\text{T}}$ at constant $[\text{Al}(\text{OH})_4^-]_{\text{T}}$ and $[\text{Hpgl}^-]_{\text{T}}$ indicates the formation of at least three complexes with different degrees of deprotonation.

Quantitative data analysis based on the potentiometric and polarimetric experiments

During the fitting procedure, first the values of $\log K_p$ and $\log K_a$ were fixed to the data presented in *Tables 3* and *4*, whereas the $\log K_w$ was set to -14.26 [131]. Second, the stoichiometric numbers q , r and s were systematically varied in order to minimize the FP.

To determine the stoichiometry and the corresponding stability constants of the individual complexes, the datasets of the pH-, Hpgl^- - and $\text{Al}(\text{OH})_4^-$ -dependent titrations were fitted

simultaneously, while the protonation and deprotonation constants of the ligand were fixed. (Figure 14).

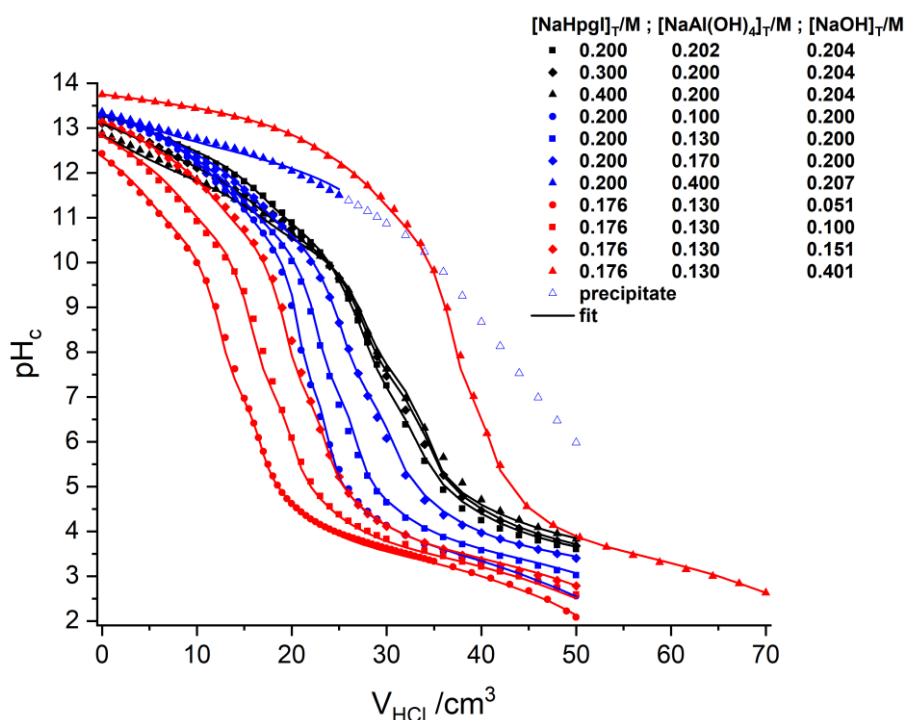


Figure 14 Measured pH values as a function of added titrant volume in solutions consisting of Hpgl^- , Al(OH)_4^- and NaOH. Experimental conditions: $t = (25 \pm 0.1)^\circ\text{C}$ and $I = 4\text{ M (NaCl)}$; the initial compositions of the samples are shown in the legend. Symbols represent the measured data, whereas lines were fitted are the results of the fits based of the speciation model discussed in the text and provided in *Table 8*.

Assuming the formation of $\text{Al(OH)}_4^-:\text{Hpgl}^- = 1:1$ stoichiometry species and its various protonated forms, *i.e.*, the $\text{Al(OH)}_5\text{Hpgl}^{3-}$, $\text{Al(OH)}_4\text{Hpgl}^{2-}$, $\text{Al(OH)}_3\text{Hpgl}^-$, Al(OH)Hpgl^+ and AlHpgl^{2+} as well as HpglH_{-1}^{2-} and HpglH , the fitting parameter, FP, was calculated to be 37.47 mV (or 0.63 pH_c units). (To improve the quality of the fit, inclusion of other hydroxido complexes of aluminum, *i.e.*, Al(OH)^{2+} , Al(OH)^+ , Al(OH)_0 , $\text{Al}_2(\text{OH})_4^{2+}$, $\text{Al}_3(\text{OH})_5^{4+}$ and $\text{Al}_{13}\text{O}_4(\text{OH})_{24}^{7+}$, were also attempted [106]. However, the assumption of these species resulted only in a minor decrease in the FP.) The second series of titrations (blue curves) consisted of solutions containing $[\text{Hpgl}^-]_T = 0.200\text{ M}$ and $[\text{Al(OH)}_4^-]_T = 0.100 - 0.400\text{ M}$, while the third set (red curves) of measurements were performed at $[\text{Hpgl}^-]_T = 0.200\text{ M}$ and $[\text{Al(OH)}_4^-]_T = 0.130\text{ M}$ with the variation of the initial concentration of sodium hydroxide from 0.050 M to 0.400 M. Upon increasing the metal:ligand ratio there was no significant change in the initial value of E_{cell} and the structure of the curves was practically identical, however a systematic shift towards lower cell potential values could be observed. Additionally, the formation of precipitation could be detected when $[\text{Al(OH)}_4^-]_T$ exceeded $[\text{Hpgl}^-]_T$. The increment of $[\text{NaOH}]_T$ yielded lower E_{cell} values with congruent curves.

Overall, the incompleteness of the fit strongly indicates that the inclusion of further species in the model is necessary. To this end, the formation of numerous polynuclear complexes was taken into account. In the light of the above results, the inclusion of polynuclear complexes for further improvement was considered. The inclusion of polynuclear species, such as the bis-complexes $\text{Al}(\text{OH})_5\text{Hpgl}^{4-}_2$ and $\text{Al}_2(\text{OH})_6\text{Hpgl}$, the dimeric species $\text{Al}_2(\text{OH})_4\text{Hpgl}^0_2$ and $\text{Al}_2(\text{OH})_5\text{Hpgl}^-_2$ and trinuclear $\text{Al}_3(\text{OH})_{10}\text{Hpgl}^{2-}$ complexes was indispensable, resulting $\text{FP} = 4.37$ mV (or 0.07 pH units).

The above speciation model was augmented by the joint fitting of polarimetric and potentiometric data. The prepared solutions and the corresponding degrees of rotation were as follows:

$$\begin{array}{ll} [\text{Hpgl}^-]_{\text{T}} = 0.175 \text{ M} / [\text{OH}^-]_{\text{T}} = 0.200 \text{ M} & \alpha = 0.4^\circ \\ [\text{Al}(\text{OH})_4^-]_{\text{T}} = 0.250 \text{ M} / [\text{OH}^-]_{\text{T}} = 0.200 \text{ M} & \alpha = 0.0^\circ \\ [\text{OH}^-]_{\text{T}} = 0.200 \text{ M} & \alpha = 0.0^\circ \end{array}$$

The first solution contained heptagluconate dissolved in sodium hydroxide to avoid lactonization. This way the ligand is mainly in the form of Hpgl^- and the extent of deprotonation, referring to one of the alcoholic OH groups, was $\approx 37\%$. The other two solutions were control measurements with components not contributing directly to the optical rotation. This approach ensured, that the observed change in the degrees of rotation was exclusively caused by the metal–ligand interaction.

Keeping the specific rotation of Hpgl^- constant, the simultaneous evaluation of polarimetric and potentiometric data with the software PSEQUAD was carried out. First the model obtained by potentiometry was fitted, considering the possible species forming in the highly alkaline region ($\text{pH} \approx 13$). Accordingly, fitting $\text{Al}(\text{OH})_4\text{Hpgl}^{2-}$, $\text{Al}(\text{OH})_5\text{Hpgl}^{3-}$ and $\text{Al}(\text{OH})_5\text{Hpgl}^{4-}_2$ resulted a systematic deviation between the calculated and measured optical rotation gradually increased with higher $[\text{Hpgl}^-]_{\text{T}}$, implying the existence of additional (polynuclear) species. Supposing the formation of $\text{Al}_3(\text{OH})_{13}\text{Hpgl}^{6-}_2$ and $\text{Al}_4(\text{OH})_{15}\text{Hpgl}^{6-}_3$, significantly improved the structure of the fitted curves, with a fitting parameter of $\text{FP} = 5.47$. This slight deterioration in the FP value can be attributed to the difference in the accuracy of the used methods, *i.e.*, they are not in the same order of magnitude. Another thing to mention is the relatively large standard deviation of the calculated $\log \beta_{043-15}$, which stems from the high correlation of the species included in the model. Nevertheless, the simultaneous fitting of the two types of data required the inclusion of these two additional complexes, which in turn greatly improved the structure of the fitted curves, thus they are excellently describing both datasets.

Table 7 Specific rotation of the individual species forming in the $\text{Al}(\text{OH})_4^- / \text{Hpgl}^-$ system. Experimental conditions: $t = (25 \pm 2)^\circ\text{C}$ and $I = 4\text{ M}$ (NaCl). Total concentrations: $[\text{Al}(\text{OH})_4^-]_{\text{T}} = 0 - 0.800\text{ M}$ and $[\text{Hpgl}^-]_{\text{T}} = 0.100 - 0.400\text{ M}$.

Species	$[\alpha]_{\text{D}} / ^\circ \cdot \text{dm}^{-1} \cdot \text{cm}^3 \cdot \text{g}^{-1}$
HpglH_1^{2-}	5.80
$\text{Al}(\text{OH})_3\text{Hpgl}^{3-}$	60.69
$\text{Al}(\text{OH})_4\text{Hpgl}^{2-}$	27.09
$\text{Al}(\text{OH})_5\text{Hpgl}_2^{4-}$	15.08
$\text{Al}_3(\text{OH})_{13}\text{Hpgl}_2^{6-}$	45.40
$\text{Al}_4(\text{OH})_{15}\text{Hpgl}_3^{6-}$	76.78

The thus obtained molar rotations of the respective species, and their formation constants are listed in *Tables 7* and *8*, respectively. The simulated titration curves and optical rotations are depicted in *Figures 14* and *15*.

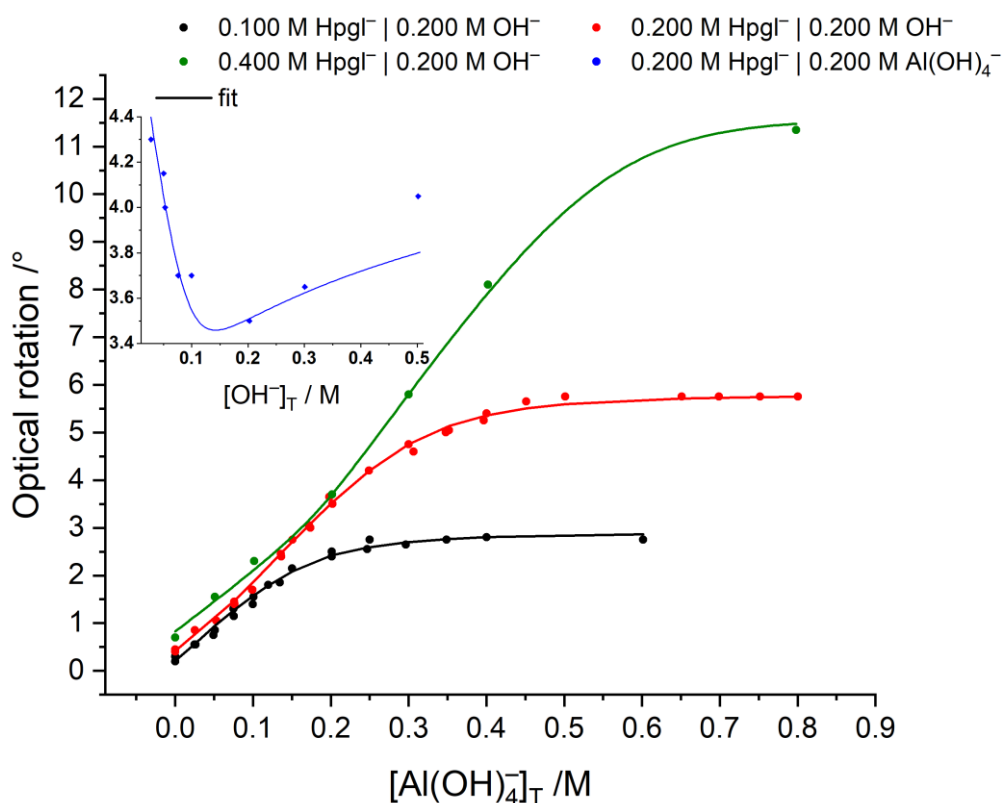


Figure 15 Optical rotation of D-heptagluconate as a function of added $[\text{Al}(\text{OH})_4^-]_{\text{T}}$ (circle) and pH (diamond). Experimental conditions: $t = (25 \pm 2)^\circ\text{C}$ and $I = 4\text{ M}$ (NaCl). Total concentrations: $[\text{Al}(\text{OH})_4^-]_{\text{T}} = 0 - 0.800\text{ M}$ and $[\text{Hpgl}^-]_{\text{T}} = 0.100 - 0.400\text{ M}$. Symbols and lines refer to the measured and calculated values, respectively.

A speciation diagram corresponding to $[\text{Al}(\text{OH})_4^-]_{\text{T}} = [\text{Hpgl}^-]_{\text{T}} = 0.2\text{ M}$ is shown in *Figure 16*. We observe distinct complexation patterns. First, the formation of AlHpgl^{2+} takes place between $\text{pH} = 2$ and 4 , and undergoes stepwise deprotonation yielding $\text{Al}(\text{OH})\text{Hpgl}^+$, $\text{Al}(\text{OH})_3\text{Hpgl}^-$, $\text{Al}(\text{OH})_4\text{Hpgl}^{2-}$ and $\text{Al}(\text{OH})_5\text{Hpgl}^{3-}$; the latter can bind a further ligand to form

$\text{Al}(\text{OH})_5\text{Hpgl}_2^{4-}$. We cannot discern the formation of the intermediate $\text{Al}(\text{OH})_2\text{Hpgl}^0$ species, however, we believe that it readily dimerizes, which manifests in the appearance of $\text{Al}_2(\text{OH})_4\text{Hpgl}_2^0$ at $\text{pH} > 3$. This species is further deprotonated yielding $\text{Al}_2(\text{OH})_5\text{Hpgl}_2^-$.

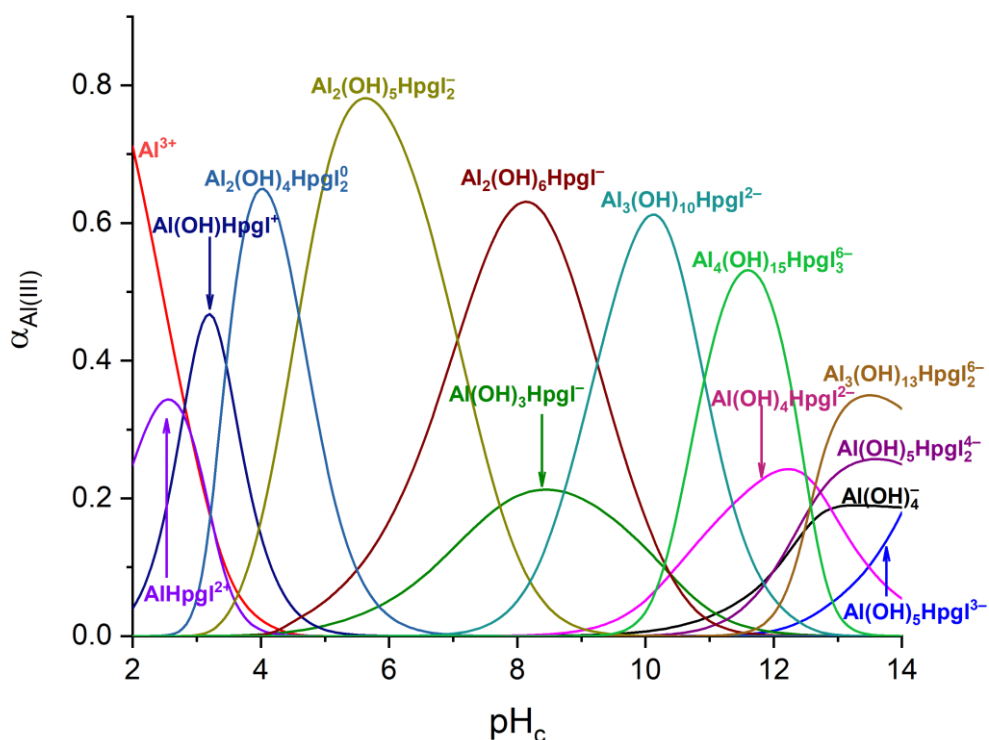


Figure 16 Speciation diagrams as a function of pH with regard to Al(III). The calculations were performed using the stability constants provided in *Table 8*, corresponding to $t = 25$ °C and $I = 4$ M (NaCl). Total concentrations: $[\text{Al}(\text{OH})_4^-]_{\text{T}} = [\text{Hpgl}^-]_{\text{T}} = 0.200$ M.

Furthermore, the formation of $\text{Al}_2(\text{OH})_6\text{Hpgl}^-$ and $\text{Al}_3(\text{OH})_{10}\text{Hpgl}^{2-}$ can be interpreted as the abstraction of one or two aluminate ions by $\text{Al}(\text{OH})_2\text{Hpgl}^0$. Two other polynuclear species appears above $\text{pH} \approx 8$, namely, the $\text{Al}_4(\text{OH})_{15}\text{Hpgl}_3^{6-}$ and $\text{Al}_3(\text{OH})_{13}\text{Hpgl}_2^{6-}$ ones. The tetranuclear $\text{Al}_4(\text{OH})_{15}\text{Hpgl}_3^{6-}$ complex may be formed via the association of $\text{Al}_3(\text{OH})_{10}\text{Hpgl}^{2-}$ and $\text{Al}(\text{OH})_5\text{Hpgl}_2^{4-}$, while the appearance of $\text{Al}_3(\text{OH})_{13}\text{Hpgl}_2^{6-}$ may be the result of the aggregation of $\text{Al}(\text{OH})_4\text{Hpgl}^{2-}$, $\text{Al}(\text{OH})_5\text{Hpgl}^{2-}$ and $\text{Al}(\text{OH})_4^-$. Additionally, this trinuclear species is the one that gives rise to the marked increase in the optical rotation under hyperalkaline conditions ($\text{pH} \geq 13$); see the speciation diagram in *Figure 17*.

Given the complexity of the system and hence the difficulty to pinpoint and properly quantify all individual equilibrium processes, one may question the reliability of the compositions of these complexes. Nevertheless, their inclusion in the model is necessary to give an appropriate proper description for the experimental data and their formation indicates that at high concentrations, simple mononuclear species tend to aggregate.

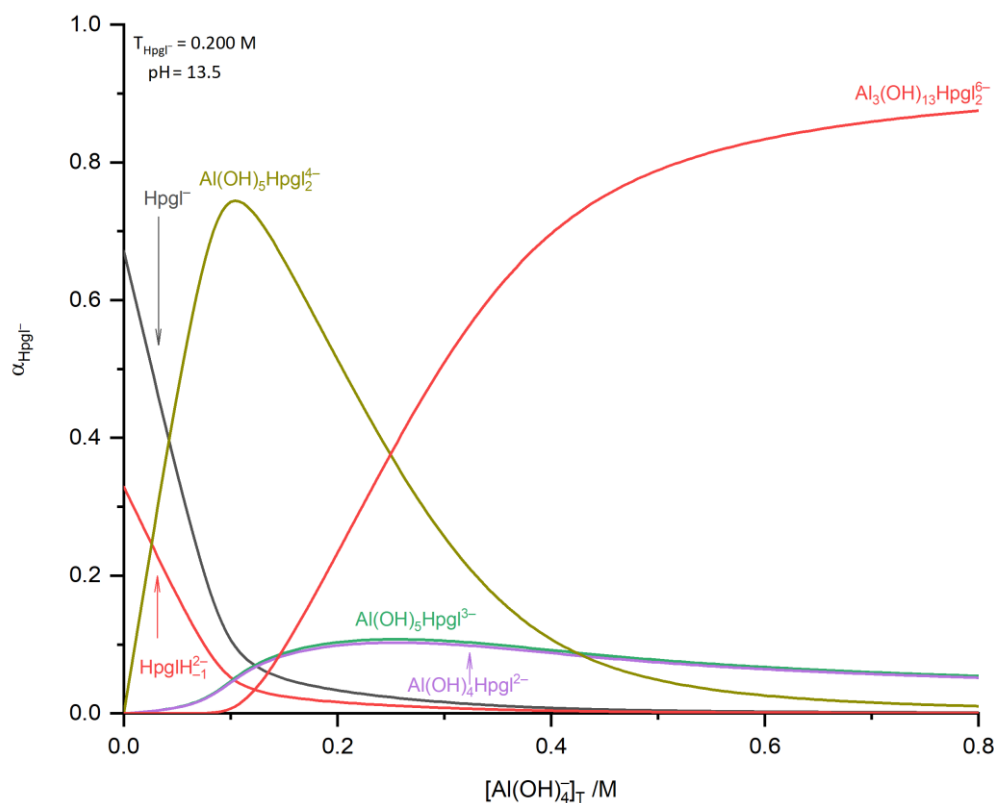


Figure 17 Speciation diagrams as a function of $[\text{Al}(\text{OH})_4^-]_{\text{T}}$ in regard to Hpgl^- . The calculations were on the basis of stability constants provided in *Table 8.*, corresponding to $t = (25 \pm 0.1)^\circ\text{C}$ and $I = 4\text{ M}$ (NaCl). Total concentrations: $[\text{Al}(\text{OH})_4^-]_{\text{T}} = 0 - 0.800\text{ M}$ and $[\text{Hpgl}^-]_{\text{T}} = 0.200\text{ M}$.

The plethora of solution species found in this system is rather unexpected, based on previous findings for Gluc^- [123–126,145], *i.e.*, the exclusive formation of mononuclear species. We would like to emphasize, however, that those previous measurements were conducted in the millimolar concentration range. (Albeit measurements at $\text{pH} > 12$ were undertaken at $[\text{Al}(\text{OH})_4^-]_{\text{T},0} \approx [\text{Gluc}^-]_{\text{T},0} \approx 0.1\text{ M}$ [126], the authors did not study the concentration-dependence of the titrations curves, which is essential to detect polynuclear complexes). In such concentration ranges, the effect of polynuclear complexes is significantly lower, therefore harder to fit them during calculation. Setting $[\text{Al}(\text{OH})_4^-]_{\text{T}}$ to 0.002 M and $[\text{Hpgl}^-]_{\text{T}}$ to 0.004 M , the complexation equilibria simplifies to that proposed previously (*Figure 18*), however $\text{Al}(\text{OH})_2\text{Hpgl}^0$ remains interchangeable with its dimer.

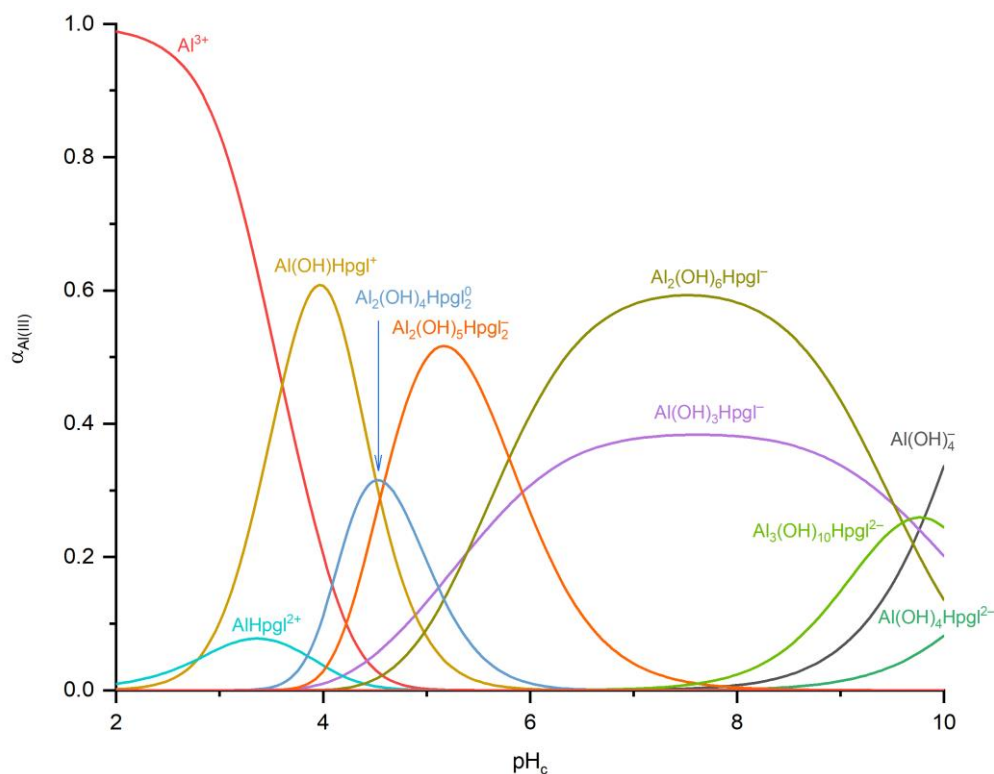


Figure 18 Speciation diagrams as a function of pH with regard to Al(III). The calculations were performed using the stability constants provided in *Table 8*, corresponding to $t = 25\text{ }^{\circ}\text{C}$ and $I = 4\text{ M}$ (NaCl). Total concentrations: $[\text{Al}(\text{OH})_4^-]_{\text{T}} = 0.002\text{ M}$, $[\text{Hpgl}^-]_{\text{T}} = 0.004\text{ M}$.

As for the analogous gluconate complexes, we find that the stability constants are in fair agreement with our data (*Table 8*); the deviations can be attributed to the much lower ionic strength (0.1–0.2 M) applied in Refs. [123–126,145]. (Since the primary species was Al^{3+} in these references, we converted them using the formation constant of $\text{Al}(\text{OH})_4^-$, taken from Ref. [106].) Based on these similarities between the two ligands, we propose that multinuclear species are likely to be formed with Gluc^- in concentrated solutions. This assumption is supported by the fact that the $\text{Ca}_3\text{L}_2(\text{OH})_4^0$ species dominates the complexation equilibria for both ligands, in concentrated solutions of CaCl_2 [64,131,97].

Table 8 Stability constants, $\log \beta_{qsr}$, determined for the various reactions taking place in the $\text{Al(OH)}_4^- / \text{HpgI}^-$ system. Experimental conditions: $t = 25^\circ\text{C}$, $I = 4\text{ M}$ (NaCl). In parentheses, the triple standard error is given. For analogous gluconate complexes, literature data are also provided.

Reaction	$\log \beta_{qsr}$	Method ^a	Ref ^b
$\text{H}_2\text{O} \rightleftharpoons \text{H}^+ + \text{OH}^-$	-14.26 ^c	H ₂ /Pt	[8]
$\text{HpgI}^- + \text{H}^+ \rightleftharpoons \text{HpgIH} + \text{H}_2\text{O}$	3.64(1) 3.38(2) ^c 2.49(2) ^c	GLE / POL GLE GLE / ¹ H NMR	p. w. [22] [18]
$\text{Gluc}^- + \text{H}^+ \rightleftharpoons \text{HpgIH} + \text{H}_2\text{O}$	3.73(5) ^c	GLE	[23]
$\text{HpgI}^- \rightleftharpoons \text{HpgIH}_{-1}^{2-} + \text{H}^+$	-13.81(1) -13.41(2) ^c	H ₂ /Pt / POL H ₂ /Pt / POL	p. w. [18]
$\text{Gluc}^- \rightleftharpoons \text{GlucH}_{-1}^{2-} + \text{H}^+$	-14.08(3) ^c -13.90(3) ^c	H ₂ /Pt ¹³ C NMR	[8] [8]
$\text{Al(OH)}_4^- + 4\text{H}^+ \rightleftharpoons \text{Al}^{3+} + 4\text{H}_2\text{O}$	22.81(19) 23.23 ^d 23.40 ^e	H ₂ /Pt / POL	p. w. [24] [12]
$\text{Al(OH)}_4^- + \text{HpgI}^- + 4\text{H}^+ \rightleftharpoons \text{AlHpgI}^{2+} + 4\text{H}_2\text{O}$	24.85(29)	H ₂ /Pt / POL	p. w.
$\text{Al(OH)}_4^- + \text{Gluc}^- + 4\text{H}^+ \rightleftharpoons \text{AlGluc}^{2+} + 4\text{H}_2\text{O}$	25.21 ^{c,d} 25.24(6) ^{c,d} 25.78(3) ^{c,e}	GLE GLE GLE	[9] [10] [12]
$\text{Al(OH)}_4^- + \text{HpgI}^- + 3\text{H}^+ \rightleftharpoons \text{Al(OH)HpgI}^+ + 3\text{H}_2\text{O}$	22.06(13)	H ₂ /Pt / POL	p. w.
$\text{Al(OH)}_4^- + \text{Gluc}^- + 3\text{H}^+ \rightleftharpoons \text{Al(OH)Gluc}^+ + 3\text{H}_2\text{O}$	22.34 ^{c,d} 22.35(12) ^{c,d} 22.39(6) ^{c,d} 21.91(6) ^{c,e}	GLE GLE GLE GLE	[9] [10] [11] [12]
$\text{Al(OH)}_4^- + \text{HpgI}^- + \text{H}^+ \rightleftharpoons \text{Al(OH)}_3\text{HpgI}^- + \text{H}_2\text{O}$	12.28(26)	H ₂ /Pt / POL	p. w.
$\text{Al(OH)}_4^- + \text{Gluc}^- + \text{H}^+ \rightleftharpoons \text{Al(OH)}_3\text{Gluc}^- + \text{H}_2\text{O}$	13.05 ^{c,d} 13.05(24) ^{c,d} 12.52(6) ^{c,d} 11.41(3) ^{c,e}	GLE GLE GLE GLE	[9] [10] [11] [12]
$\text{Al(OH)}_4^- + \text{HpgI}^- \rightleftharpoons \text{Al(OH)}_4\text{HpgI}^{2-}$	1.89(17)	H ₂ /Pt / POL	p. w.
$\text{Al(OH)}_4^- + \text{Gluc}^- \rightleftharpoons \text{Al(OH)}_4\text{Gluc}^{2-}$	2.4(1.2) ^c 2.2(0.6) ^c	¹ H NMR POL	[13] [13]
$\text{Al(OH)}_4^- + \text{HpgI}^- + \text{H}_2\text{O} \rightleftharpoons \text{Al(OH)}_5\text{HpgI}^{3-} + \text{H}^+$	-11.59(29)	H ₂ /Pt / POL	p. w.
$\text{Al(OH)}_4^- + 2\text{HpgI}^- + \text{H}_2\text{O} \rightleftharpoons \text{Al(OH)}_5\text{HpgI}_2^{4-} + \text{H}^+$	-9.02(15)	H ₂ /Pt / POL	p. w.
$2\text{Al(OH)}_4^- + \text{HpgI}^- + 2\text{H}^+ \rightleftharpoons \text{Al}_2(\text{OH})_6\text{HpgI}^- + 2\text{H}_2\text{O}$	24.98(21)	H ₂ /Pt / POL	p. w.
$2\text{Al(OH)}_4^- + 2\text{HpgI}^- + 4\text{H}^+ \rightleftharpoons \text{Al}_2(\text{OH})_4\text{HpgI}_2^0 + 4\text{H}_2\text{O}$	37.99(21)	H ₂ /Pt / POL	p. w.
$2\text{Al(OH)}_4^- + 2\text{HpgI}^- + 3\text{H}^+ \rightleftharpoons \text{Al}_2(\text{OH})_5\text{HpgI}_2^- + 3\text{H}_2\text{O}$	33.41(20)	H ₂ /Pt / POL	p. w.
$3\text{Al(OH)}_4^- + \text{HpgI}^- + 2\text{H}^+ \rightleftharpoons \text{Al}_3(\text{OH})_{10}\text{HpgI}^{2-} + 2\text{H}_2\text{O}$	28.23(26)	H ₂ /Pt / POL	p. w.
$3\text{Al(OH)}_4^- + 2\text{HpgI}^- + \text{H}_2\text{O} \rightleftharpoons \text{Al}_3(\text{OH})_{13}\text{HpgI}_2^{6-} + \text{H}^+$	-6.52(26)	H ₂ /Pt / POL	p. w.
$4\text{Al(OH)}_4^- + 3\text{HpgI}^- + \text{H}^+ \rightleftharpoons \text{Al}_4(\text{OH})_{15}\text{HpgI}_3^{6-} + \text{H}_2\text{O}$	21.74(39)	H ₂ /Pt / POL	p. w.

^a H₂/Pt, GLE: potentiometry applying a platinum H₂ or glass electrode, POL: polarimetry, NMR: nuclear (¹H or ¹³C) magnetic resonance spectroscopy.

^b In the present work, the constants were determined via the simultaneous fit of potentiometric and polarimetric data.

^c The stability products correspond to $I = 0.1\text{ M KNO}_3$ [9], 0.1 M NaCl [10], 0.1 M NaNO_3 [11,23], 0.2 M KCl [12], 1 M NaCl [13,18] and 4 M NaCl [8,24].

^d The stability products of the analogous gluconate complexes were converted from the literature data [9–11] using the formation constant of Al(OH)_4^- ($I = 0.1\text{ M}$) reported in Ref. [24].

^e The stability products of the analogous gluconate complexes were converted from the literature data [12] using the formation constant of Al(OH)_4^- ($I = 0.2\text{ M}$) reported in Ref. [12].

Model validation and the possible structure of the $\text{Al}_2(\text{OH})_6\text{Hpgl}^-$ complex

ESI-MS measurements and the structural iteration of $\text{Al}_2(\text{OH})_6\text{Hpgl}^-$ complex

We performed ESI-MS measurements to gain further experimental support for the chemical speciation proposed in the previous section. The negative ion-mode spectrum shown in *Figure 19* refers to a solution containing $[\text{Al}(\text{OH})_4^-]_{\text{T}} = 0.001 \text{ M}$ and $[\text{Hpgl}^-]_{\text{T}} = 0.001 \text{ M}$ at $\text{pH} = 7$. To estimate which species is formed under the conditions of the MS experiments, we calculated the speciation using the data in *Table 8*. Accordingly, $\text{Al}_2(\text{OH})_6\text{Hpgl}^-$ dominates the pH range 6–8 (the degree of its formation is $\approx 40\%$ relative to $[\text{Hpgl}^-]_{\text{T}}$).

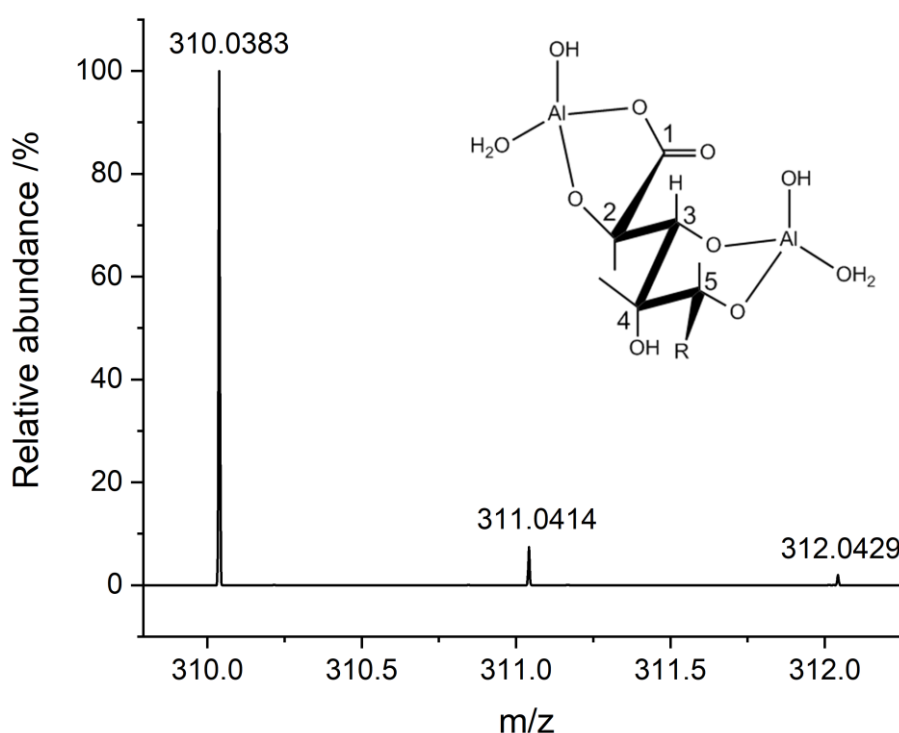


Figure 19 ESI-MS spectrum of a solution containing $[\text{Al}(\text{OH})_4^-]_{\text{T}} = [\text{Hpgl}^-]_{\text{T}} = 0.001 \text{ M}$ at $\text{pH} = 7$. The spectrum was recorded in negative ion mode. The peak at 310.0383 m/z corresponds to the $\text{Al}_2(\text{OH})_6\text{Hpgl}^-$ species, predominant in this solution. The inset shows the proposed structure of this species, where 'R' represents the C(6)HOH-C(7)H₂OH moiety and the hydrogens are omitted for clarity.

The experimental mass spectrum matches perfectly with a species having a chemical formula of $\text{Al}_2\text{C}_7\text{H}_{12}\text{O}_{10}^-$, that is, $\text{Al}_2(\text{OH})_2\text{HpglH}_3^-$, where HpglH_3^{4-} refers to the threefold deprotonated ligand. This formula corresponds to the $\text{Al}_2(\text{OH})_6\text{Hpgl}^-$ complex, supporting the validity of the proposed model. Since Al^{3+} is a negligible species as compared to $\text{Al}(\text{OH})_4^-$ in ligand-free solutions at this pH [146], the complex is likely to be formed *via* the binding of aluminates. That is, one $\text{Al}(\text{OH})_4^-$ ion is coordinated by the COO^- and the adjacent OH group

of the ligand, the other is bound by two other OH functionalities (for instance, the C3(OH) and C5(OH) ones). The binding is followed by the dissociation of an OH⁻ ion due to COO⁻ coordination and by three condensation steps between the OH-s of Hpgl⁻ and Al(OH)₄⁻, releasing three water molecules. Simultaneously, one OH⁻ ion attached to each Al³⁺ ion is being protonated yielding H₂O. These two coordinated water molecules are likely to dissociate from the complex during the evaporation process. The possible structure of the complex is depicted in the inset of *Figure 19*. Here we assume the geometry of the metal center to be tetrahedral.

Freezing Point Depression (FPD) measurements

Additional experimental data were collected to reinforce the obtained speciation model. This simple method proved to be handy to support the results obtained by other experimental methods [64]. Freezing point depression, being a colligative property, is proportional to the total concentration of the ions in relatively dilute solutions:

$$\Delta T_{f,\text{theo}} = K_f \cdot \sum_{i=1}^n [X_i]_T, \quad (23)$$

where K_f is the cryoscopic constant for water (which is taken as 1.86 °C·M⁻¹, and the term $[X_i]_T$ refers to the total concentration of discrete ions in the solution. If the number of solute particles decreases, *e.g.* complex formation takes place, the freezing point depression also decreases. The measured value corresponds to the sum of equilibrium concentrations:

$$\Delta T_{f,\text{meas}} = K_f \cdot \sum_{i=1}^n [X_i]. \quad (24)$$

In order to quantify the difference between the theoretical (*i.e.*, assuming full dissociation) and the observed values, the following equation could be used:

$$\Delta \Delta T_f = T_{f,\text{theo}} - T_{f,\text{meas}} = K_f \cdot \sum_{i=1}^n ([X_i]_T - [X_i]) \quad (25)$$

where $\Delta \Delta T_f$ refers to the extent of particle decrease, therefore to the extent of association. This parameter and the measured FPD values for solutions with various NaAl(OH)₄, NaHpgl, NaOH and NaCl are presented in *Table 9*. Examining the first seven solutions, which are exclusively strong electrolytes, the value $\Delta T_{f,\text{meas}}$ agrees well with those calculated assuming the full dissociation of the species ($\Delta T_{f,\text{theo}}$). In these solutions the $\Delta \Delta T_f$ value refers to the uncertainty of the method and can be taken as 0.14°C. In solutions containing Al(OH)₄⁻, Hpgl⁻ and OH⁻, starting from composition *No. 8*, the parameter $\Delta \Delta T_f$ is at least two times higher than the uncertainty of the method. Since this parameter is proportional to the magnitude of association, its increase indicates the enhancement of complex formation. Regarding the first Al(OH)₄⁻-dependent solution series (*No. 9–13*), the value of $\Delta \Delta T_f$ increases until 3:2 metal:ligand ratio, where the fraction of Al₃(OH)₁₃Hpgl₆²⁻ reaches its plateau value (*Figure 17*).

hence the change of $\Delta\Delta T_f$ could be mainly credited to the formation of $Al_3(OH)_{13}Hpgl^{6-}_2$ species.

In order to attest the performance of the suggested model, the equilibrium concentration of each species (for a given sample) were calculated on the basis of compositions and stability constants presented in *Table 8*, with the aid of PSEQUAD software. Using these concentrations, the expected freezing point depression values ($\Delta T_{f,calc}$ presented in *Table 9*) were obtained and compared with the measured ones. Although the ionic strength and the temperature of the solutions used for the FPD experiments differed substantially from those which were evaluated to deduce the formation constants, the observed and predicted values agree reasonably well.

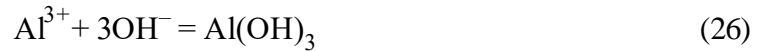
Table 9 Freezing point depression measurements for the system containing various amounts of $NaAl(OH)_4$, $NaHpgl$, $NaOH$ or $NaCl$. $\Delta\Delta T_f$ refers to the difference between the theoretical ($\Delta T_{f,theo}$, calculated by assuming complete dissociation of each compound) and measured ($\Delta T_{f,meas}$) FPD. The term $\Delta\Delta T_f$ is the extent of particle decrease. The calculated FPD values are listed in column $\Delta T_{f,calc}$.

#	$[NaAl(OH)_4]_T$ / M	$[NaHpgl]_T$ / M	$[NaOH]_T$ / M	$[NaCl]_T$ / M	$\Delta T_{f,theo}$ / °C	$\Delta T_{f,meas}$ / °C	$\Delta\Delta T_f$ / °C	$\Delta T_{f,calc}$ / °C
1	0.200	0	0.205	0	1.50	1.49	0.02	1.51
2	0	0.090	0	0	0.33	0.33	0.01	0.33
3	0	0.175	0	0	0.65	0.61	0.04	0.65
4	0	0.174	0	0	0.65	0.62	0.03	0.65
5	0	0.271	0	0	1.01	0.93	0.08	1.01
6	0	0.445	0	0	1.66	1.51	0.14	1.66
7	0	0	0.197	0	0.73	0.72	0.01	0.73
8	0	0.175	0.197	0	1.38	1.11	0.28	1.29
9	0.101	0.178	0.202	0	1.79	0.94	0.85	1.35
10	0.200	0.175	0.205	0	2.16	1.19	0.97	1.60
11	0.401	0.175	0.201	0.209	3.67	2.56	1.11	2.95
12	0.600	0.175	0.200	0.414	5.16	3.89	1.28	4.41
13	0.800	0.175	0.205	0.615	6.68	5.82	0.85	5.91

Solubility simulations: the effect of NaHpgl on the solubility of $Al(OH)_3(s)$

The effect caused by $NaHpgl$ on the solubility of gibbsite was estimated by calculating the solubility curves of $Al(OH)_3$ for every initial composition used during potentiometry and polarimetry. Our working hypothesis was as follows: if no complexation occurs between aluminum and $Hpgl^-$, gibbsite may precipitate from the solution. The stability constants used in the calculations are listed in *Table 8*. The solubility product of $Al(OH)_3$ was assessed using the value ($\log K^*_{sp,Al(OH)_3} = 9.49$) found in the literature obtained at $5.0 \text{ mol}\cdot\text{kg}^{-1}$ ($\approx 5.74 \text{ M}$ [147]) $NaCl$ [106]; therefore the range, where gibbsite is expected to precipitate is only approximate.

The pH ranged from 2 to 14 and the individual solution compositions were listed in the legend of *Figure 20*. Given the following reaction, the solubility product of gibbsite can be calculated as follows:



$$K_{\text{sp}}^* = \frac{[\text{Al}^{3+}][\text{H}^+]^{-3}}{c^{-2}} \quad (27)$$

Increasing the metal-to-ligand ratios, a considerable shift of the solubility curves can be observed. Surprisingly, in the pH range where gibbsite was predicted to form, no precipitate was observed. This phenomenon could be explained by the findings of *Rossiter et al.*, that is, sodium gluconate dramatically inhibits the formation of $\text{Al}(\text{OH})_3(\text{s})$ precipitation by blocking the active crystal growth surfaces of gibbsite seeds [148]. These conclusions were further confirmed by *Beckham et al.*, who revealed that the interaction between D-gluconate and gibbsite is solely a physical adsorption process, which can be properly described using a modified Langmuir isotherm. Gluconate is reported to have a strong selectivity for flaws created during the formation of crystal growth sites, thus able to block 50% more of the actually covered sites [149].

In accordance with the publications above, the formation of $\text{Al}_2(\text{OH})_6\text{Hpgl}^-$, $\text{Al}(\text{OH})_3\text{Hpgl}^-$ and $\text{Al}_3(\text{OH})_{10}\text{Hpgl}^{2-}$ particles is accompanied by a large excess of free ligand in the pH range from 6 to 11, thus implying the stabilizing role of the ligand in this domain. In conclusion, the lack of precipitate is due to the formation of ligand stabilized hydroxides.

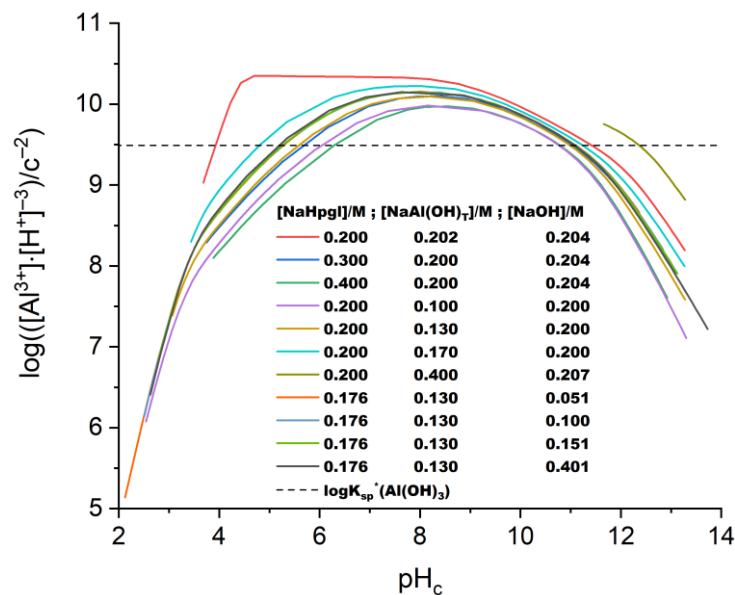


Figure 20 Solubility of $\text{Al}(\text{OH})_3$ regarding to pH. The calculations were performed on the basis of stability constants corresponding to $t = 25^\circ\text{C}$ and $I = 4\text{ M}$ (NaCl). The dashed line refers to the $\log K_{\text{sp},\text{Al}(\text{OH})_3}^*$ value, above which $\text{Al}(\text{OH})_3(\text{s})$ is expected to precipitate.

NMR study on the structural aspects of the complexation reactions and the possible metal binding sites

Complexation of Al^{3+} in the acidic region

To gain structural insight into the complex formation, a series of ^1H and ^{13}C NMR spectra as a function of pH and $[\text{Al}(\text{OH})_4^-]_{\text{T}}$ were recorded. Before any analysis concerning complexation, we have to note that for the pH-dependent ^1H and ^{13}C NMR spectra, as well as the $[\text{Al}(\text{OH})_4^-]_{\text{T}}$ -dependent ^1H and ^{13}C NMR spectra at pH = 4 (Figure 21, 22, 23 and 24, respectively), there are several peaks marked as 'L'. These signals are most likely to belong to the lactone form of heptagluconic acid. The formation of such ring compounds is common for hydroxycarboxylic acids, such as gluconic acid [63]. Due to their rigid structure, the lactones are in general do not participate in metal complexation; hence, we focus solely on the ligand peaks in the following discussion.

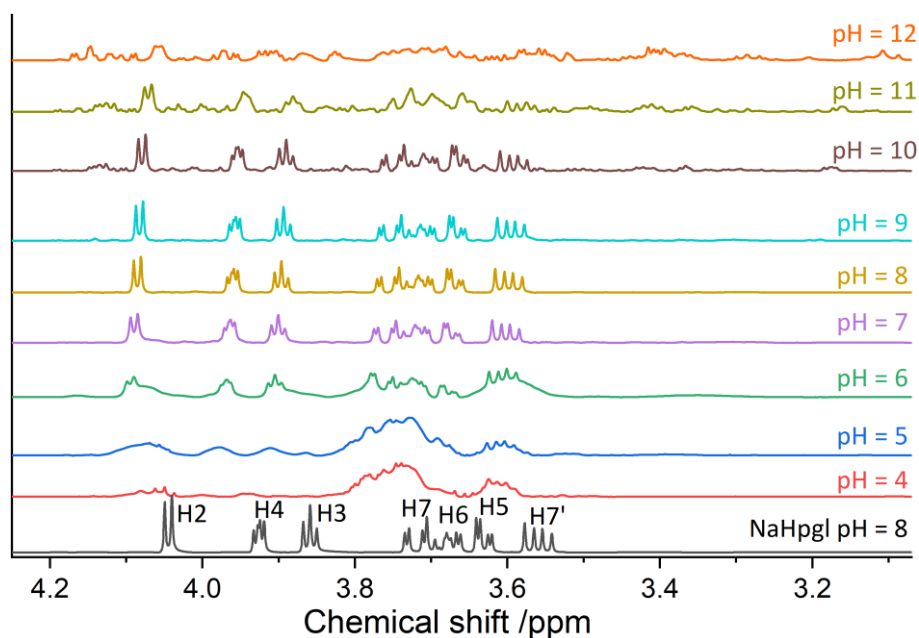


Figure 21 ^1H NMR spectra of solutions containing $[\text{Al}(\text{OH})_4^-]_{\text{T}} = [\text{HpgI}^-]_{\text{T}} = 0.200 \text{ M}$ as a function of the nominal pH at $(25 \pm 1) \text{ }^\circ\text{C}$.

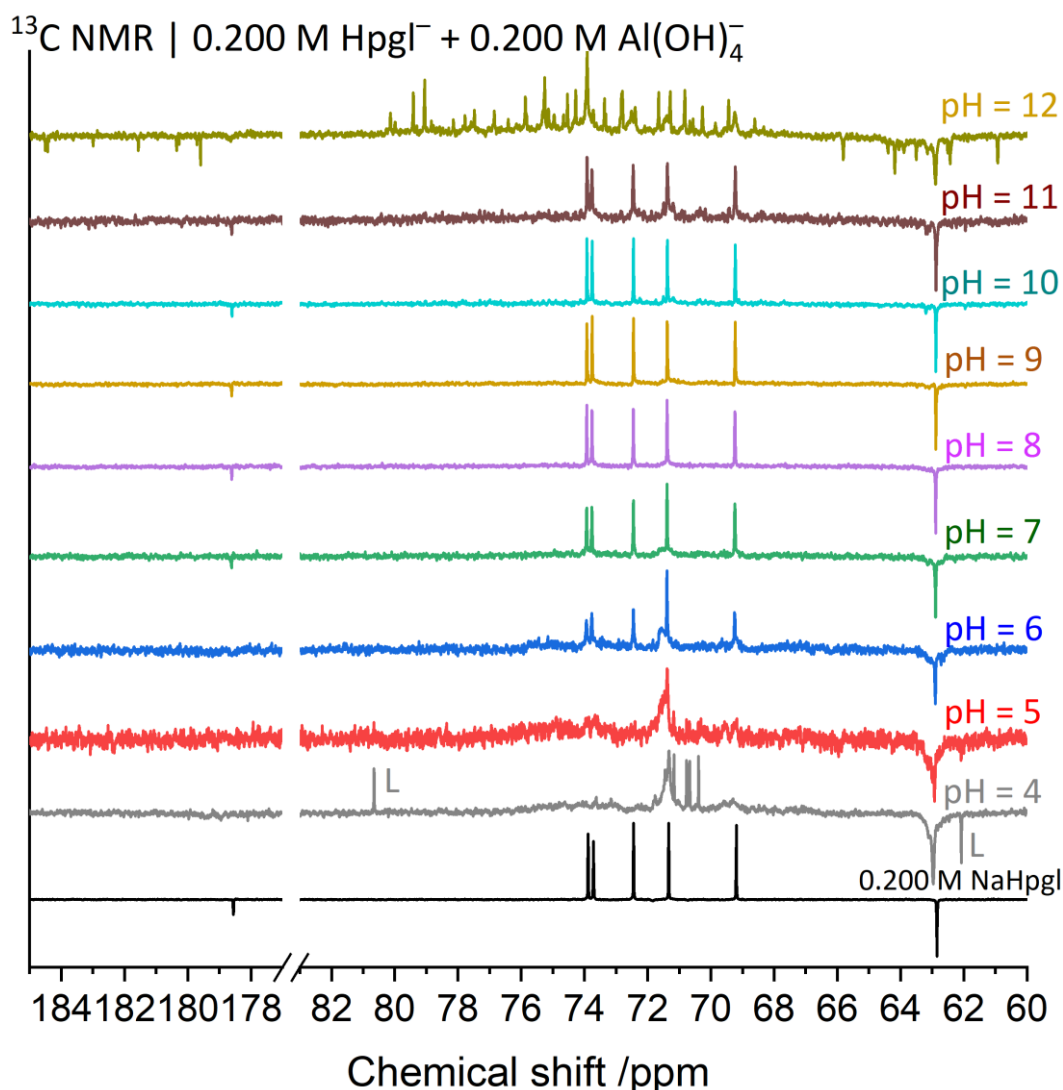


Figure 22 ^{13}C NMR spectra of solutions containing $[\text{Al}(\text{OH})_4]_{\text{T}} = [\text{HpgI}]_{\text{T}} = 0.200 \text{ M}$ as a function of the nominal pH at $(25 \pm 1) \text{ }^\circ\text{C}$.

For the solution with $[\text{Al}(\text{OH})_4]_{\text{T}} = [\text{HpgI}]_{\text{T}} = 0.200 \text{ M}$ and at $\text{pH} = 4$, the dominant species is the $\text{Al}_2(\text{OH})_4\text{HpgI}_2^0$ dimer; see the speciation diagram of heptagluconate in *Figure 16*. The ^1H spectrum (*Figure 21*) shows that the chemical exchange between the free and complexed ligand is rather slow, giving rise to broad and thus not well-resolved signals. This is in line with the $[\text{Al}(\text{OH})_4]_{\text{T}}$ -dependent spectra at the same pH (*Figure 23*); that is, the signal half-widths increase gradually, particularly the C2H(OH), C3H(OH) and the C4H(OH) ones. This indicates their vital roles as coordination sites. As for the ^{13}C NMR spectra (*Figure 24*), the drop in the relative intensity of the C1–C5 signals also suggests their participation in the metal-ion binding.

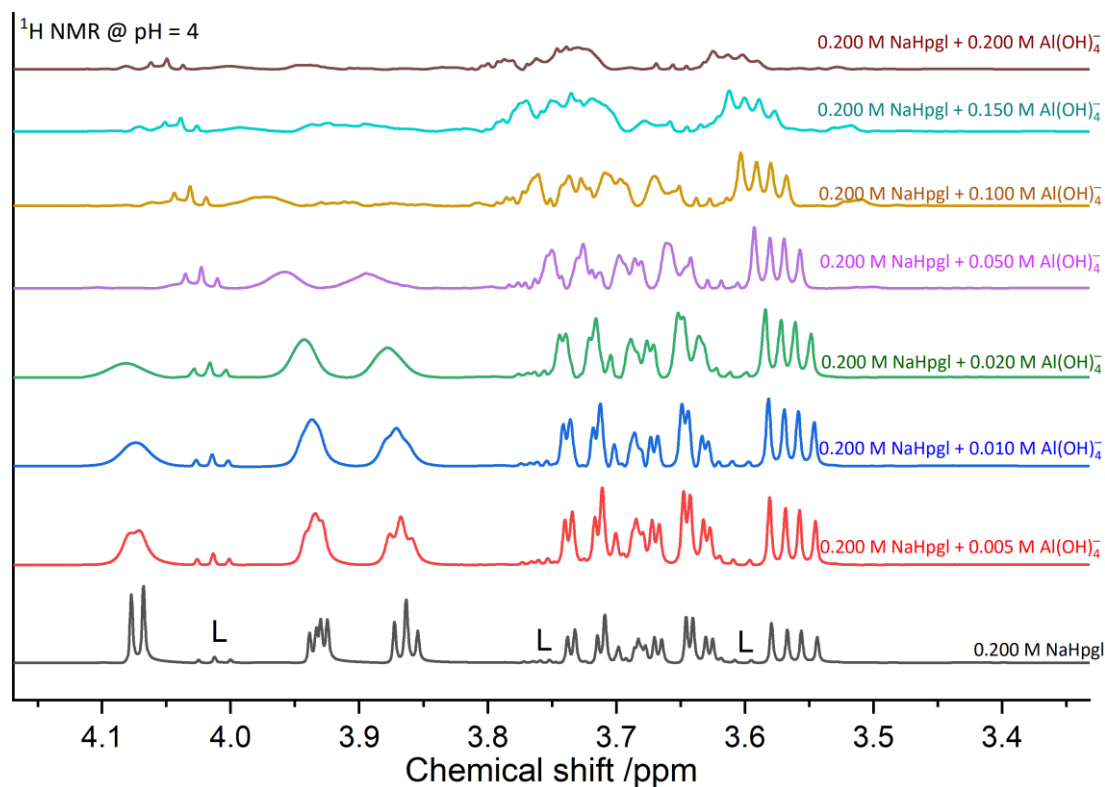


Figure 23 ¹H NMR spectra of solutions containing $[\text{HpgI}]_{\text{T}} = 0.200 \text{ M}$ as a function of $[\text{Al}(\text{OH})_4]_{\text{T}}$ at pH = 4 and $(25 \pm 1)^\circ\text{C}$

Furthermore, the slow exchange is indicative of strong metal-ligand interactions. We can elucidate this feature by the high charge density of the metal, resulting in strong coordinative bonds between Al^{3+} and the COO^- as well as the OH groups. In turn, the coordination of Al^{3+} leads to the weakening of the O–H bonds. In turn, the acidity of the OH function decreases, that is, the deprotonation of the OH group can occur at much lower pH than in the metal-free system ($\text{pK} = 13.8$, *Table 8*). This is the well-known metal-ion-induced ligand deprotonation and its driving force is the formation of stable chelate rings with the Al^{3+} ion being bound to the COO^- and (at least) one alcoholate moiety.

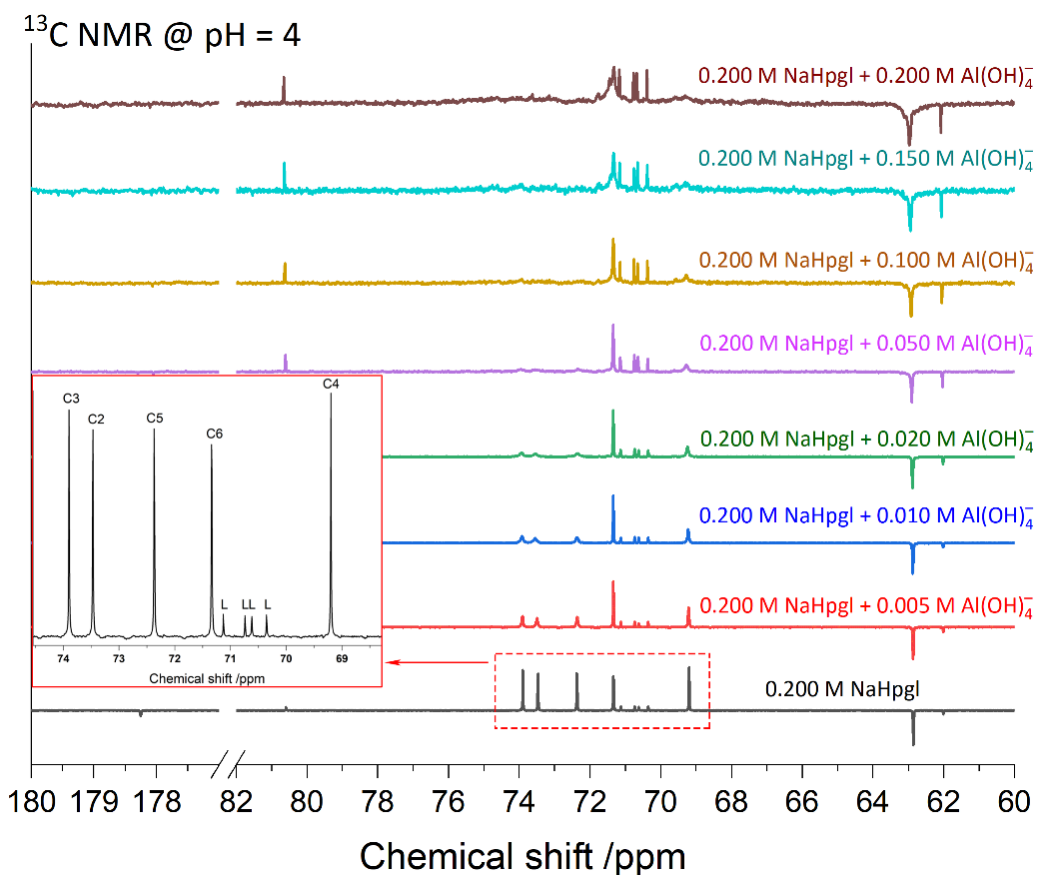


Figure 24 ¹³C NMR spectra of solutions containing [Hpgl]⁻_T = 0.200 M as a function of [Al(OH)₄⁻]_T at pH = 4 and (25 ± 1) °C. The assignment of the peaks is depicted in the inset. Due to the decreasing relative intensity of the C1 to C5 peaks, the lactone peaks become comparable to them.

This is further supported by the fact that the first deprotonation step referring to the reaction:



with a pK of 3.6 ($\log\beta_{0114} - \log\beta_{0113}$, *Table 8*), being much lower than that of the Al³⁺ aquation (pK = 5.5 at I = 3 M NaCl [106]). This indicates that the first deprotonation step indeed occurs on the ligand rather than on a metal-coordinated water molecule, similarly to the Al(III)/Gluc⁻ system [125]. Whether the second deprotonation takes place on the ligand or on a water molecule yielding the putative Al(OH)₂Hpgl⁰ species (and its dimer), however, is not deductible from the NMR spectra.

Complexation of Al³⁺ in the close-to-neutral region

Increasing the pH further up to 9, the recovery of the spectrum of the plain ligand can be observed (*Figures 21 and 22*). This becomes obvious when we compare the spectrum at pH = 8 with the one of Hpgl⁻ at the same pH (*Figure 21*). Moreover, increasing [Al(OH)₄⁻]_T at pH = 8

results in only a minor downfield shift of the ^1H peaks (*Figure 25*) and no noticeable variations in the ^{13}C spectra (*Figure 26*). Consequently, the complexes formed in the pH range of 6–9 are in fast exchange with the free ligand. The acceleration of the chemical exchange upon the pH increase implies the weakening of metal-ligand interactions. A possible (albeit somewhat speculative) explanation for this striking feature is that further deprotonation takes place on coordinated water molecules. The strong bond between Al^{3+} and OH^- ions leads to the apparent destabilization of those between Al^{3+} and Hpgl^- . This scenario seems to be valid for all species formed in this range, particularly for $\text{Al}_2(\text{OH})_6\text{Hpgl}^-$ being the predominant one (see the distribution diagram in *Figure 27*). Furthermore, $n_{\text{OH}} : n_{\text{Al}} \geq 3$ holds for all complex compositions, suggesting the formation of $\text{Al}(\text{OH})_3$ moieties being loosely bound to the ligand through the COO^- group.

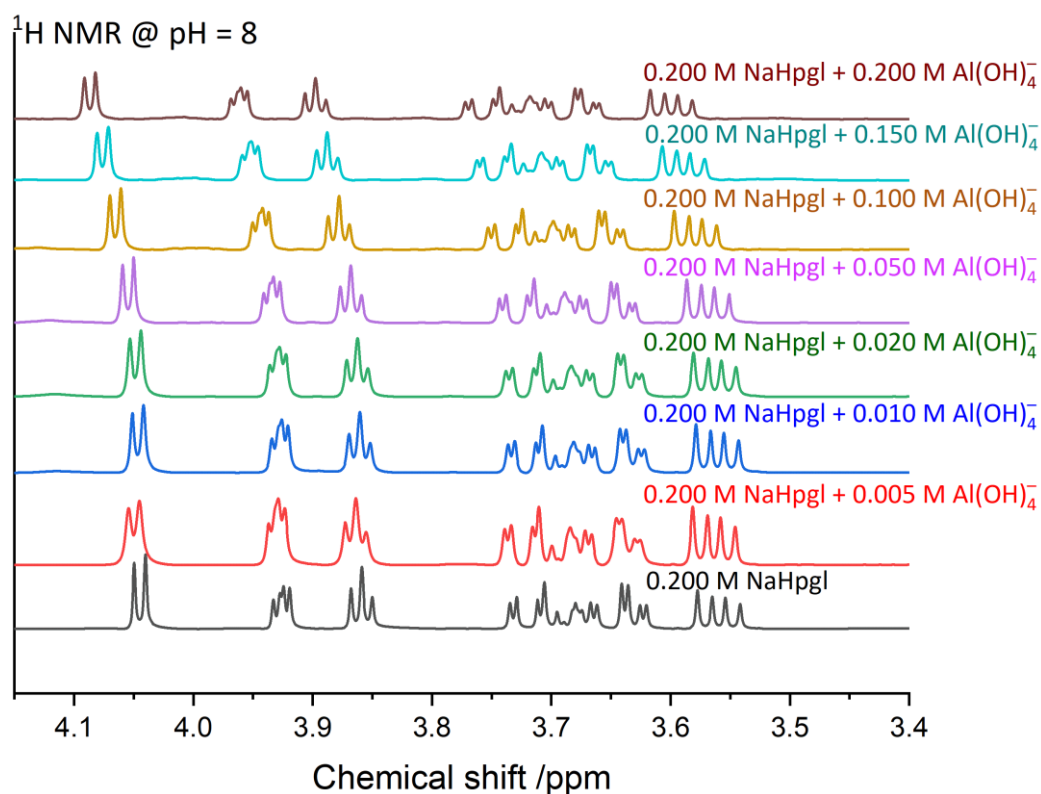


Figure 25 ^1H NMR spectra of solutions containing $[\text{Hpgl}^-]_{\text{T}} = 0.200 \text{ M}$ as a function of $[\text{Al}(\text{OH})_4^-]_{\text{T}}$ at $\text{pH} = 8$ and $25^\circ\text{C} \pm 1^\circ\text{C}$

Concerning $\text{Al}_2(\text{OH})_6\text{Hpgl}^-$, this finding is in contradiction with the structure outlined in *Figure 19*, where strong Al-O-C bonds are present. As an attempt to resolve this contradiction, we propose this species to be in the form of $\text{Al}_2(\text{OH})_6\text{Hpgl}^-$ in solution with Al^{3+} being sixfold coordinated. A possible isomerization of the metal center from octa- to tetrahedral geometry during the MS measurement may facilitate the condensation reactions, resulting in the

formation of the $\text{Al}_2(\text{OH})_2\text{HpglH}_3^-$ complex (Figure 19). Interestingly, such change in the coordination number was suggested for the $\text{Al}(\text{OH})_3\text{Gluc}^-$ complex previously [145].

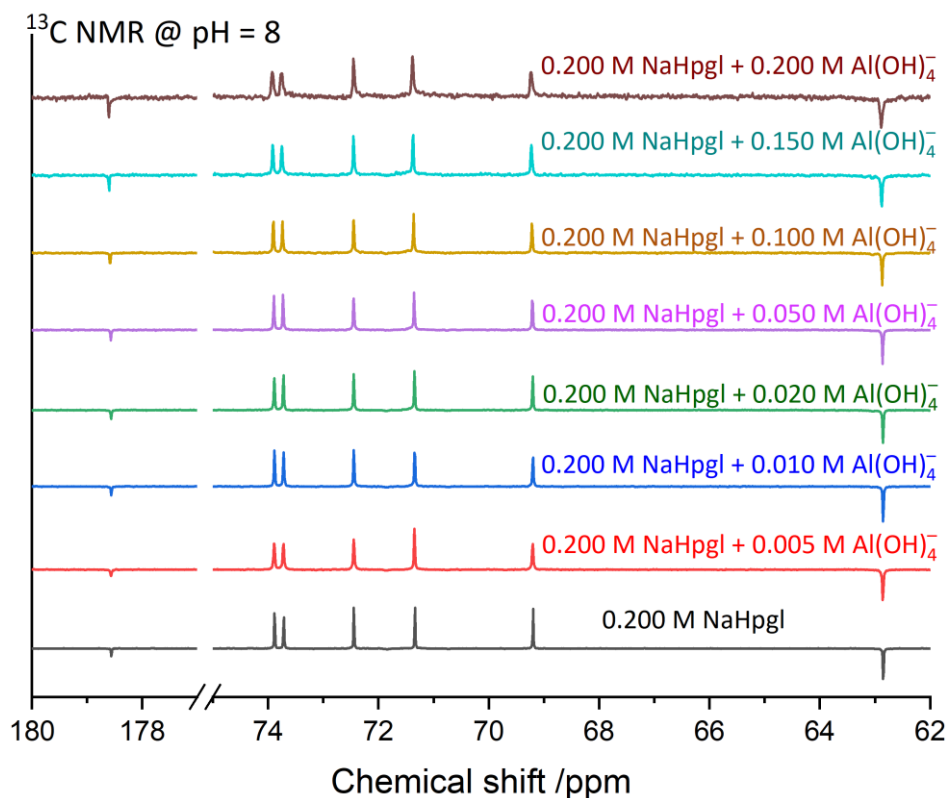


Figure 26 ^{13}C NMR spectra of solutions containing $[\text{Hpgl}^-]_{\text{T}} = 0.200 \text{ M}$ as a function of $[\text{Al}(\text{OH})_4^-]_{\text{T}}$ at $\text{pH} = 8$ and $25^\circ\text{C} \pm 1^\circ\text{C}$

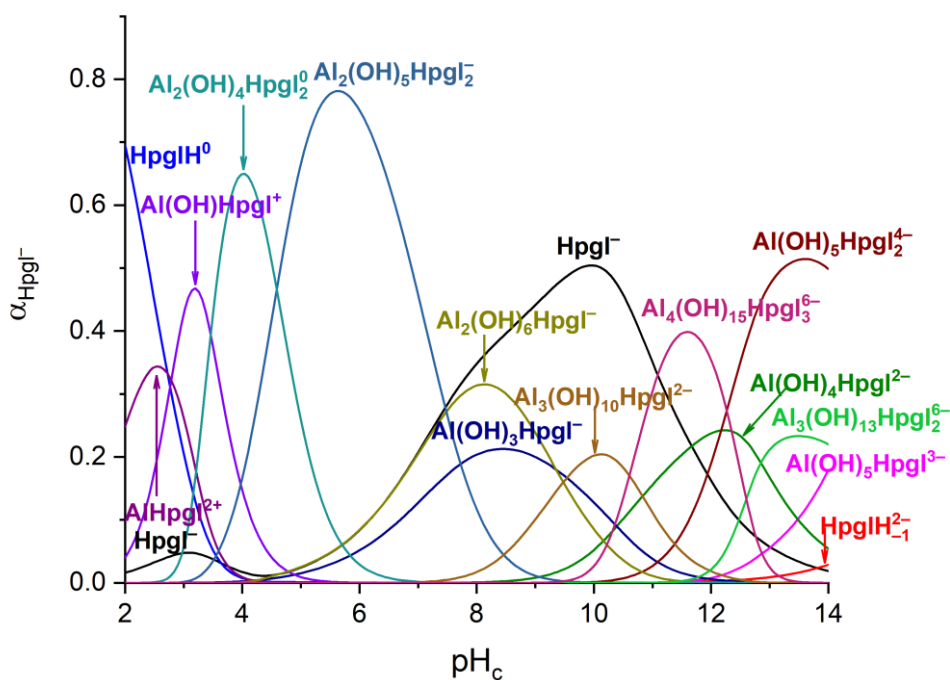


Figure 27 Speciation diagrams as a function of pH regarding Hpgl^- . The calculations were on the basis of stability constants provided in Table 8, corresponding to $t = (25 \pm 0.1)^\circ\text{C}$ and $I = 4 \text{ M}$ (NaCl). Total concentrations: $[\text{Al}(\text{OH})_4^-]_{\text{T}} = 0.200 \text{ M}$ and $[\text{Hpgl}^-]_{\text{T}} = 0.200 \text{ M}$.

Complexation of Al^{3+} in the alkaline region

Both the 1H and ^{13}C spectra above $pH = 10$ (Figures 21 and 22) exhibit salient variations, namely, the appearance of new peaks which correspond to newly formed complexes. This is apparent in the $[Al(OH)_4^-]_T$ -dependent 1H and ^{13}C spectra at $pH = 12$ (Figures 28 and 29). The emergence of distinct peaks of the complexes indicates that the ligand exchange rate is even slower than the one at $pH = 4$.

The slowdown of the exchange processes signals the formation of species that are considered to be inert on the NMR timescale and again reflects strong metal-ligand interactions. This must be the consequence of Al–O–C ethereal-type bonds of highly covalent nature, forming via intermolecular condensation reactions. (This mechanism and the concomitant slow exchange is known for the Al(III)/Gluc⁻ system [126].) On the other hand, the deprotonation of the ligand results in similar Al–O–C bonds being present already at $pH = 4$ (Figures 23 and 24). Why in that case the exchange rate is somewhat faster might be answered by the different geometry. That is, the dissociation of the complexes is slower when coordination geometry of the metal center is tetrahedral when it is octahedral. This leads to the interesting presumption that the change in the coordination geometry occurs in the neutral to mildly alkaline pH regime.

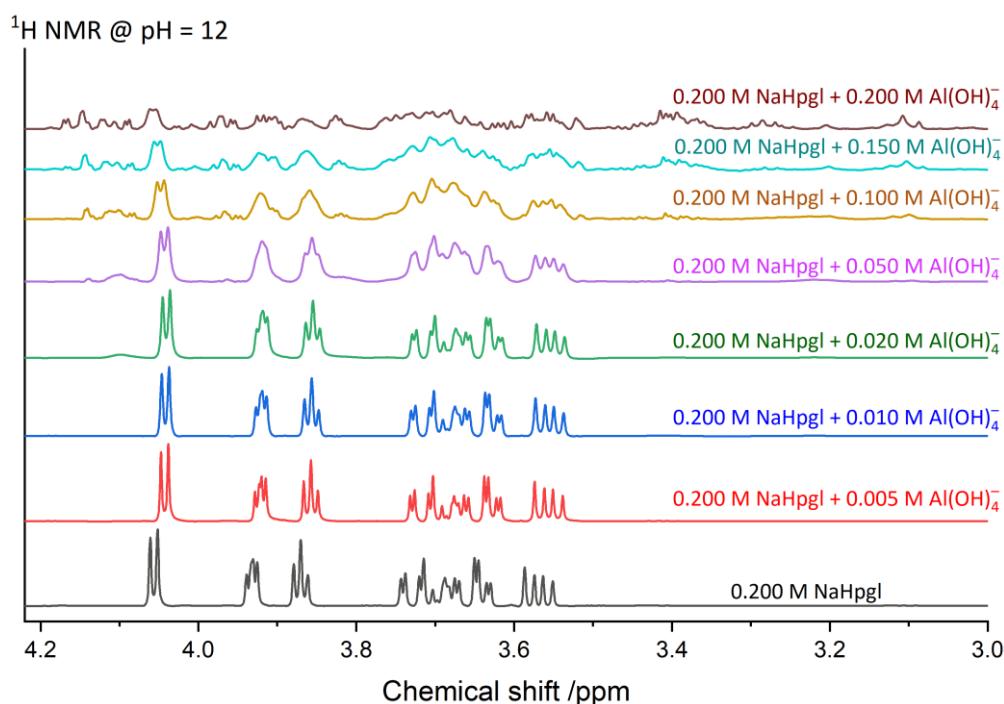


Figure 28 1H NMR spectra of solutions containing $[Hpgl^-]_T = 0.200$ M as a function of $[Al(OH)_4^-]_T$ at $pH = 12$ and $(25 \pm 1)^\circ C$

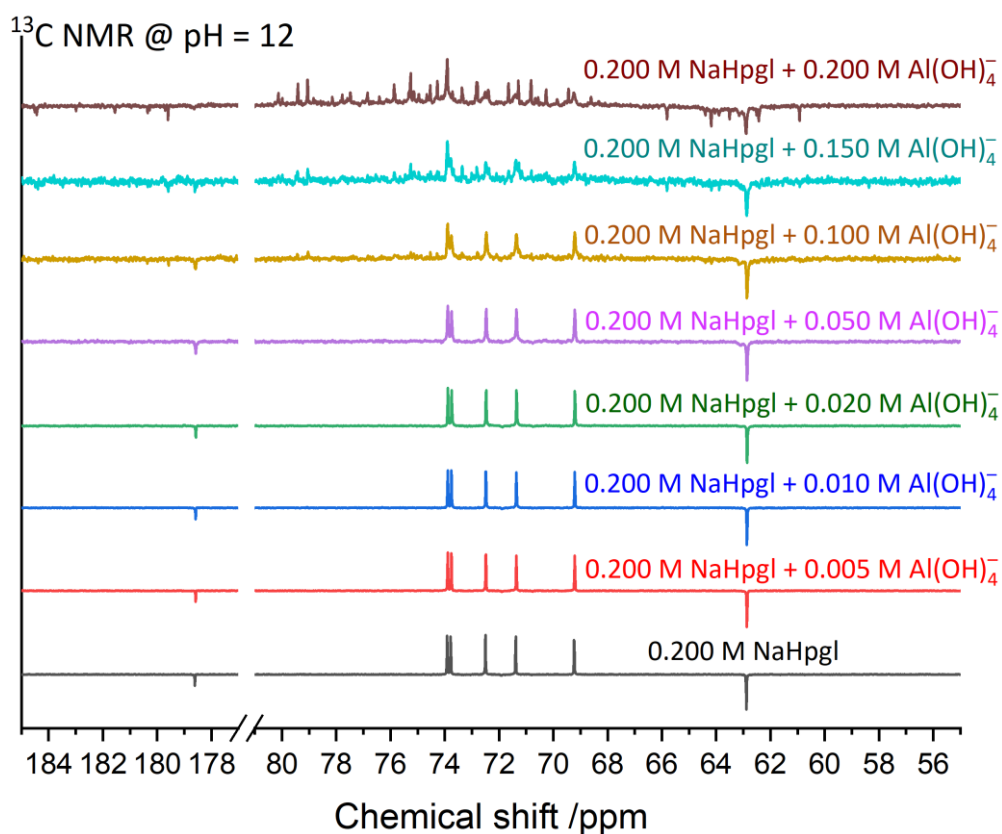


Figure 29 ^{13}C NMR spectra of solutions containing $[\text{HpgI}]_{\text{T}} = 0.200 \text{ M}$ as a function of $[\text{Al}(\text{OH})_4^-]_{\text{T}}$ at $\text{pH} = 12$ and $(25 \pm 1) ^\circ\text{C}$

Furthermore, the ^{13}C spectrum at $\text{pH} = 12$ (*Figure 30*) exhibits eight additional peaks around the C1 as well as the C7 peaks of the free ligand (being present at $\approx 20\%$, see *Figure 27*). In addition to HpgI^- , three complexes dominate the equilibria, namely $\text{Al}(\text{OH})_4\text{HpgI}^{2-}$, $\text{Al}(\text{OH})_5\text{HpgI}^{4-}$ and $\text{Al}_4(\text{OH})_{15}\text{HpgI}^{6-}$. The presence of at least eight complex signals clearly shows that these species exist in isomeric forms. It is also important to note that at these concentrations, a further deprotonation occurs on $\text{Al}(\text{OH})_4\text{HpgI}^{2-}$ yielding $\text{Al}(\text{OH})_5\text{HpgI}^{3-}$ (and $\text{Al}(\text{OH})_5\text{HpgI}^{4-}$, see *Figure 27*). The existence of a five-coordinated Al^{3+} in strongly alkaline medium is a long-running conundrum in the inorganic chemistry society [150]. Whether this is the case in the present system cannot be concluded from our experiments, but future extended X-ray absorption fine structure (EXAFS) measurements could probably address this question.

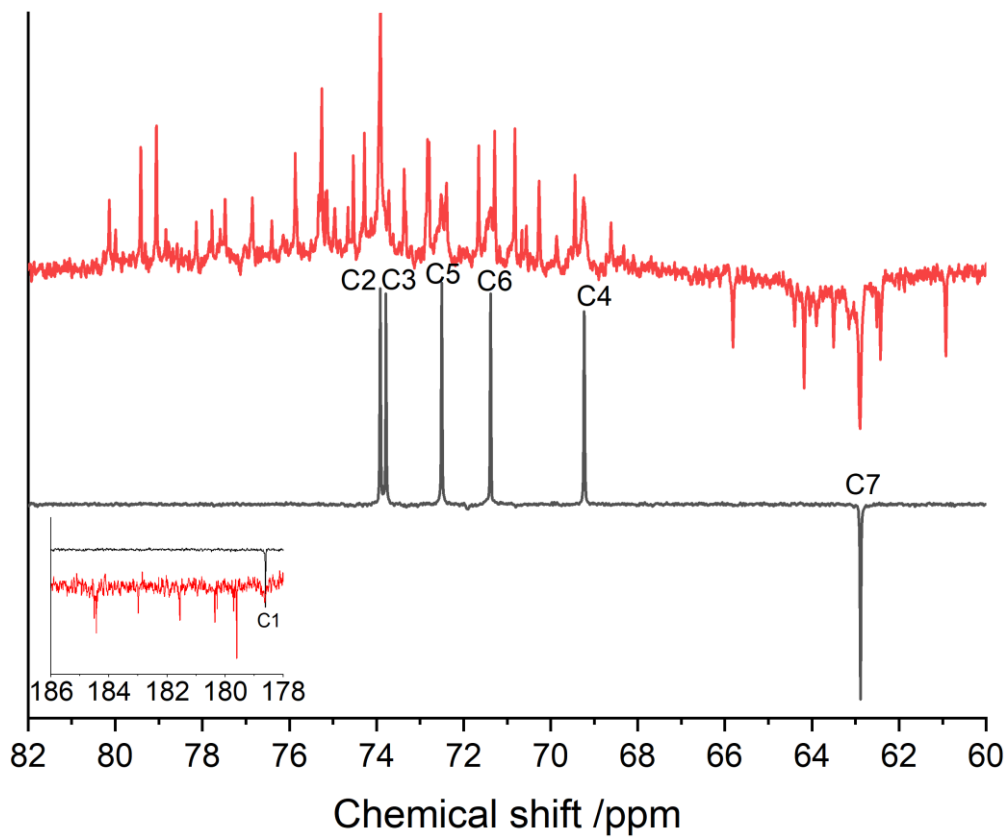


Figure 30 Comparison of ^{13}C NMR spectra of a solution containing only $[\text{Hpgl}^-]_{\text{T}} = 0.200 \text{ M}$ (black spectrum) with one containing $[\text{Hpgl}^-]_{\text{T}} = 0.200$ and $[\text{Al}(\text{OH})_4^-]_{\text{T}} = 0.200$ (red spectra) at $\text{pH} = 12$ and $(25 \pm 1) ^\circ\text{C}$

The structural and thermal analysis of the solid compounds forming in systems containing Ca^{2+} , Al^{3+} and heptagluconate ions

Crystallinity study of the prepared solids and reference compounds

First, the powder X-ray diffractograms of the precipitates as well as the Na- and Ca-heptagluconate reference compounds were recorded to gain information on the reflection patterns and crystallinity. The NaHpgl hydrate has sharp and well-separated reflections (*Figure 31a*), whereas the XRD traces of the $\text{Ca}(\text{Hpgl})_2 \cdot 2\text{H}_2\text{O}$ reference and the as-prepared binary Ca-Hpgl and Al-Hpgl samples are rather broad and not well-structured indicating the amorphous nature of the binary complexes. Similarly, the diffractogram of the ternary Ca-Al-Hpgl-5 sample shows broad reflections with low signal-to-noise ratio (*Figure 31a*; for the other ternary compounds, see *Figure 31b*), referring again to a low degree of crystallinity. This finding is in line with the formation of amorphous Ca-Al-gluconate solid phases, reported previously [151].

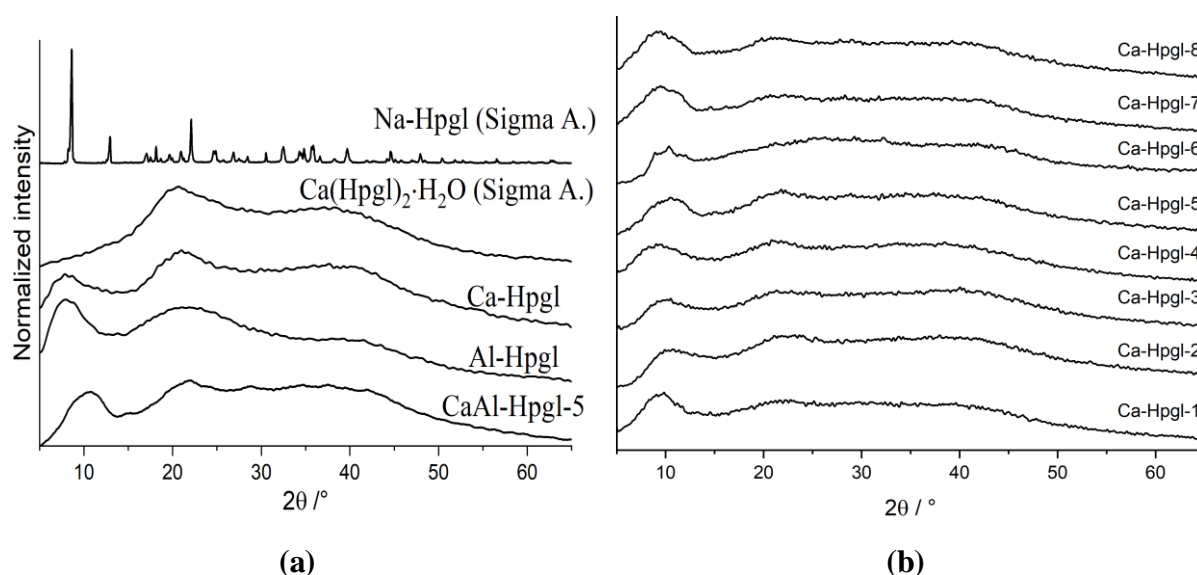


Figure 31 X-ray diffractograms of **a)** the reference heptagluconate (Hpgl⁻) salts, the as-prepared binary Ca- and Al-Hpgl solid compounds, and a typical ternary Ca-Al-Hpgl compound; **b)** all ternary compounds.

The morphology of precipitates: comparison of binary and ternary solids with the reference compounds

The morphology of the forming solid phase was studied with scanning electron microscopy. Compared to the angular particles of the well-crystallized sodium heptagluconate, the ternary and binary solids exhibit a rather amorphous, therefore significantly different morphologies (*Figure 32*), which is in line with the findings of XRD experiments.

For all these samples, exclusively highly aggregated particles (in the range of 500–1000 nm merged into few micron sizes) with planar shape and smooth edges could be registered without

the occurrence of crystallites. Meanwhile, the SEM-EDX analysis of the ternary samples (see *Figure 32* for CaAl-Hpogl) shows rather uniform distribution of calcium and aluminum atoms implying that this compound is indeed a ternary complex and not a heterogeneous mixture of two binary solids.

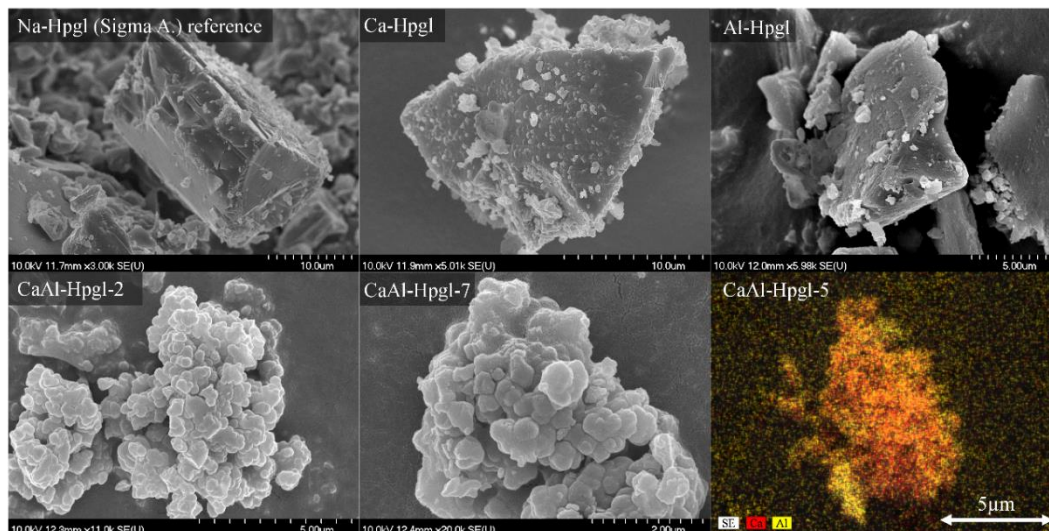


Figure 32 SEM images of sodium heptagluconate (NaHpogl) and its binary (Ca-Hpogl, Al-Hpogl) as well as ternary (CaAl-Hpogl) complexes with Ca^{2+} and Al^{3+} ions. The images of CaAl-Hpogl-2 and CaAl-Hpogl-7 represent the typical morphology, while the image of CaAl-Hpogl-5 represents the metal distribution in the samples.

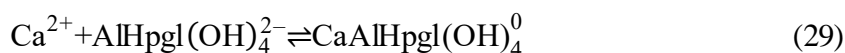
Calculation of the possible stoichiometries of the precipitates

The total concentrations of Ca^{2+} and Al^{3+} for the binary and ternary samples (dissolved in ≈ 2 M HCl) were determined by ICP-OES, while the concentration of heptagluconate was estimated on the basis of UV-vis spectrophotometry (see *Experimental Part* for further discussion). The calculated mass percentages of Ca^{2+} , Al^{3+} and Hpogl^- are listed in *Table 10*. The molar fraction of OH^- was determined applying the charge balance equation and any residual mass was ascribed to the presence of surface or lattice water. The molar fractions of all components were referenced to that of Al^{3+} (which was set to unity) and the thus obtained cumulative stoichiometries are presented also in *Table 10*.

As a result, the Ca-Hpogl binary complex is most probably in the form of partially deprotonated CaHpogl_2 , whereas the formula of Al-Hpogl binary sample ($\text{AlHpogl}_{0.4}(\text{OH})_{2.6}$) can be assigned to the trinuclear $\text{Al}_3\text{Hpogl}(\text{OH})_8^0$ complex, whose stoichiometry is similar to the previously reported $\text{Al}_3\text{Hpogl}(\text{OH})_{10}^{2-}$ solution species, which was found to be formed in alkaline solutions (see the distribution diagram in *Figure 27*).

To assess the composition of the ternary products, we have simulated the speciation of the Al^{3+} - and Hpogl^- -containing species for the applied $[\text{Al}(\text{OH})_4^-]_{\text{T}}$ and $[\text{Hpogl}^-]_{\text{T}}$ concentrations (see in *Table 2*), using the stability constants provided in *Table 8*. Under these conditions, the

dominant solution species are the $\text{AlHpgl}_2(\text{OH})_5^{4-}$ and $\text{AlHpgl}(\text{OH})_4^{2-}$ ones. Adding CaCl_2 to these solutions, the formation of the solid phase could be observed. According to the preliminary results from XRD and EDX studies, the formation of at least one low-solubility heteropolynuclear Ca-Al-Hpgl complex could be inferred. Examining the calculated cumulative stoichiometries listed in *Table 10*, three types of complexes can be conceived: in the first case, when the $n_{\text{OH}}/n_{\text{Hpgl}}$ ratio is above 1.0 (samples CaAl-Hpgl-1 to 4), both the formation of $\text{CaAlHpgl}(\text{OH})_4^0$ and $\text{Ca}_2\text{AlHpgl}_2\text{OH}_5^0$ is possible:



The most plausible explanation for the calculated stoichiometries is that the samples contained a mixture of ternary (or binary) compounds, which could be interpreted by the products described in *Equations 29* and *30*.

On the other hand, for samples with $n_{\text{OH}}/n_{\text{Hpgl}} < 1.0$, one major compound with a more sophisticated structure could be inferred. Examining the calculated stoichiometries for samples CaAl-Hpgl-5 to 8, the differences among them are only minor implying the exclusive formation of only one complex, $\text{Ca}_3\text{Al}_2\text{Hpgl}_3(\text{OH})_9^0$ which may be formed by the (formal) 1:1 combination of $\text{CaAlHpgl}(\text{OH})_4^0$ and $\text{Ca}_2\text{AlHpgl}_2\text{OH}_5^0$. In addition, the stoichiometry of the metal ions in $\text{Ca}_3\text{Al}_2\text{Hpgl}_3(\text{OH})_9^0$ strongly resembles that of TCA, $\text{Ca}_3\text{Al}_2(\text{OH})_{12}$, which may contribute to the understanding of the results published by *Kim et al.* [151,152].

Table 10 w/w% distribution of the components and the calculated cumulative stoichiometry

Sample ID	Ca ²⁺ (w/w%)	Al ³⁺ (w/w%)	Hpgl ⁻ (w/w%)	Calculated cumulative stoichiometry
Ca-Hpgl	7.6	-	74.9	$\text{CaHpgl}_{1.8}\text{OH}_{0.3} \times 4.9 \text{ H}_2\text{O}$
Al-Hpgl	-	17.0	60.5	$\text{AlHpgl}_{0.4}\text{OH}_{2.6}$
CaAl-Hpgl-1	16.7	5.7	58.0	$\text{Ca}_2\text{AlHpgl}_{1.2}\text{OH}_{5.7}$
CaAl-Hpgl-2	13.4	3.3	67.9	$\text{Ca}_{2.8}\text{AlHpgl}_{2.5}\text{OH}_{6.0} \times 0.5 \text{ H}_2\text{O}$
CaAl-Hpgl-3	12.6	4.1	66.6	$\text{Ca}_{2.1}\text{AlHpgl}_{1.9}\text{OH}_{5.2} \times 0.6 \text{ H}_2\text{O}$
CaAl-Hpgl-4	14.8	2.9	62.3	$\text{Ca}_{3.5}\text{AlHpgl}_{2.6}\text{OH}_{7.4} \times \text{H}_2\text{O}$
CaAl-Hpgl-5	11.6	4.4	63.9	$\text{Ca}_{1.8}\text{AlHpgl}_{1.8}\text{OH}_{4.8} \times 1.3 \text{ H}_2\text{O}$
CaAl-Hpgl-6	12.4	5.7	64.9	$\text{Ca}_{1.5}\text{AlHpgl}_{1.4}\text{OH}_{4.6} \times 0.1 \text{ H}_2\text{O}$
CaAl-Hpgl-7	13.4	6.8	61.3	$\text{Ca}_{1.3}\text{AlHpgl}_{1.2}\text{OH}_{4.5} \times 0.6 \text{ H}_2\text{O}$
CaAl-Hpgl-8	12.0	5.4	63.9	$\text{Ca}_{1.5}\text{AlHpgl}_{1.4}\text{OH}_{4.6} \times 0.6 \text{ H}_2\text{O}$

The effect of metal-ion coordination on the infrared and Raman spectra of sodium heptagluconate

The information provided by the infrared and Raman spectra of the same sample is complementary to each other, since their general selection rules are different. The intensities of the infrared spectrum are proportional to the square of the transitional dipole moment, while the magnitude of Raman-effect is determined by the change of the polarizability tensor during the transition. Therefore, the vibrational normal modes of the D-heptagluconate ion can be classified from this point of view.

The normal modes dominated by the displacement of the hydrogen atoms in the O–H groups produce high transitional dipole moment, but hardly influence the polarizability tensor of the molecule. Their intensities are high in the absorption spectrum, and they are practically invisible in the Raman spectrum. On the other hand, the normal modes, dominated by the combinations of the stretching vibrations of C–C bonds alter the polarizability tensor but produce negligible change in the dipole moment. Hence, their signals are weak on the infrared and relatively intense in the Raman spectrum.

The normal modes governed by the carboxylate group have both effects, since the delocalized 4π electron system strongly shifted to the direction of the oxygen atoms, although they are prone to further polarization, hence they are seen on both spectra. Consequently, the infrared spectra of the samples provide information mainly on the coordination properties of the ligand, whereas the Raman spectra report predominantly on the conformation of the backbone. This difference is most spectacular in the O–H stretching range and that of the carboxylate group:

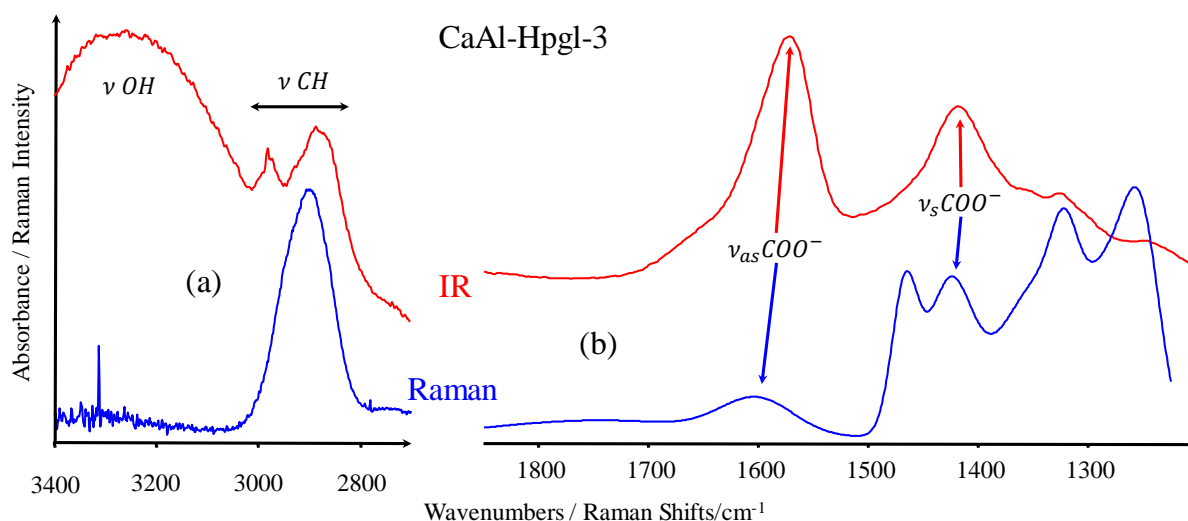


Figure 33 Comparison of the IR and Raman signals in the O-H and C-O-O stretching vibration ranges in case on sample CaAl-Hppl-3

The C–C stretching range of the Raman spectra divides the solid ternary specimens into two groups, showing a clear difference in the conformation of the backbone of Hpgl⁻ (Figure 34). The Raman spectra of samples from CaAl-Hpgl-1 to CaAl-Hpgl-4 differ somewhat only in the wavenumber range below 800 cm⁻¹, which is in the out-of-plane deformation range of the carboxylate and C–H groups (Figure 34, left (a)). Only slight relative intensity differences can be identified elsewhere in the spectra.

The other group of samples from CaAl-Hpgl-5 to CaAl-Hpgl-8 show much more uniform Raman spectra (they are indistinguishable), except around 1600 cm⁻¹, which is the carboxylate stretching region (Figure 34, left (b)).

The C–C stretching region of the two groups differ essentially, indicating the difference in the conformation of the carbon chain. This range is rather complicated in the spectra of CaAl-Hpgl-1 to CaAl-Hpgl-4, but the other series of spectra shows very clearly a set of nearly equidistant bands, the so-called „band progression”, *i.e.*, the sign of a fully stretched carbon backbone [153].

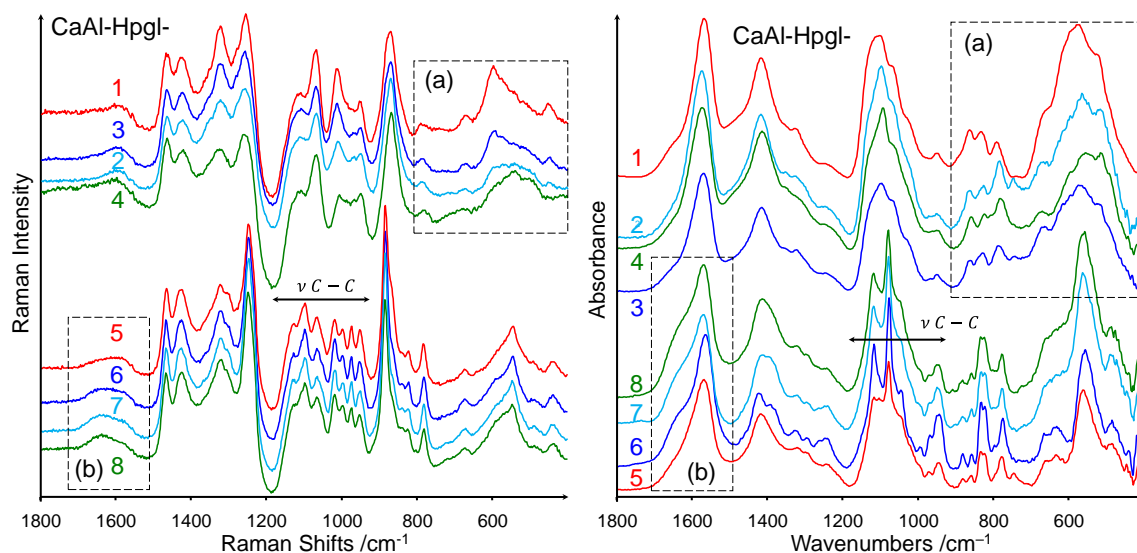


Figure 34 Raman and IR spectra of the ternary compounds. The difference between the C–C stretching region of the two groups indicates the difference in the conformation of the carbon chain.

The corresponding infrared spectra seem to confirm our conclusions drawn from the Raman spectra (Figure 34, right): the magnitude of differences for both groups of spectra are essentially the same, therefore the division of samples into two groups from CaAl-Hpgl-1 to CaAl-Hpgl-4 and from CaAl-Hpgl-5 to CaAl-Hpgl-8 is appropriate.

Another interesting feature of the spectra is the carboxylate region, which is seen on Figure 33b. The position of the peaks, tentatively assigned to the carboxylate stretching modes, did not coincide on the corresponding infrared and Raman spectra of the samples. Since the

selection rules do not justify this difference, there were only two possibilities to consider. One possible explanation is that the ligands are arranged in central symmetry around the metal ions, resulting the separation of the *gerade* and *ungerade* species into the Raman and into the infrared spectra, respectively. The other possibility is that the positions of the peaks could arise from overlapping bands with various intensities, indicated by the differences in the carboxylate stretching region depicted in *Figure 34b* [153].

A straightforward way of verifying this assumption is the analysis of the Fourier self-deconvoluted spectra between 1850 and 1200 cm^{-1} . A typical result of the Fourier self-deconvolution is shown in *Figure 35*.

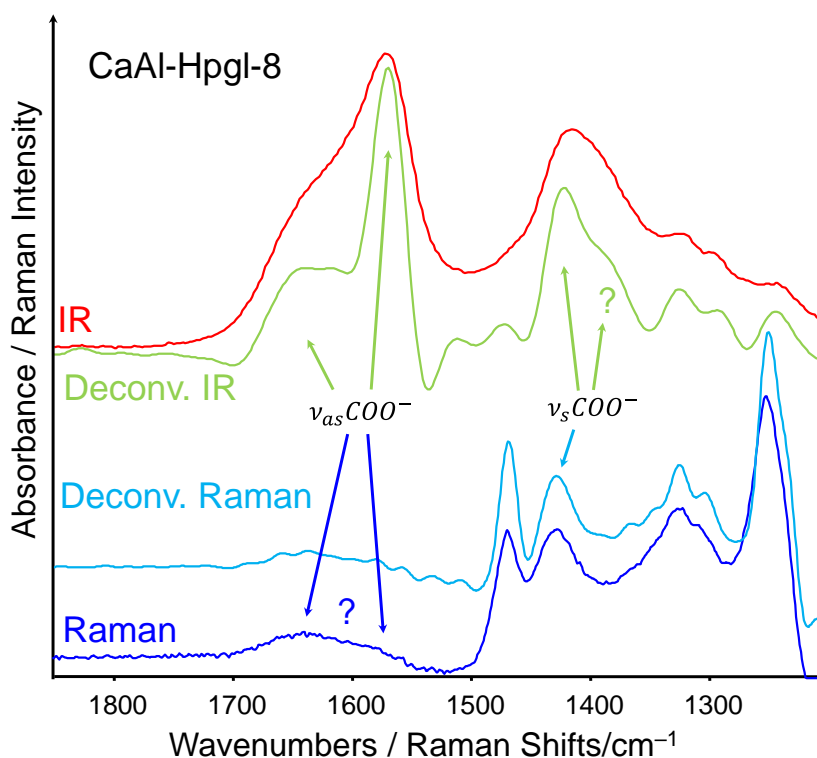


Figure 35 Fourier self-deconvolution performed on the IR and Raman spectra of sample CaAl-Hppl-8.

The carboxylate stretching peaks indeed split into at least two components in the infrared spectra. However, the deconvolution of the same range of the Raman spectra provided less information, since the peak around 1600 cm^{-1} being too weak and too broad for a reliable Fourier self-deconvolution. Nevertheless, the self-deconvoluted spectrum does not indicate the presence of overlapping bands.

In conjunction with Fourier self-deconvolution, peak fitting was performed with each spectrum in the same region. An example of such spectral decomposition for sample CaAl-Hppl-8 is depicted in *Figure 36*.

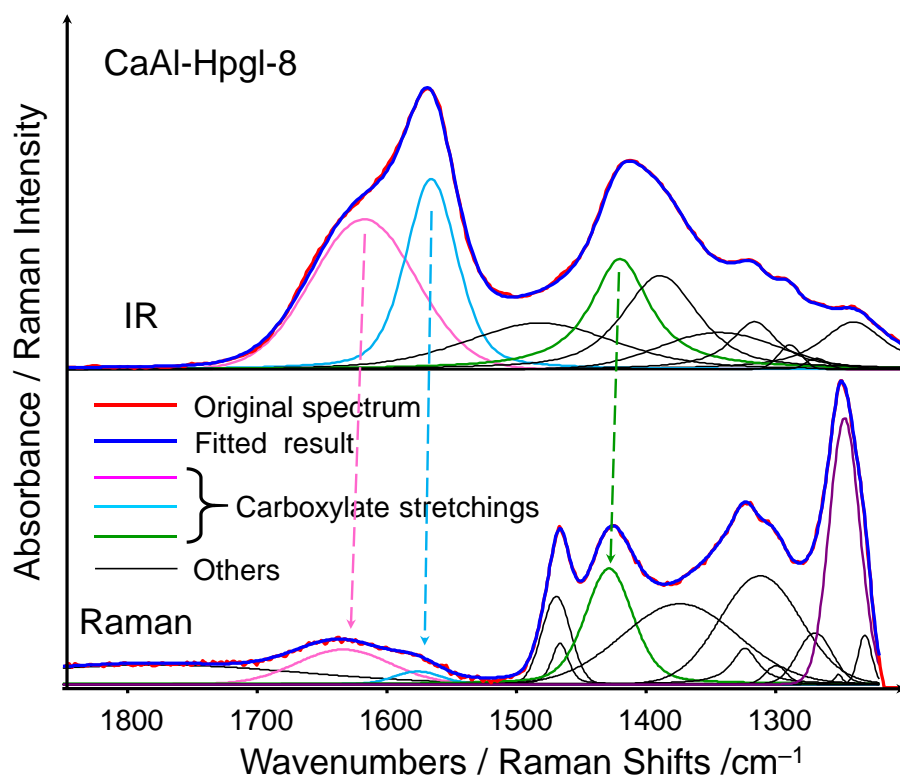


Figure 36 The result of peak fitting demonstrated on sample CaAl-Hppl-8. The position of the fitted carboxylate stretching bands imply a symmetry center between the ligands.

As a result, there were apparent deviations between the two aforementioned groups of samples. Generally, fewer peaks were sufficient for a satisfactory fit of the spectra of samples from CaAl-Hppl-1 to CaAl-Hppl-4, than for samples from CaAl-Hppl-5 to CaAl-Hppl-8. More importantly, no analogous bands could be found in the Raman spectra of the first group of samples between 1600 and 1500 cm^{-1} matching the strong infrared band of the antisymmetric carboxylate stretching mode. Besides, the fitting of the Raman spectra would have been inadequate for the second set of samples, without the corresponding, very low intensity bands. The positions of the fitted carboxylate stretching bands on the infrared and Raman spectra are satisfactorily close to each other, ruling out the presence of a symmetry center between the ligands. (For detailed data, see *Table 11*).

Table 11 Results of the peak fitting, performed in the carboxylate region (1850–1200 cm⁻¹) of the IR (plain background) and Raman (grey background) spectra.

Sample ID	ν_1 /cm ⁻¹	Lorentz %	$\frac{Area_{n+1}}{Area_n}$ / %	ν_2 /cm ⁻¹	Lorentz %	$\frac{Area_{n+1}}{Area_n}$ / %	ν_3 /cm ⁻¹	Lorentz %	$\frac{Area_{n+1}}{Area_n}$ / %
Ca-Hpg1	–	–	–	1590	0.63	0.4	1413	0.00	3.3
	1609	0.00	–	–	–	–	1428	0.00	1.1
Al-Hpg1	1634	0.00	–	1554	0.21	2.2	1393	0.47	2.4
	1650	0.31	0.5	–	–	–	1405	0.00	2.0
CaAl-Hpg1-1	1621	0.27	1.9	1569	0.25	1.6	1418	1.00	2.0
	1600	0.00	–	–	–	–	1427	0.00	1.5
CaAl-Hpg1-2	1609	0.01	1.3	1574	0.04	1.7	1419	0.81	2.0
	1601	0.00	–	–	–	–	1426	0.00	1.4
CaAl-Hpg1-3	1614	0.01	1.6	1571	0.01	1.4	1419	0.86	2.1
	1602	0.00	–	–	–	–	1427	0.00	1.4
CaAl-Hpg1-4	1613	0.34	1.2	1574	0.01	1.6	1417	0.64	2.1
	1603	0.00	–	–	–	–	1426	0.00	1.7
CaAl-Hpg1-5	1604	0.13	0.8	1568	0.34	1.7	1419	1.00	2.3
	1631	0.00	0.4	1581	0.00	–	1429	0.00	1.7
CaAl-Hpg1-6	1625	0.34	1.7	1565	0.60	0.6	1426	1.00	3.6
	1631	0.00	0.2	1576	0.00	8.9	1429	0.21	1.6
CaAl-Hpg1-7	1619	0.00	0.6	1569	0.00	1.0	1423	0.50	3.5
	1634	0.00	0.2	1576	0.00	8.8	1429	0.33	1.7
CaAl-Hpg1-8	1621	0.01	0.7	1569	0.39	0.8	1423	0.96	4.0
	1634	0.00	0.2	1576	0.00	10.6	1429	0.33	1.6

The spectra of the binary samples Ca-Hppl and Al-Hppl were also studied. Their spectra, together with the fitted carboxylate stretching bands were shown in *Figure 37*.

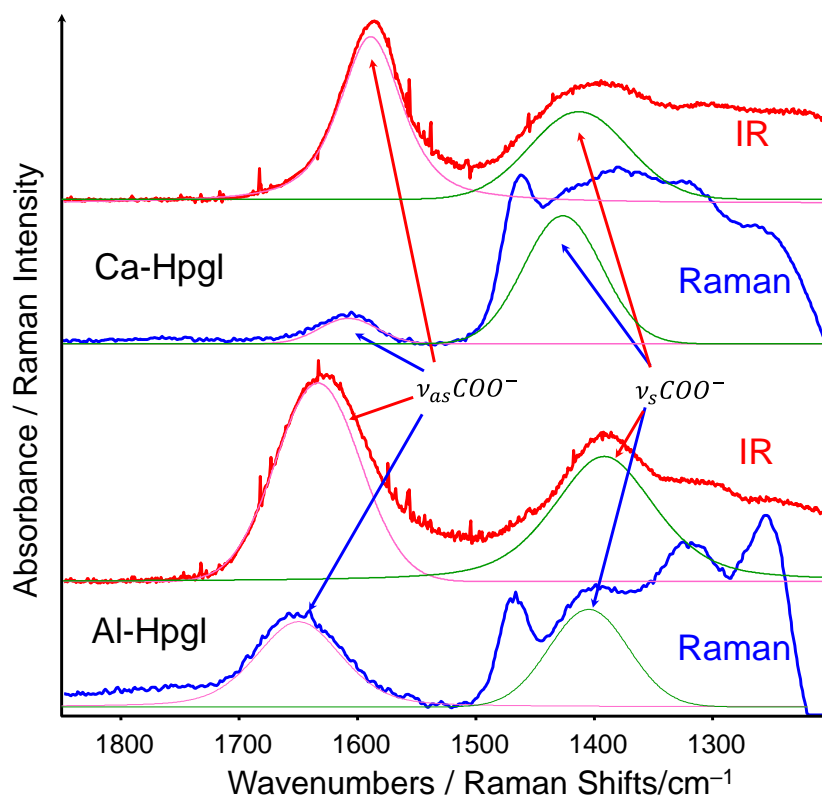


Figure 37 Fitting results of the Ca-Hppl and Al-Hppl binary samples. The antisymmetric carboxylate stretching mode of Hppl^- above 1600 cm^{-1} refers to the coordination with Al(III), whereas the region of $1600 - 1500\text{ cm}^{-1}$ is indicative of Ca(II) complexation.

Comparing the fitted peak positions to those of the ternary compounds, one can infer that the presence of two bands in the antisymmetric carboxylate stretching region arises from the coordination of Ca(II) and Al(III) ions to Hppl^- ligands. Explicitly, the antisymmetric stretching mode above 1600 cm^{-1} corresponds to the coordination of Al(III), while the band between 1600 cm^{-1} and 1500 cm^{-1} may be the sign of coordination to Ca(II) [154–156].

Finally, the ratios of the integrated intensities of the fitted antisymmetric carboxylate bands above and below 1600 cm^{-1} corroborate the existence of the two types of solid compounds: the ratios were above 1.0 for the samples from CaAl-Hppl-1 to CaAl-Hppl-4, and below 1.0 for CaAl-Hppl-5 to CaAl-Hppl-8 (*Table 11*), indicating that the relative amount of Al(III) as compared to Ca(II) is higher for the latter precipitates in the second group. This agrees well with the results obtained from the ICP-OES analysis.

Thermal analysis of the ternary complexes

The thermograms of both the Al- and Ca-Hpgl solids (*Figure 38a* and *Figure 40a-b*) as well as the CaAl-Hpgl-7 ternary complex (*Figure 38b*) exhibit well-distinguishable mass loss processes. For all compounds, the physically adsorbed water (*i.e.*, the fraction of water which is bound to the surface) evaporate first at 50 °C, followed by the release of lattice water below ~180°C.

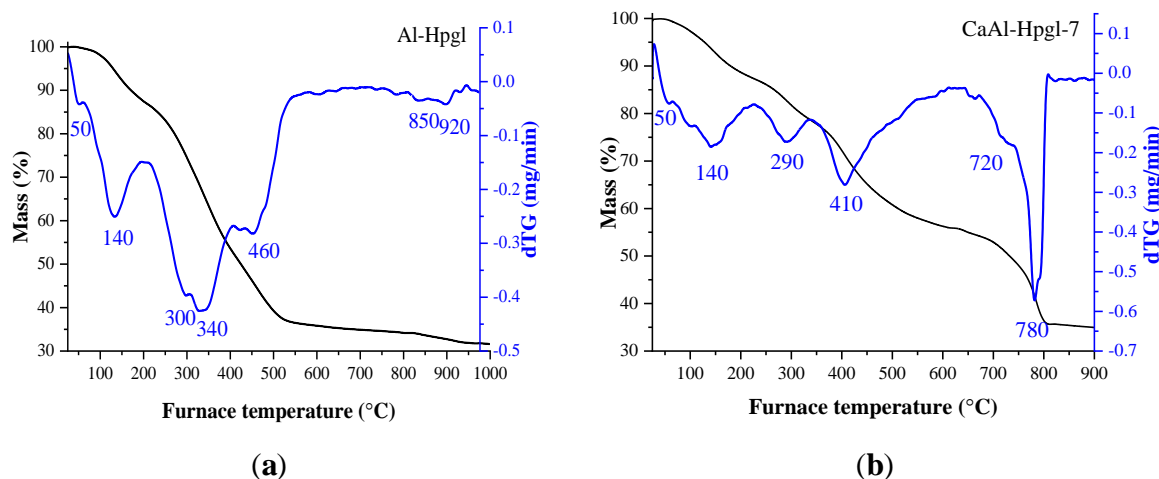


Figure 38 Thermograms (left axis, black solid line) and differential thermograms (right axis, blue solid line) of the Al-binary (a) and a typical ternary (CaAl-Hpgl-7) complex (b).

The next major loss peak appears between 180 and 400 °C (Al-Hpgl) or 180 and 350 °C (Ca-Hpgl and CaAl-Hpgl-5). To reveal the underlying chemical processes, infrared spectra of the CaAl-Hpgl-7 solid calcined at 200, 310, 340 and 500 °C (*Figure 39a*) were recorded. The sample calcined at 200 °C remains essentially intact, since the peaks of the corresponding spectrum are in similar positions and of similar shape as compared to the untreated solid (*Figure 34*, right). However, above 310 °C marked variations can be observed: namely, the intensities of the ligand O–H/C–H stretching vibrational modes at 2750–3750 cm^{-1} decrease gradually, in conjunction with the weakening of the C–O bands between 900 and 1200 cm^{-1} . Parallel to the mineralization of the heptagluconate, the dehydration of the $\text{Al}(\text{OH})_x^{(3-x)+}$ ion may also occur, as this step takes place < 300 °C in the case of $\text{Al}(\text{OH})_3$ [72].

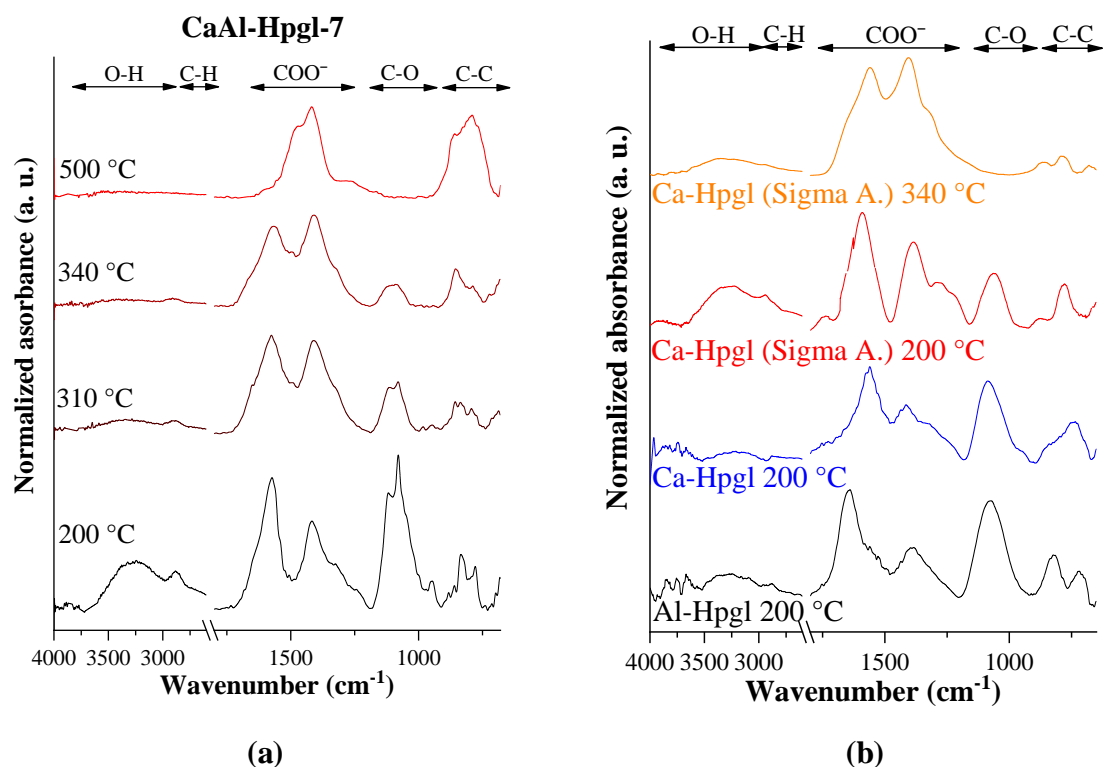


Figure 39 Infrared spectra of the CaAl-Hpogl-7 ternary solid compound after heat treatment at different temperatures (a), and the binary and commercial solids at 200 °C and 340 °C (b).

Between 340 and 500 °C, the caramelization of the ligand proceeds with similar mass losses (16–22%), presumably along with the dehydration of the $\text{Ca}(\text{OH})_y^{(2-y)+}$ (which occurs at ~460 °C, see the TG curve of $\text{Ca}(\text{OH})_2$ in *Figure 40c*). The infrared spectrum of the solids calcined at 500 °C shows the disappearance of the C–H and C–O bonds. The collapse of the heptagluconate moiety is also shown by the variation of asymmetric and symmetric vibrations of the COO^- groups (at 1570 and 1410 cm^{-1}). Meanwhile, a signal at 1420 cm^{-1} ascribed to the surface-adsorbed CO_2 molecules as well as a resonance mode at 1480 cm^{-1} corresponding to the *in situ* generated calcite phase appeared [127].

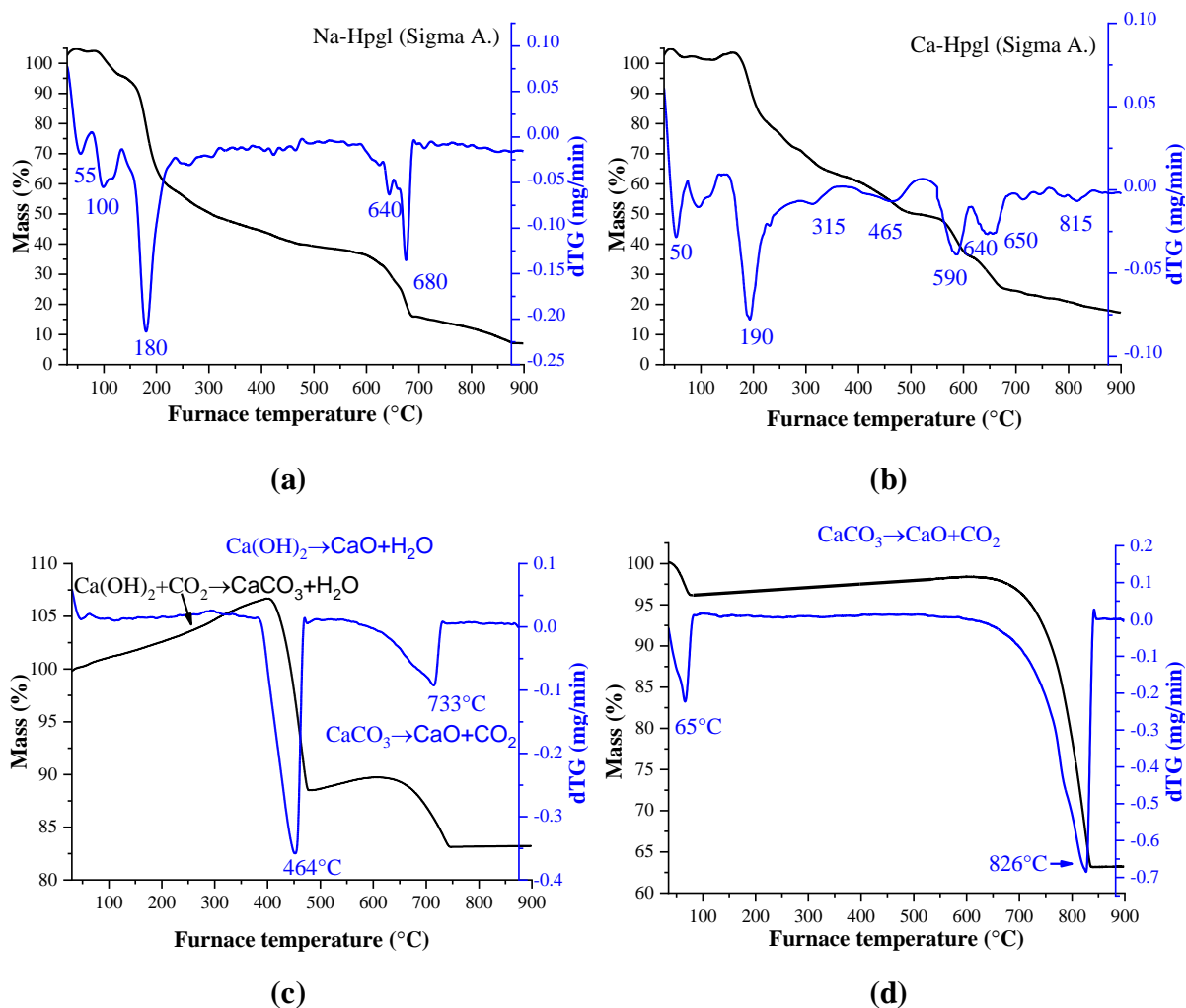


Figure 40 Thermograms of the commercial heptagluconate sodium- (a), and calcium salts (b) from Sigma. Aldrich as well as Ca(OH)_2 (c) and CaCO_3 (d).

Above 500 °C, the merger of calcite phase decomposition (*Figure 40c*) with the final-step mineralization of Hpgl^- could be observed; the decarbonization processes took place in the most substantial amounts (24–30% mass losses). A notable feature of the Al-Hpgl and Ca-Hpgl binary samples is that the decomposition of Hpgl^- started at higher temperatures, than for the commercially available sodium and calcium salts of heptagluconate. Furthermore, the ternary samples exhibited even greater thermal stabilities: for the binary solids heat-treated at 200 °C a significant decrease in the intensities of their C–O peaks (900–1200 cm^{-1}) in their infrared spectra could be observed (*Figure 39b*), while those of the ternary compounds were unscathed. This enhanced thermal stability of Hpgl^- is more evident for the calcination of samples at 340 °C: the C–O bands and even the O–H/C–H stretching modes (2750–3750 cm^{-1}) of the Na- and Ca-salts of heptagluconate disappeared on the spectrum, while these peaks were still observable for CaAl-Hpgl-7 heat-treated at 340 °C. Moreover, the calculated mass losses remained under ~13% for the ternary solids between 200 and 350 °C, and these values were

significantly larger, 21 and 34%, in the case of binary precipitates (*Table 12.*). Ultimately, these observations could indicate that the heteropolynuclear complexes are more stable than the binary ones, explicable by the intuition that the simultaneous binding of Ca^{2+} and Al^{3+} yields overall stronger metal-ligand interactions.

Table 12 Mass losses of the solids at different temperature ranges.

Sample ID	Mass loss under 200 °C (%)	Mass loss 200–350 °C (%)	Mass loss 350–500 °C (%)	Mass loss above 500 °C (%)
Ca-Hpgl	9	20.9	22.1	24.6
Al-Hpgl	12.5	33.8	17.1	4.9
CaAl-Hpgl-1	14.9	7.4	15.8	26.6
CaAl-Hpgl-2	13.2	12.6	15.8	29.7
CaAl-Hpgl-3	12.7	11.0	16.3	28.4
CaAl-Hpgl-4	13.5	10.6	14.4	29.7
CaAl-Hpgl-5	10.5	12.0	17.2	29.5
CaAl-Hpgl-6	11.3	10.9	17.0	26.2
CaAl-Hpgl-7	12.7	10.8	17.4	27.0
CaAl-Hpgl-8	14.7	11.0	16.8	24.9

Ca²⁺ / Al³⁺ / heptagluconate complexes in the pH range of 8–14: Preliminary insights into the solution equilibria and speciation

The cardinal step in our work was to describe the interactions in solutions containing Ca²⁺, Al³⁺ and heptagluconate ions. The characterization of such a complex system required a holistic approach, therefore multiple experimental methods were employed, including potentiometry, polarimetry as well as ¹H and ¹³C NMR spectroscopy.

The interpretation of the pH-potentiometric and polarimetric data

First, potentiometric titrations were conducted on solutions containing Ca²⁺, Al³⁺ and heptagluconate ions (hereafter ternary solutions). Due to the overlapping solution equilibria detected previously in the case of the Al³⁺-Hpgl⁻ system, an appropriate description of the system required studying it in a broad pH range.

Comparing the titration curves of the plain ligand with those of the binary and ternary solutions, the gradual shift towards lower pH could be observed (*Figure 41*). Among these, the introduction of both metal ions caused the most spectacular pH effect, implying the formation of complexes with remarkable stability.

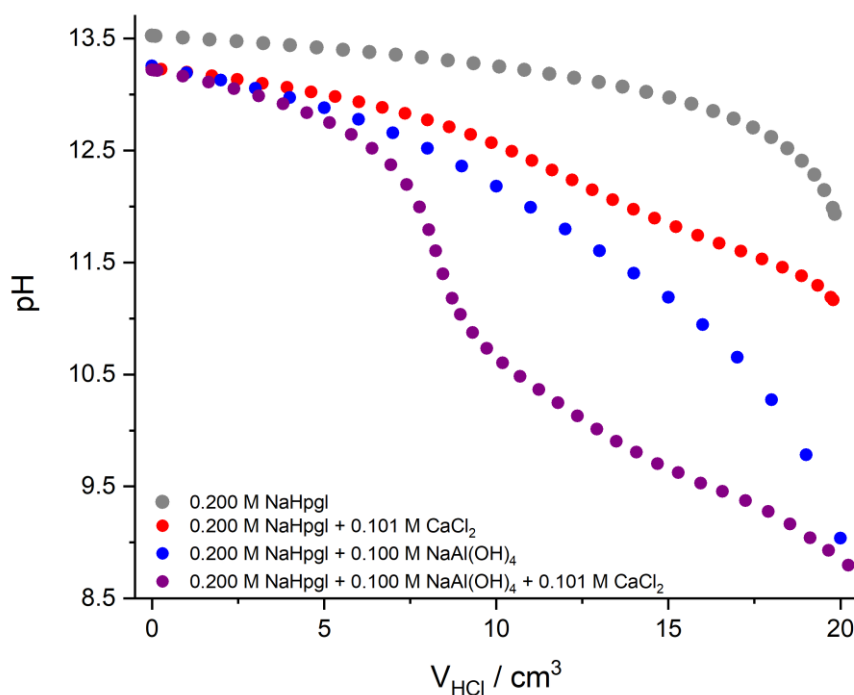


Figure 41 The effect of Ca²⁺ and Al³⁺ ions on the titration curve of heptagluconate (Hpgl⁻). Experimental conditions: $t = 25^{\circ}\text{C}$, $I = 4\text{ M}$ (NaCl), $[\text{NaOH}]_{\text{T},0} = 0.250\text{ M}$. The titrant was 1 M HCl.

Although the introduction of both metal ions resulted in extensive proton release, the large pH effects already seen for the binary solutions indicates that the contribution of these binary species to the overall equilibria is not negligible. To check to which extent the observed pH effects are due to the formation of ternary complexes, the titration curves of the binary systems were simulated using the PSEQUAD software and were compared to those for the ternary solutions at the same total concentrations.

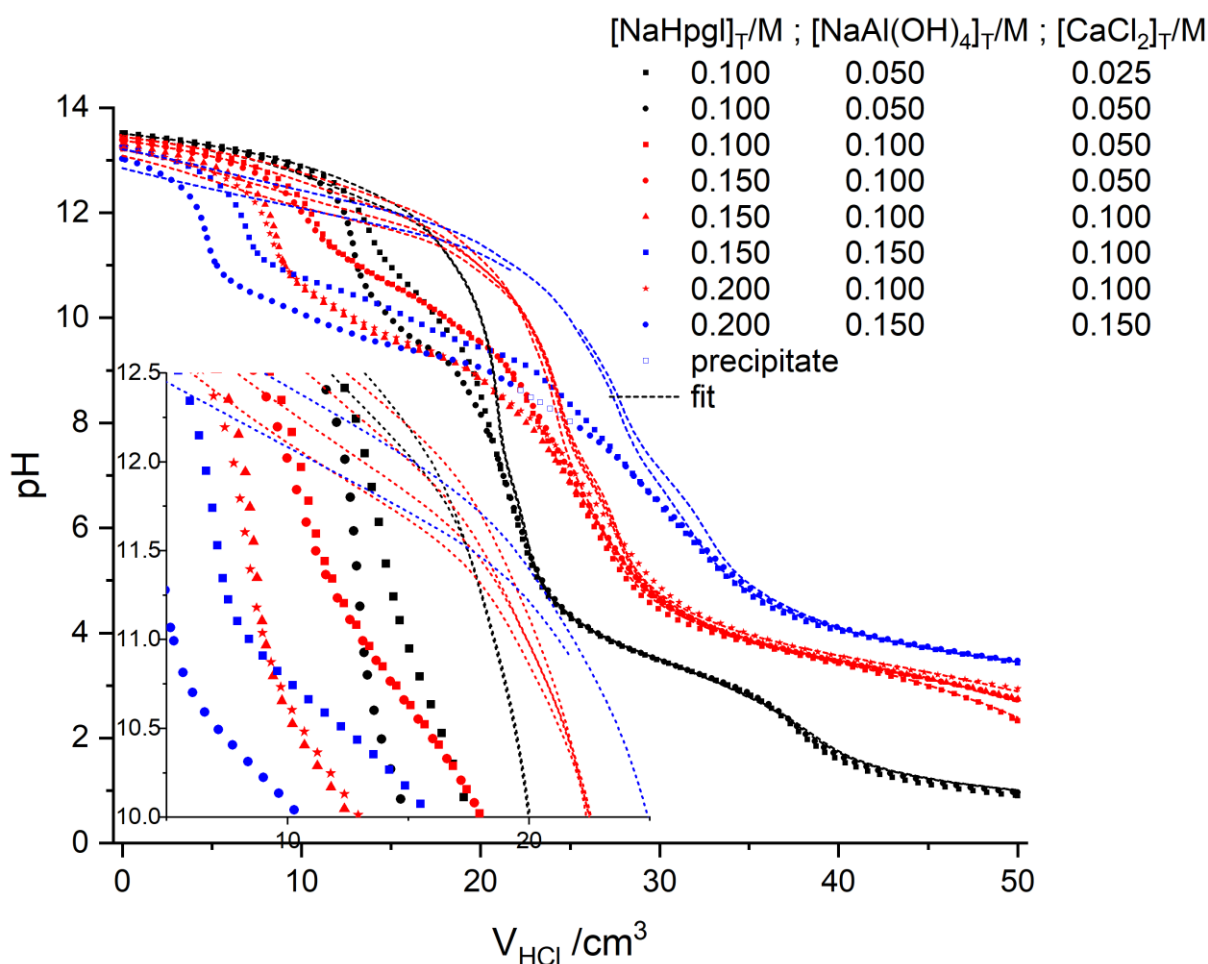


Figure 42 Measured (symbols) and calculated (dashed line) pH values for heptagluconate (Hpgl^-) in presence of Ca^{2+} and Al^{3+} ions. Experimental conditions: $t = 25^\circ\text{C}$, $I = 4\text{ M}$ (NaCl), $[\text{NaOH}]_{T,0} = 0.250\text{ M}$. The titrant was 1 M HCl . Symbols represent the experimental data, whereas solid lines are simulated curves for the binary systems containing either Ca^{2+} or Al^{3+} , based on the $\log \beta_{\text{pqrs}}$ values of $\text{Ca}_p\text{Hpgl}_r\text{H}_s^{(2p-r+s)+}$ and $\text{Al}((\text{OH})_4)_q\text{Hpgl}_r\text{H}_s^{(-q-r+s)+}$ species presented in *Tables 6* and *7*.

In the first scenario, the simulation of the measured titration curves was based on the premise, that the mere inclusion of the binary complexes of $\text{Ca}_p\text{Hpgl}_r\text{H}_s^{(2p-r+s)+}$ and $\text{Al}((\text{OH})_4)_q\text{Hpgl}_r\text{H}_s^{(-q-r+s)+}$ compositions would yield a satisfactory fit. However, looking at *Figure 42*, one can notice the significant deviation between the calculated and measured pH values starting from approximately pH 7–8. On the other hand, the inclusion of binary

complexes was sufficient to provide an adequate fit below pH = 6. Furthermore, in the pH range of 6 to 14, the structure of the curves depends mainly on the total concentration of Ca²⁺ ions. These observations provided us two important remarks, namely that (1) ternary complexes do form in these solutions and (2) they dominate the complexation equilibria in the pH range of 8 to 14.

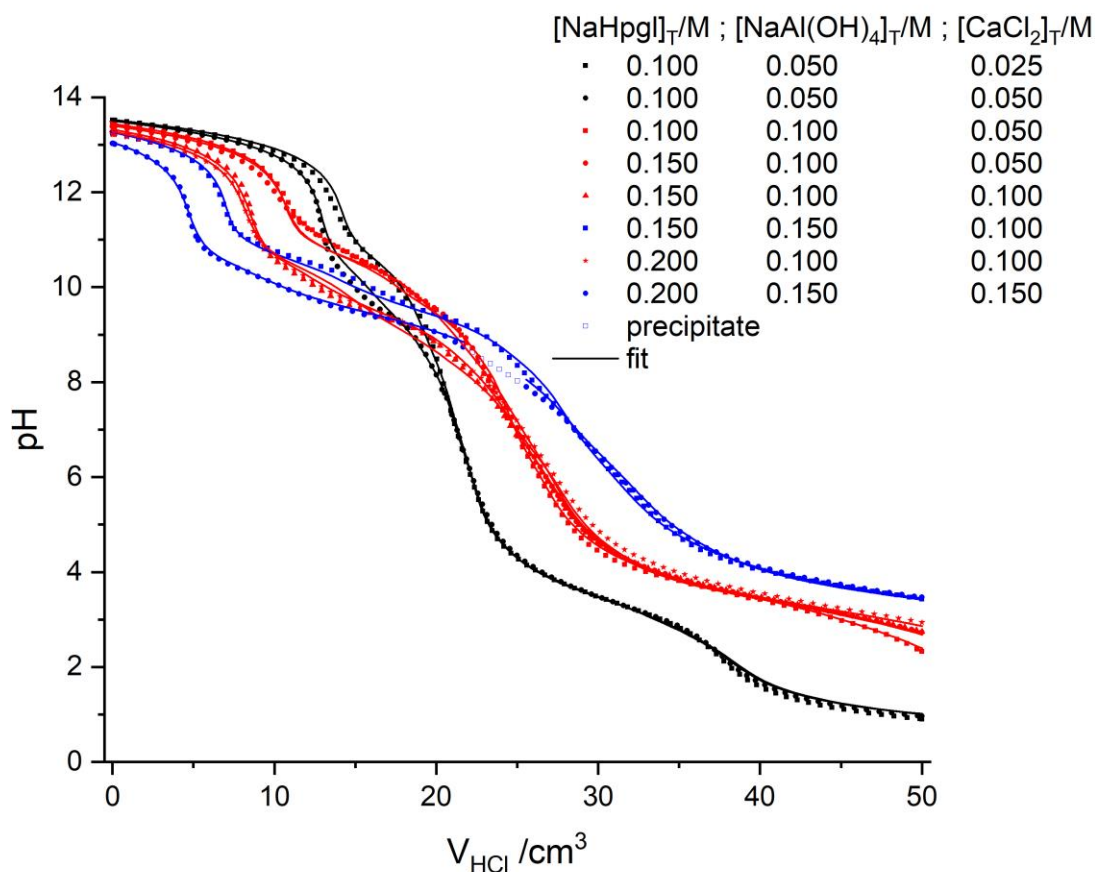


Figure 43 Measured (symbols) and calculated (dashed line) pH values for heptagluconate in presence of Ca²⁺ and Al³⁺ ions. Experimental conditions: t = 25 °C, I = 4 M (NaCl), [NaOH]_{T,0} = 0.250 M; the titrant was 1 M HCl. Symbols represent experimental data, whereas solid lines are the results of the fits based on the log β_{pqrs} values of Ca_pAl_qHpgl_r(OH)_{4q-s}^{(2p+3q-r-4q+s)+} species presented in Table 13.

The evaluation of the measured potentiometric data was performed by fitting the pH- and Ca²⁺-dependent sets simultaneously. Several various ternary species were systematically included and checked, while all the aforementioned binary particles were incorporated in the model, with their stability products fixed to the values presented in Tables 6 and 7. The best model obtained on this system yielded FP = 5.31 mV (≈0.07 pH units), which provided a satisfactory description of the measured data. The calculated species' stoichiometries and their stability products are listed below in Table 13, whereas the corresponding speciation diagram is presented in Figure 44.

Table 13 Stability constants, $\log \beta_{pqrs}$, determined for the various reactions taking place in the $\text{Ca}^{2+} / \text{Al}(\text{OH})_4^- / \text{Hpgl}^-$ system. Experimental conditions: $t = 25^\circ \text{C}$, $I = 4 \text{ M}$ (NaCl). In parentheses, the triple standard error is given.

Reaction	$\log \beta_{pqrs}$
$\text{H}_3\text{O}^+ + \text{OH}^- \rightleftharpoons 2\text{H}_2\text{O}$	14.26
$\text{Hpgl}^- + \text{H}_3\text{O}^+ \rightleftharpoons \text{HpglH} + \text{H}_2\text{O}$	3.64(1)
$\text{Hpgl}^- + \text{H}_2\text{O} \rightleftharpoons \text{HpglH}_{-1}^{2-} + \text{H}_3\text{O}^+$	-13.81(1)
$\text{Ca}^{2+} + \text{Hpgl}^- \rightleftharpoons \text{CaHpgl}^+$	0.42(19)
$2\text{Ca}^{2+} + 2\text{Hpgl}^- + 4\text{H}_2\text{O} \rightleftharpoons \text{Ca}_2\text{Hpgl}_2\text{H}_{-4}^{2-} + 4\text{H}^+$	-46.61(25)
$3\text{Ca}^{2+} + 2\text{Hpgl}^- + 3\text{H}_2\text{O} \rightleftharpoons \text{Ca}_3\text{Hpgl}_2\text{H}_{-3}^+ + 3\text{H}^+$	-31.19(19)
$3\text{Ca}^{2+} + 2\text{Hpgl}^- + 4\text{H}_2\text{O} \rightleftharpoons \text{Ca}_3\text{Hpgl}_2\text{H}_{-4}^0 + 4\text{H}^+$	-42.98(11)
$\text{Al}(\text{OH})_4^- + 4\text{H}^+ \rightleftharpoons \text{Al}^{3+} + 4\text{H}_2\text{O}$	22.81(19)
$\text{Al}(\text{OH})_4^- + \text{Hpgl}^- + 4\text{H}^+ \rightleftharpoons \text{AlHpgl}^{2+} + 4\text{H}_2\text{O}$	24.85(29)
$\text{Al}(\text{OH})_4^- + \text{Hpgl}^- + 3\text{H}^+ \rightleftharpoons \text{Al}(\text{OH})\text{Hpgl}^+ + 3\text{H}_2\text{O}$	22.06(13)
$\text{Al}(\text{OH})_4^- + \text{Hpgl}^- + \text{H}^+ \rightleftharpoons \text{Al}(\text{OH})_3\text{Hpgl}^- + \text{H}_2\text{O}$	12.28(26)
$\text{Al}(\text{OH})_4^- + \text{Hpgl}^- \rightleftharpoons \text{Al}(\text{OH})_4\text{Hpgl}^{2-}$	1.89(17)
$\text{Al}(\text{OH})_4^- + \text{Hpgl}^- + \text{H}_2\text{O} \rightleftharpoons \text{Al}(\text{OH})_5\text{Hpgl}^{3-} + \text{H}^+$	-11.59(29)
$\text{Al}(\text{OH})_4^- + 2\text{Hpgl}^- + \text{H}_2\text{O} \rightleftharpoons \text{Al}(\text{OH})_5\text{Hpgl}_2^{4-} + \text{H}^+$	-9.02(15)
$2\text{Al}(\text{OH})_4^- + \text{Hpgl}^- + 2\text{H}^+ \rightleftharpoons \text{Al}_2(\text{OH})_6\text{Hpgl}^- + 2\text{H}_2\text{O}$	24.98(21)
$2\text{Al}(\text{OH})_4^- + 2\text{Hpgl}^- + 4\text{H}^+ \rightleftharpoons \text{Al}_2(\text{OH})_4\text{Hpgl}_2^0 + 4\text{H}_2\text{O}$	37.99(21)
$2\text{Al}(\text{OH})_4^- + 2\text{Hpgl}^- + 3\text{H}^+ \rightleftharpoons \text{Al}_2(\text{OH})_5\text{Hpgl}_2^- + 3\text{H}_2\text{O}$	33.41(20)
$3\text{Al}(\text{OH})_4^- + \text{Hpgl}^- + 2\text{H}^+ \rightleftharpoons \text{Al}_3(\text{OH})_{10}\text{Hpgl}^{2-} + 2\text{H}_2\text{O}$	28.23(26)
$3\text{Al}(\text{OH})_4^- + 2\text{Hpgl}^- + \text{H}_2\text{O} \rightleftharpoons \text{Al}_3(\text{OH})_{13}\text{Hpgl}_2^{6-} + \text{H}^+$	-6.52(26)
$4\text{Al}(\text{OH})_4^- + 3\text{Hpgl}^- + \text{H}^+ \rightleftharpoons \text{Al}_4(\text{OH})_{15}\text{Hpgl}_3^{6-} + \text{H}_2\text{O}$	21.74(39)
$\text{Ca}^{2+} + \text{Al}(\text{OH})_4^- + 2\text{Hpgl}^- + \text{H}_2\text{O} \rightleftharpoons \text{CaAl}(\text{OH})_5\text{Hpgl}_2^{2-} + \text{H}^+$	-2.46(13)
$\text{Ca}^{2+} + \text{Al}(\text{OH})_4^- + 2\text{Hpgl}^- \rightleftharpoons \text{CaAl}(\text{OH})_4\text{Hpgl}_2^-$	7.67(8)
$\text{Ca}^{2+} + \text{Al}(\text{OH})_4^- + 2\text{Hpgl}^- + \text{H}^+ \rightleftharpoons \text{CaAl}(\text{OH})_3\text{Hpgl}_2^0$	15.73(11)
$\text{Ca}^{2+} + 2\text{Al}(\text{OH})_4^- + 2\text{Hpgl}^- + 2\text{H}_2\text{O} \rightleftharpoons \text{CaAl}_2(\text{OH})_{10}\text{Hpgl}_2^{4-} + 2\text{H}^+$	-10.52(9)
$2\text{Ca}^{2+} + \text{Al}(\text{OH})_4^- + 2\text{Hpgl}^- + 2\text{H}_2\text{O} \rightleftharpoons \text{Ca}_2\text{Al}(\text{OH})_6\text{Hpgl}_2^- + 2\text{H}^+$	-10.44(29)
$2\text{Ca}^{2+} + 2\text{Al}(\text{OH})_4^- + 2\text{Hpgl}^- + 2\text{H}_2\text{O} \rightleftharpoons \text{Ca}_2\text{Al}_2(\text{OH})_{10}\text{Hpgl}_2^{2-} + 2\text{H}^+$	-7.33(18)
$3\text{Ca}^{2+} + \text{Al}(\text{OH})_4^- + 4\text{Hpgl}^- + 3\text{H}_2\text{O} \rightleftharpoons \text{Ca}_3\text{Al}(\text{OH})_7\text{Hpgl}_4^{2-} + 3\text{H}^+$	-13.33(28)
$3\text{Ca}^{2+} + \text{Al}(\text{OH})_4^- + 4\text{Hpgl}^- + 2\text{H}^+ \rightleftharpoons \text{Ca}_3\text{Al}(\text{OH})_2\text{Hpgl}_4^{3+} + 2\text{H}_2\text{O}$	27.36(42)

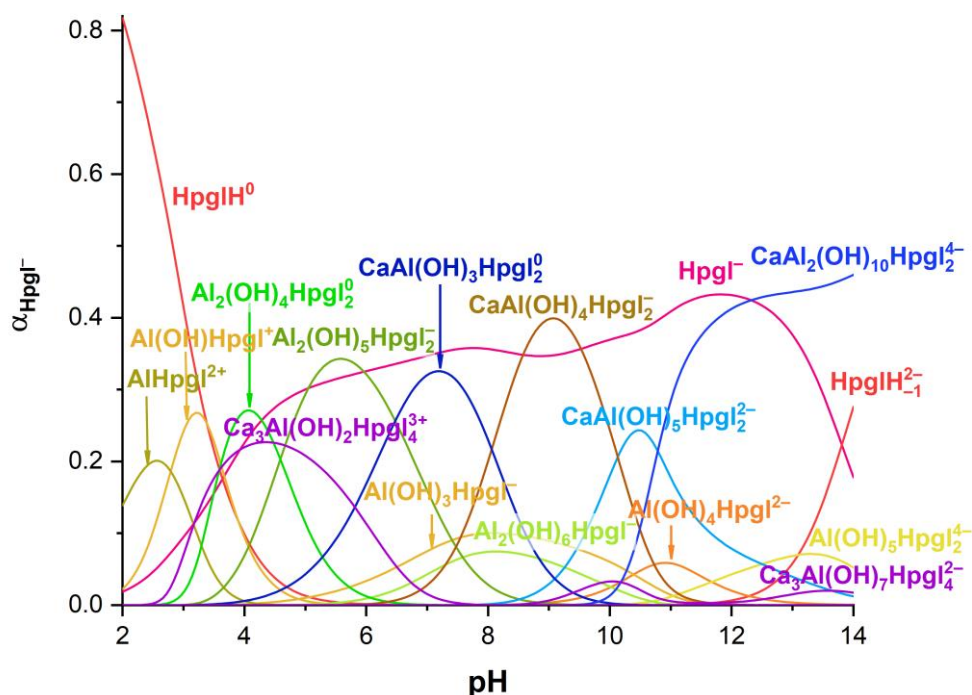


Figure 44 Speciation diagrams as a function of pH regarding to Hpgl^- . The calculations were performed using the stability constants provided in *Table 13*, corresponding to $t = 25^\circ\text{C}$ and $I = 4\text{ M}$ (NaCl). Total concentrations: $[\text{Hpgl}^-]_{\text{T}} = 0.200\text{ M}$, $[\text{Al}(\text{OH})_4^-]_{\text{T}} = 0.100\text{ M}$, $[\text{Ca}^{2+}]_{\text{T}} = 0.050\text{ M}$.

The obtained speciation presented on *Figure 44* indeed demonstrates that ternary complexes are the prevailing ones in the alkaline pH region, although some ternary species (*i.e.*, $\text{Ca}_3\text{Al}(\text{OH})_2\text{Hpgl}_4^{3+}$) do form in the slightly acidic region as well. According to the present model, three major ternary species could be identified, *i.e.*, the $\text{CaAl}(\text{OH})_3\text{Hpgl}_2^0$, $\text{Ca}_3\text{Al}(\text{OH})_2\text{Hpgl}_4^{3+}$ and their deprotonated forms, as well as the $\text{CaAl}_2(\text{OH})_{10}\text{Hpgl}_2^{4-}$ complex dominating the strongly alkaline regime. The formation process of the former could be described by the initial coordination of a Ca^{2+} ion to the binary $\text{Al}(\text{OH})_3\text{Hpgl}^-$ complex, yielding $\text{CaAl}(\text{OH})_3\text{Hpgl}_2^0$. This step is followed by its gradual deprotonation, which ultimately leads to the formation of $\text{CaAl}(\text{OH})_5\text{Hpgl}_2^{2-}$. Regarding the $\text{CaAl}_2(\text{OH})_{10}\text{Hpgl}_2^{4-}$ complex, the substitution of one $\text{Al}(\text{OH})_3$ moiety of the $\text{Al}_3(\text{OH})_{13}\text{Hpgl}_2^{6-}$ binary complex to a Ca^{2+} ion could be a plausible explanation on its formation. Nevertheless, these working hypotheses will need further verification in the future by spectroscopic methods.

In addition, Ca^{2+} -dependent polarimetric and potentiometric measurements were also conducted on solutions containing $\text{Al}(\text{OH})_4^-$ and Hpgl^- ions. Polarimetry proved to be a handy tool in detecting complexes forming in a pH-independent process, thereby giving us a more complete understanding of the speciation. Besides, fitting the acquired data with the already existing model is a simple method for the validation of the speciation.

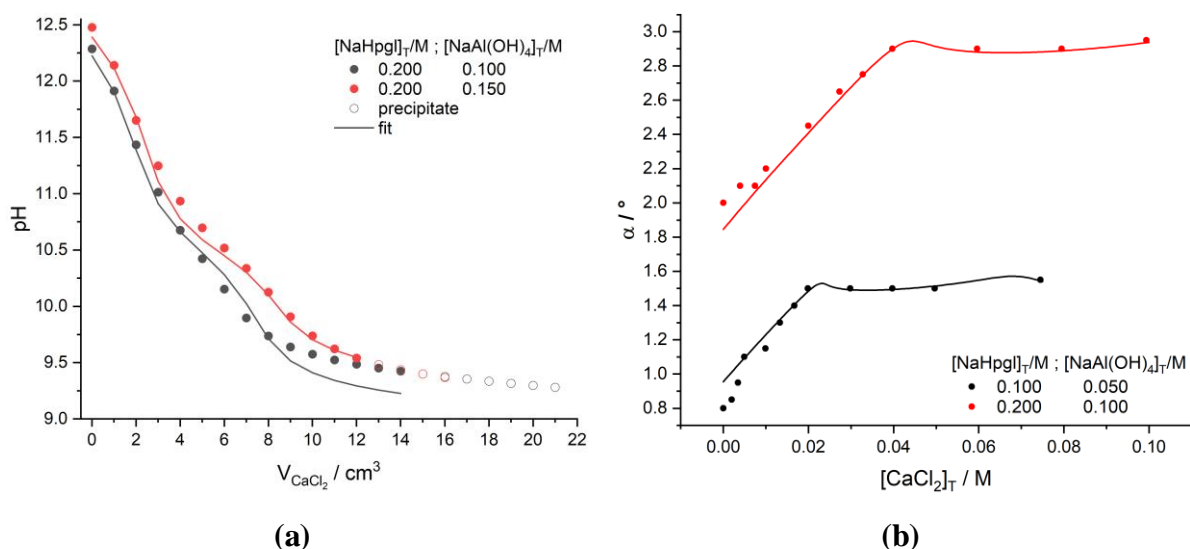


Figure 45 Measured (symbols) and calculated (lines) Ca^{2+} -dependent potentiometric and polarimetric data calculated on the basis of stability constants listed in *Table 13*. Experimental conditions: $t = 25^\circ\text{C}$, $I = 4\text{ M}$ (NaCl) and (a) $[\text{NaOH}]_{\text{T},0} = 0.050$; (b) $[\text{NaOH}]_{\text{T}} = 0.250$. The titrant was 1 M CaCl_2 .

Fitting the Ca^{2+} -dependent data together with the pH-dependent potentiometric data did not introduce additional particles. The recalculation of the model together with these datasets yielded $\text{FP} = 5.34$ and provided only small errors between the measured and calculated data, although a significant deviation could be observed in the initial stage of polarimetry (*Figure 45b*). This error could be attributed to the lack of the $\text{CaAl}(\text{OH})_5\text{Hpgl}^-$ complex, however due to the high correlation with $\text{Ca}_2\text{Al}_2(\text{OH})_{10}\text{Hpgl}_2^{2-}$, both species could not have been included into the final model. Based on this fit, the specific rotations of the corresponding complexes were obtained and are presented in *Table 14*.

Table 14 Specific rotation of the individual species forming in the $\text{Ca}^{2+} / \text{Al}(\text{OH})_4^- / \text{Hpgl}^-$ system. Experimental conditions: $t = (25 \pm 2)^\circ\text{C}$ and $I = 4\text{ M}$ (NaCl). Total concentrations: $[\text{Ca}^{2+}]_{\text{T}} = 0\text{--}100\text{ M}$, $[\text{Al}(\text{OH})_4^-]_{\text{T}} = 0.050\text{--}0.100\text{ M}$ and $[\text{Hpgl}^-]_{\text{T}} = 0.100\text{--}0.200\text{ M}$.

Species	$[\alpha]_{\text{D}} / ^\circ \cdot \text{dm}^{-1} \cdot \text{cm}^3 \cdot \text{g}^{-1}$
$\text{CaAl}(\text{OH})_5\text{Hpgl}_2^{2-}$	-50.30
$\text{CaAl}_2(\text{OH})_{10}\text{Hpgl}_2^{4-}$	45.84
$\text{Ca}_2\text{Al}(\text{OH})_6\text{Hpgl}_2^-$	28.08
$\text{Ca}_3\text{Al}(\text{OH})_7\text{Hpgl}_4^{2-}$	16.65

The effect of ternary complex formation on the ^1H and ^{13}C NMR spectra of heptagluconate

In order to gain information on the preferable metal-ion binding sites of the ligand, ^1H and ^{13}C NMR spectra of heptagluconate at varying $[\text{CaCl}_2]_{\text{T}}$ in the presence and absence of $\text{Al}(\text{OH})_4^-$ were recorded. In solutions containing $[\text{Hpgl}^-]_{\text{T}} = 0.100$ M the signals of heptagluconate go through spectacular changes upon addition of CaCl_2 . With increasing $[\text{Ca}^{2+}]_{\text{T}}$, significant line broadening occurs in the ^1H NMR spectra (Figure 46a), which stems predominantly from the slowdown of the chemical exchange processes between the free and bound ligand molecules. This line broadening is most remarkable for the H2 and H4 signals suggesting the participation of the C(2) H_2OH and C4(2) H_2OH groups in the coordination of Ca^{2+} ions [64,66,101]. As for the ^{13}C NMR spectra (Figure 46b), significant line broadening is seen for all peaks (except for C7), hence the coordination sites cannot be deduced unambiguously. Nevertheless, the C1 signals completely merge into the baseline already at 0.01 M CaCl_2 (see the inset in Figure 46b), supporting the plausible coordination of the COO^- group.

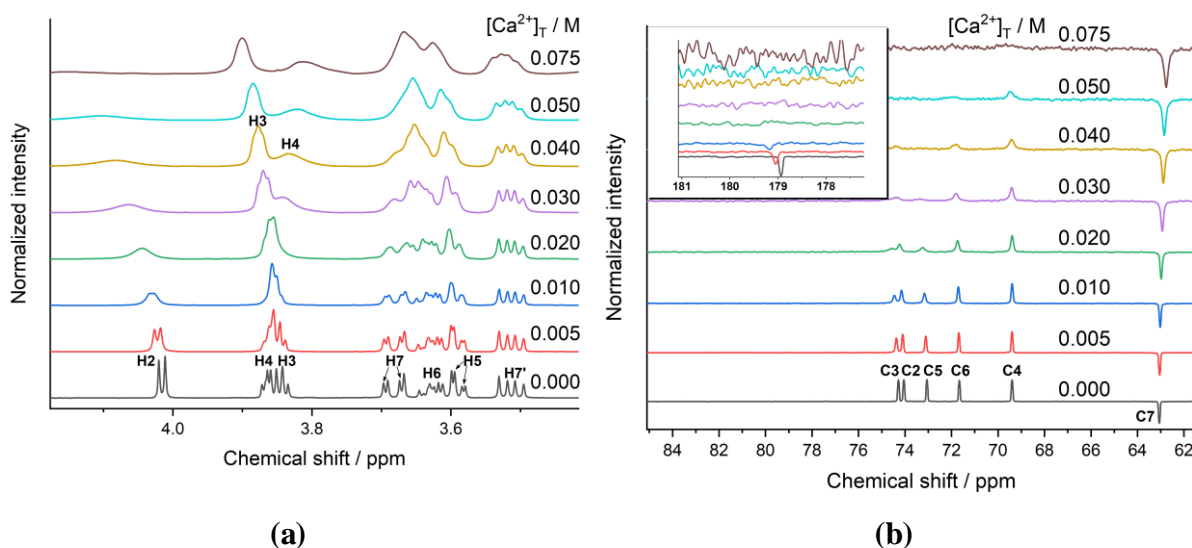
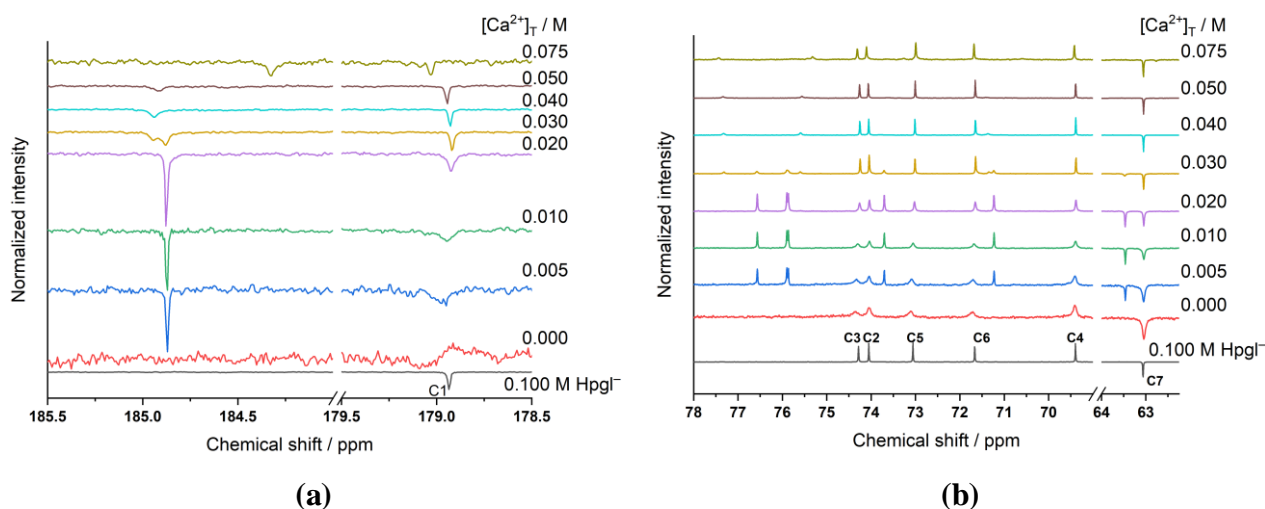


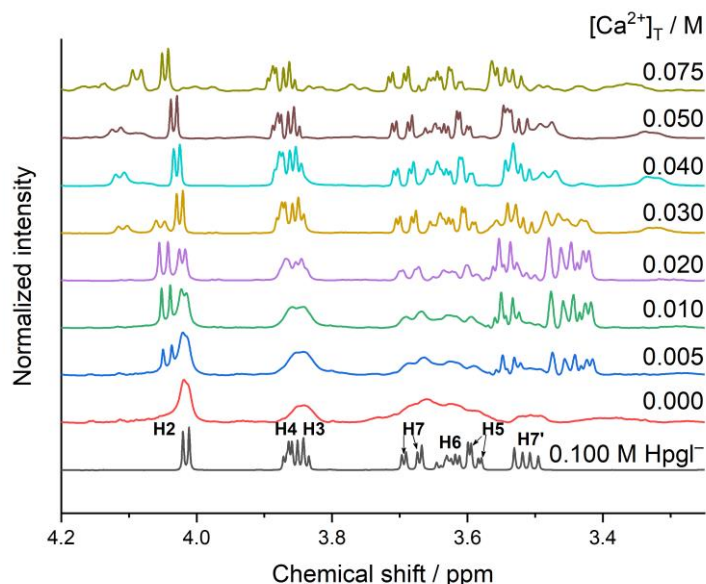
Figure 46 ^1H and ^{13}C NMR spectra of heptagluconate as a function of $[\text{CaCl}_2]_{\text{T}}$. Experimental conditions: $t = 25$ °C, $I = 4$ M (NaCl); $[\text{NaHpgl}]_{\text{T}} = 0.100$ M, $[\text{CaCl}_2]_{\text{T}} = 0 - 0.075$ M, $[\text{NaOH}]_{\text{T}} = 0.255$ M. The appropriate nuclei and their numbering are indicated in the legend.

Conversely, in solutions containing $[\text{NaHpgl}]_{\text{T}} = 0.100$ M and $[\text{Al}(\text{OH})_4^-]_{\text{T}} = 0.050$ M, several new peaks appear with increasing $[\text{Ca}^{2+}]_{\text{T}}$ (Figure 47). These new signals indicate that the chemical exchange becomes even slower on the NMR timescale, than in the case of the binary complexes, which may refer to the strengthening of metal-ligand interactions. According to the speciation based on the stability constants presented in Table 13, the predominant aluminate binary complex is $\text{Al}(\text{OH})_5\text{Hpgl}_2^{4-}$. At this composition, the C1 peak of Hpgl^- could not be identified and the overall signal-to-noise ratio is rather low. However, increasing $[\text{Ca}^{2+}]_{\text{T}}$ only

to 0.005 M, salient changes occur on the spectrum: a distinct peak emerges at 184.8 ppm, which is indicative of a newly forming ternary complex (*Figure 47a*). (Note that this variation cannot be attributed to a binary Ca(II) complex, since the C1 peak is invisible in the absence of aluminate; see the inset in *Figure 46b*.) Likewise, five new peaks appear in the range of 62–78 ppm (*Figure 47b*) as a token of ternary complex formation. Increasing $[\text{Ca}^{2+}]_{\text{T}}$ above 0.030 M, these peaks essentially disappear, while new albeit low-intensity signals show up at 184.9, 184.2, 77.5 and 75.5 ppm signaling the appearance of yet another ternary species. These observations are in line with the qualitative changes seen in the ^1H NMR spectra (*Figure 47c*).

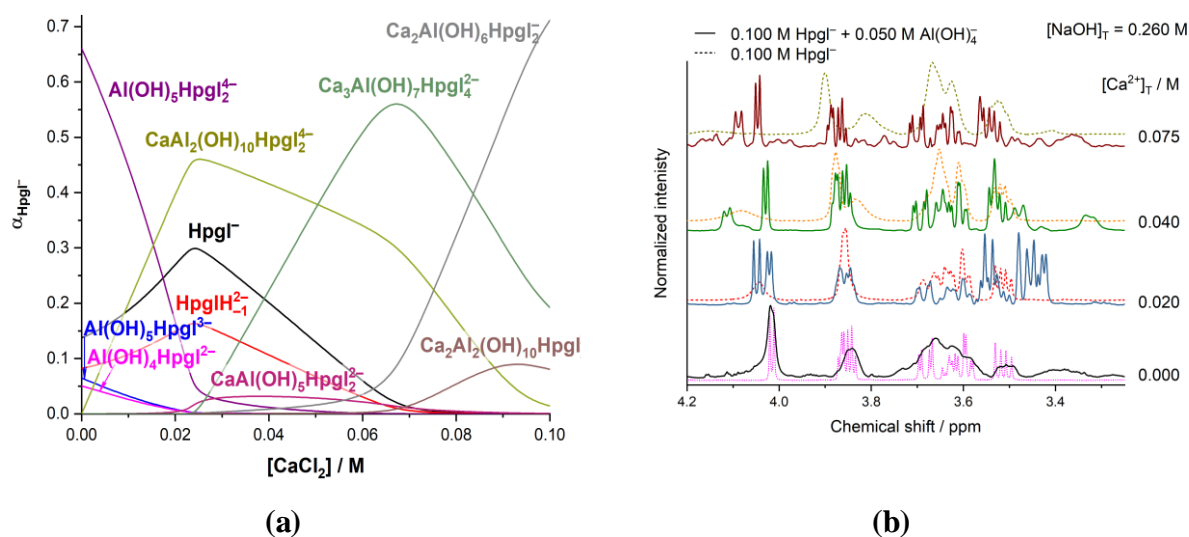
Based on the speciation diagram depicted in *Figure 48*, the new signals can be assigned to the formation of the $\text{CaAl}_2(\text{OH})_{10}\text{Hpgl}_2^{4-}$ ($[\text{CaCl}_2]_{\text{T}} = 0.005\text{--}0.030$ M) and that of the $\text{Ca}_3\text{Al}(\text{OH})_7\text{Hpgl}_4^{2-}$ ($[\text{CaCl}_2]_{\text{T}} = 0.030\text{--}0.075$ M). It is intriguing that the most intensive peaks at the highest $[\text{CaCl}_2]_{\text{T}}$ (0.075 M) strongly resembles those of the free ligand (obvious in both ^1H and ^{13}C spectra), yet the fraction of free Hpgl^- is essentially zero. To resolve this contradiction, one explanation is that the ligand-like spectra actually belong to the $\text{Ca}_2\text{Al}(\text{OH})_6\text{Hpgl}_2^{2-}$ species (see *Figure 48*), which is possibly an anion-stabilized mixed Al(III)-Ca(II) hydroxide, similarly to the Al(III)- Hpgl^- binary system in the pH range of 7–10 (see *Figure 16*). Nevertheless, this interpretation need further verification.





(c)

Figure 47 ^{13}C NMR (a, b) and ^1H (c) and spectra of heptagluconate as a function of $[\text{CaCl}_2]_{\text{T}}$. Experimental conditions: $t = 25\text{ }^\circ\text{C}$, $I = 4\text{ M}$ (NaCl); $[\text{NaHpg}]_{\text{T}} = 0.100\text{ M}$, $[\text{Al}(\text{OH})_4]_{\text{T}} = 0.050\text{ M}$, $[\text{CaCl}_2]_{\text{T}} = 0\text{--}0.075\text{ M}$, $[\text{NaOH}]_{\text{T}} = 0.255\text{ M}$. The appropriate nuclei and their numbering are indicated in the legend.



(a)

(b)

Figure 48 (a) Distribution diagram of Hpgl^- -containing species regarding to $[\text{Ca}^{2+}]_{\text{T}}$ referring to $[\text{Hpgl}^-]_{\text{T}} = 0.100\text{ M}$, $[\text{Al}(\text{OH})_4]_{\text{T}} = 0.050\text{ M}$ and $[\text{NaOH}]_{\text{T}} = 0.260\text{ M}$. The calculations were made based on the stability products presented in Table 13. (b) ^1H NMR spectra of the binary (dashed lines) and ternary (solid lines) complexes of heptagluconate with regard to the increasing $[\text{Ca}^{2+}]_{\text{T}}$. The well distinguishable spectral changes are in line with the simulated speciation.

Equilibria in solutions approaching industrial conditions: The temperature dependence of the calcium complexation properties of D-gluconate

The comprehensive description of the Ca(II)-containing binary systems at elevated temperatures played a pivotal role during our project, since no equilibrium model is useful for industrial purposes without ample information on the solution species under these extreme conditions. Strictly speaking, such type of experimental work would require advanced instrumentation, therefore the valid implementation of necessary analysis would have been quite challenging in a laboratory environment. An elegant way to tackle this obstacle is to determine the thermodynamic properties of the corresponding system, so they could be utilized to extrapolate the distribution model to higher temperatures. In the following section, the temperature-dependent characterization of the calcium-gluconate binary system and the determination of the corresponding enthalpy and entropy changes will be described.

Determination of the ionic product of water at various temperatures – validation of the measuring system

In order to check the robustness of the electrochemical cell and the reliability of the titration protocol used for our measurements, the determination of the ionic product of water (pK_w) at 25, 50 and 75 °C was undertaken.

First, a weak acid-strong base (malonic acid, H_2Mal , vs. NaOH) titration was performed using a H_2/Pt electrode. H_2Mal is available in sufficiently high-purity form, thus, it can be used as primary standard. For the titrations, $[H_2Mal]_{T,0}$ was set to 0.01 M. As a next step, a strong acid-strong base (HCl versus NaOH) titration was carried out with $[HCl]_{T,0}$ being approximately 0.01 M. For both measurements, the titrant was 0.1 M NaOH. The resulted data points were used to determine the exact concentration of the titrant base solution and to estimate its actual carbonate concentration (usually between 0.1 and 0.2 mol% of the base; inevitably, this value was found to gradually increase with time). Additionally, the intercept and slope of the electrode, the pK_w as well as the first and second pK_a of H_2Mal were calculated using the non-linear fitting procedure of the pHCal software. On the other hand, the two acidity constants of H_2CO_3 , corresponding to $t = 25$ °C and $I = 4$ M $[(CH_3)_4NCl]$, were taken from the literature [157]. (It should be noted that the actual value of the acidity constants of H_2CO_3 had only an insignificant effect on the obtained results due to the very low concentration of the carbonate in these calibrating solutions.) Due to experimental difficulties concerning the determination of

pK_a of HCO_3^- and especially that of H_2CO_3 at elevated temperatures, the data corresponding to 25 °C were used at each temperature.

For all the three temperatures, two parallel measurements were performed and the thus obtained six pK_w values (*Figure 49*) were fitted linearly as a function of reciprocal temperature (in K^{-1}) according to the van t' Hoff equation:

$$\ln K = -\frac{\Delta H}{RT} + \frac{\Delta S}{R} \quad (31)$$

The standard enthalpy and entropy of reaction **32** were directly determined from the intercept and slope of the fitted line.



The results of these calculations are presented in *Table 15*. The pK_w versus T^{-1} relation showed good linearity, demonstrated by the value of the correlation coefficient, R^2 (0.9963). The accepted values of pK_w (*Table 15*) were then obtained via recalculating them from the ΔH and ΔS parameters.

At 25 °C, the pK_w was found to be 14.26, which agrees well with 14.29 [129], which was determined previously with similar methodology under the same experimental conditions. The corresponding ΔH and ΔS values were determined to be $-56 \text{ kJ} \cdot \text{mol}^{-1}$ and $85 \text{ J} \cdot \text{mol}^{-1} \cdot \text{K}^{-1}$, respectively. These values are in satisfactory agreement with the ones reported in the literature ($\Delta H = -55.8 \text{ kJ} \cdot \text{mol}^{-1}$ and $\Delta S = 80.8 \text{ J} \cdot \text{mol}^{-1} \cdot \text{K}^{-1}$), which led us to the conclusion, these pK_w determination experiments could be considered as validation of the experimental protocol.

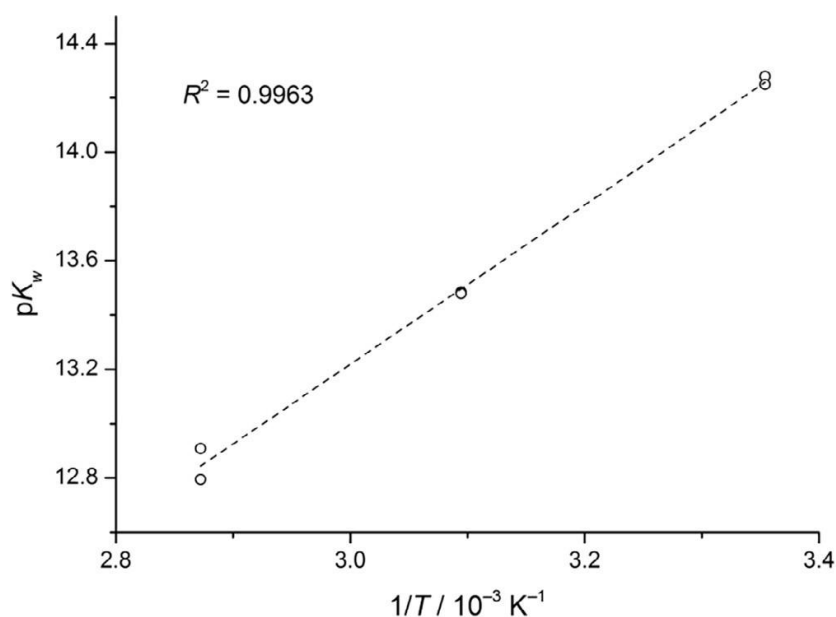


Figure 49 The ionic product of water, pK_w , as a function of $1/T$ at $I = 4 \text{ M}$ (NaCl). The results of linear fitting are depicted as dashed line.

Table 15 Stability constants, standard enthalpies and entropies determined for the various reactions taking place in the $\text{Ca}^{2+}/\text{Gluc}^-/\text{OH}^-$ system. Experimental conditions: $t = 25, 50$ or 75 °C, $I = 4$ M (NaCl). In parentheses, the triple standard error is given.

Reaction	T / °C	$\log \beta_{\text{prs}}$	ΔH / $\text{kJ} \cdot \text{mol}^{-1}$	ΔS / $\text{J} \cdot \text{mol}^{-1} \cdot \text{K}^{-1}$	
$\text{H}_3\text{O}^+ + \text{OH}^- \rightleftharpoons 2\text{H}_2\text{O}$	25	14.28(7)	-56(5)	85(15)	
		14.25(5)			
		14.26 [†]			
	50	13.48(7)			
		13.48(5)			
		13.50 [†]			
	75	12.80(5)			
		12.91(5)			
		12.84 [†]			
$\text{Gluc}^- + \text{H}_2\text{O} \rightleftharpoons \text{GlucH}_{-1}^{2-} + \text{H}_3\text{O}^+$	25	-14.08(3)	57(1)	-79(4)	
		-13.90(3) [‡]			
		-13.32(3)			
50	-12.65(2)				
	75	-28.82(2)			
		25	-13.92 [*]	68(5) [*]	
50			-12.99 [*]		
75	-12.20 [*]				
$\text{Ca}(\text{H}_2\text{O})_x + \text{H}_2\text{O} \rightleftharpoons \text{Ca}(\text{H}_2\text{O})_{x-1}(\text{OH})^+ + \text{H}_3\text{O}^+$	25	-27.64 [*]	126(10) [*]		
		50		-25.94 [*]	
		75		-24.45 [*]	
$\text{Ca}(\text{H}_2\text{O})_x + 2\text{H}_2\text{O} \rightleftharpoons \text{Ca}(\text{H}_2\text{O})_{x-2}(\text{OH})_2^0 + 2\text{H}_3\text{O}^+$	25	-11.73(3)	45(7)	-73(23)	
		50			-11.17(3)
		75			-10.59(3)
$\text{Ca}^{2+} + \text{Gluc}^- + \text{H}_2\text{O} \rightleftharpoons \text{CaGlucH}_{-1}^0 + \text{H}_3\text{O}^+$	25	-46.54(3)	184(23)	-276(70)	
		50			-44.21(5)
		75			-41.91(22)
$2\text{Ca}^{2+} + 2\text{Gluc}^- + 4\text{H}_2\text{O} \rightleftharpoons \text{Ca}_2\text{Gluc}_2\text{H}_{-4}^{2-} + 4\text{H}_3\text{O}^+$	25	-43.80(3)	193(6)	-193(18)	
		50			-41.23(2)
		75			-38.95(3)

[†] These constants were recalculated from the corresponding ΔH and ΔS parameters and then were used to determine the stability products of the various $\text{Ca}_p\text{Gluc}_r\text{H}_s^{(2p-r+s)+}$ species.

[‡] These constants were determined by ^{13}C NMR spectroscopy (the others by potentiometry).

^{*} These constants were calculated from the $\text{p}K_w$ values given here and from the ΔH parameters reported in Ref. [95].

^{*} These parameters were obtained from the ΔH of neutralization given here and from the ΔH parameters reported in Ref. [95].

The Ca²⁺ complexation of gluconate ions in strongly alkaline solutions on elevated temperatures

Upon comparison, the titrations performed at 50 °C and 75 °C resulted in nearly identical titration curves as observed at 25 °C (see *Figures 11* and *50*). However, the pH range where the system was homogenous significantly shrank. (As a result, the CaCl₂-dependence of the titration curves could not be studied at 75 °C). The incidental precipitation of Ca(OH)₂ would be a plausible explanation for that, since its solubility product greatly decreases with increasing temperature [95], although the X-ray diffractogram taken for the precipitate indicated the formation of an amorphous phase, which will be discussed later. The determination of the stability constants and speciation was performed using the same boundary conditions as discussed before (see the discussion on *page 32*). The thus obtained values for the different complexation reaction are shown in *Table 15*.

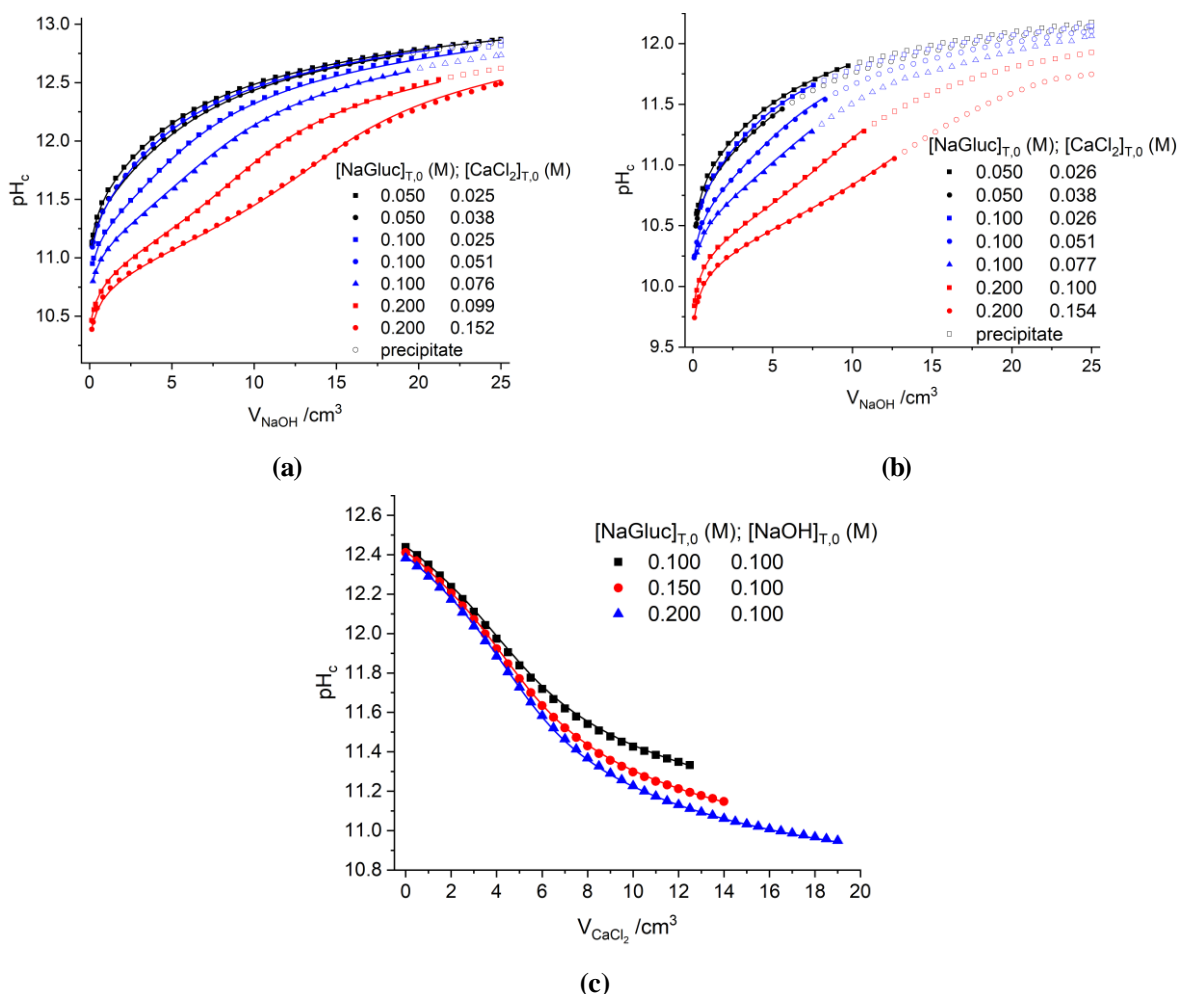


Figure 50 Measured (symbols) and calculated (lines) pH for gluconate (Gluc⁻) in presence of CaCl₂ and NaOH. Experimental conditions: **(a and c)** *t* = 50 °C, *I* = 4 M (NaCl), **(b)** *t* = 75 °C, *I* = 4 M (NaCl); **(a and b)** [NaOH]_{T,0} = 0.005 M, **(c)** [NaOH]_{T,0} = 0.100 M . The titrants were 1 M NaOH **(a, b)** and 1 M CaCl₂ **(c)**.

In the next step, the distributions of Ca(II) among free Ca^{2+} and the different Ca(II) complexes were compared at 25, 50 and 75 °C. It is important to mention that the overall pH scale is rather different at different temperatures due to the temperature-dependence of pK_w , therefore, $[\text{NaOH}]_T$ was chosen as independent variable for a reliable comparison of the species distributions. Between $[\text{NaOH}]_T = 0.01$ and 0.15 M (where the system was homogenous at each temperature), the speciation remains practically unaltered regardless of the temperature (*Figure 51*).

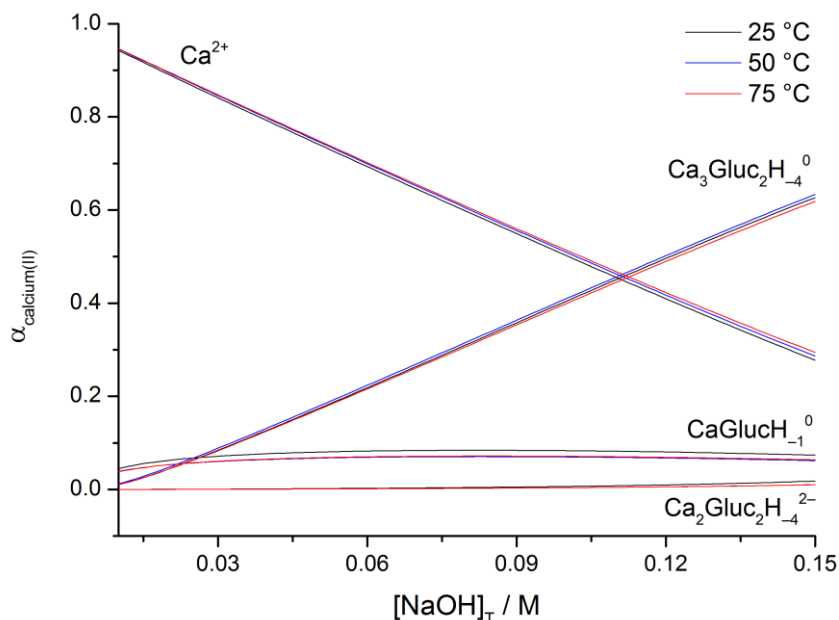


Figure 51 Distribution of calcium(II) among the various aqueous species in the presence of gluconate (Gluc^-) as a function of pH. The calculations correspond to $t = 25\text{--}75$ °C, $I = 4$ M (NaCl); $[\text{NaGluc}]_T = 0.200$ M and $[\text{CaCl}_2]_T = 0.150$ M. Calculations were performed by using the stability constants given in *Table 15*.

As in the case of the deprotonation constants, the enthalpy and entropy of these complex formation reactions (*Equation 8, page 22*) were also determined. The results are shown in *Table 15* and presented graphically in *Figure 52*. Generally, the deprotonation and Ca(II) complexation reactions of Gluc^- are all enthalpy-driven. It can also be deduced that the Ca^{2+} binding of GlucH_{-1}^{2-} described in the following reaction:



is an exothermic process with ΔH being $-12(8)$ $\text{kJ}\cdot\text{mol}^{-1}$. Conversely, the Ca^{2+} abstraction of the $\text{Ca}_2\text{Gluc}_2\text{H}_{-4}^{2-}$ complex (*Equation 21, see page 31*) is accompanied with $\Delta H \approx 0$. (Numerically, it is $9(24)$ $\text{kJ}\cdot\text{mol}^{-1}$, but the corresponding standard error is too high to consider this process endothermic.)

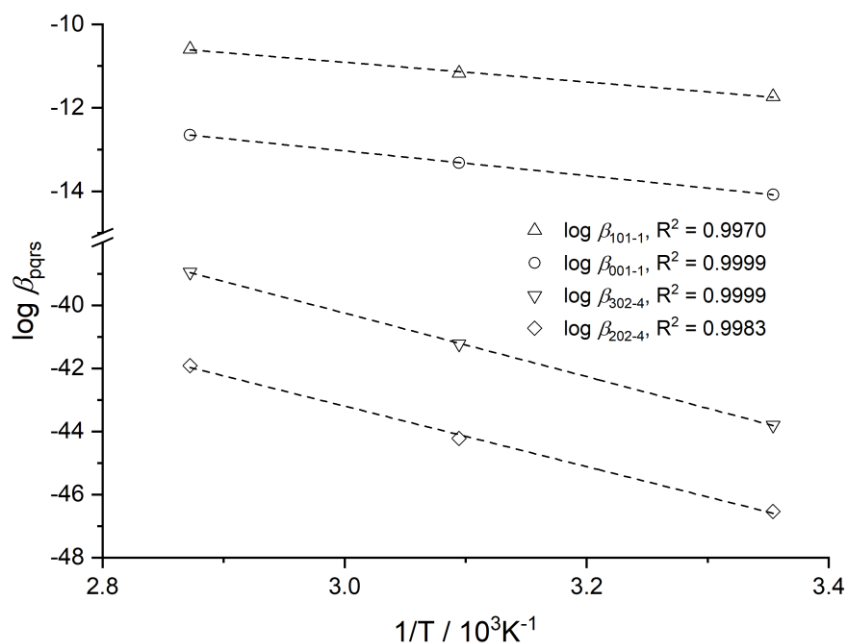


Figure 52 The deprotonation constant ($\log \beta_{001-1}$) of gluconate (Gluc) as well as the $\log \beta_{pqrs}$ stability products of the various $\text{Ca}_p\text{Gluc}_r\text{H}_s^{(2p-r+s)+}$ species as a function of $1/T$ at $I = 4 \text{ M}$ (NaCl). The results of linear fitting are depicted as dashed lines, and the calculated R^2 values are indicated in the legend.

To assess the effect of Gluc^- on the solubility of $\text{Ca}(\text{OH})_2$ under the conditions of the Bayer process [7,8,158], model calculations were performed. To take hetero- and homogenous equilibria into consideration simultaneously, the solubility product of $\text{Ca}(\text{OH})_2$ was taken from Ref. [95]. Using the enthalpies and entropies given in *Table 15* and in Ref. [95], all equilibrium constants corresponding to 100 °C were calculated. The variation in the solubility of calcium(II) is demonstrated in *Figure 53*. It is clearly seen that NaGluc has considerable impact on the concentration of dissolved calcium(II) in the whole range of $[\text{OH}^-]$ (0.01–2.51 M). At $[\text{OH}^-] = 1 \text{ M}$, the increase of $[\text{Ca}^{2+}]_T$ relative to that of the gluconate-free system is 10%, 23% and 76% at $[\text{Gluc}]_T = 0.03, 0.05$ and 0.10 M , respectively. In conclusion, the dissolution of $\text{Ca}(\text{OH})_2$ is significantly enhanced by the addition of NaGluc (as a model of organic contaminants) in agreement with previous results [7,8,158].

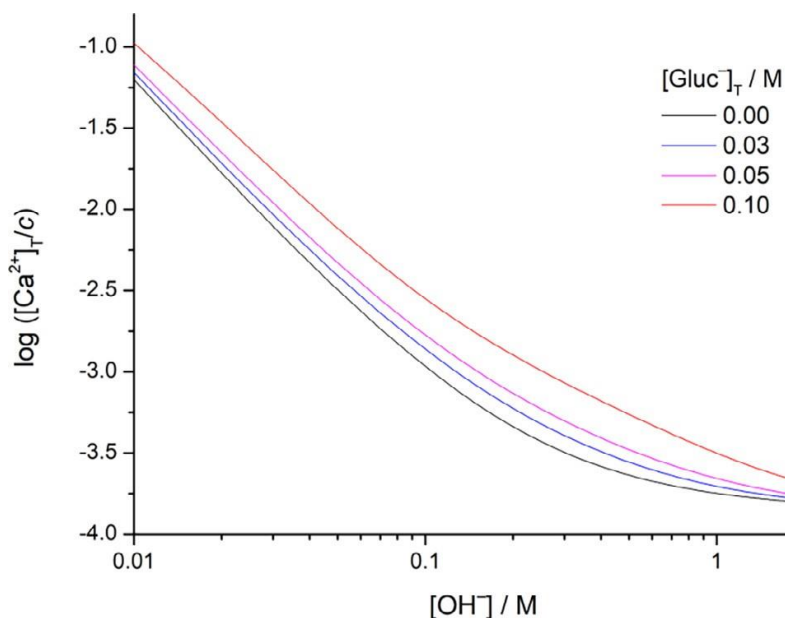


Figure 53 The solubility of calcium(II), $\log ([\text{Ca}^{2+}]_{\text{T}}/c)$, as a function of $[\text{OH}^-]$. The calculations correspond to $T = 100\text{ }^\circ\text{C}$, $I = 4\text{ M}$ (NaCl) and $[\text{NaGluc}]_{\text{T}} = 0\text{--}0.10\text{ M}$. The simulations were performed by using the $\log \beta_{\text{pqs}}$ stability products of the $\text{Ca}_p\text{Gluc}_r\text{H}_s^{(2p-r+s)+}$ complexes, the $\log K_{\text{sp}}$ solubility product of $\text{Ca}(\text{OH})_2$, and the corresponding ΔH and ΔS parameters given in *Table 15* and in Ref. [95].

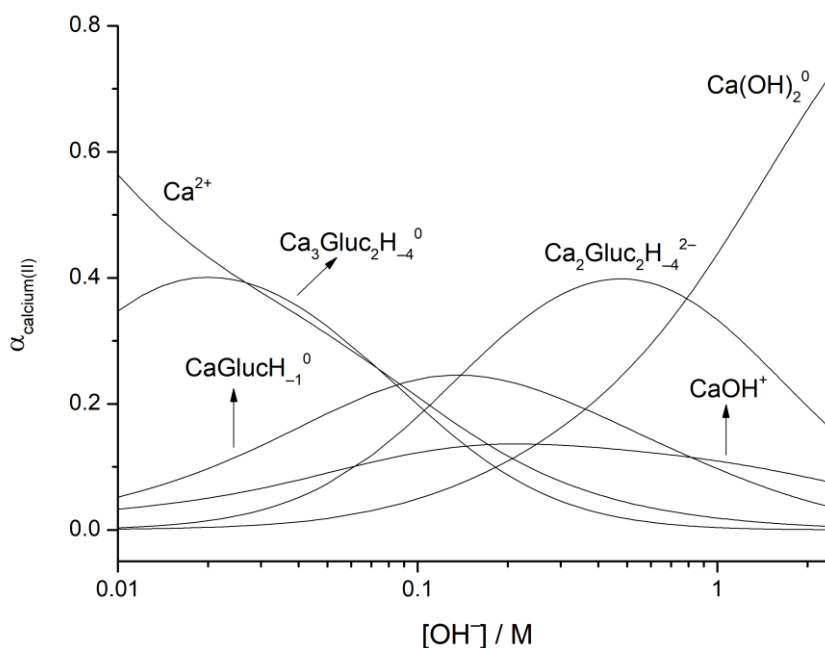


Figure 54 Distribution of calcium(II) among the various aqueous species in the presence of gluconate (Gluc^-) and $\text{Ca}(\text{OH})_2(\text{s})$ as a function of $[\text{OH}^-]$. The calculations correspond to $T = 100\text{ }^\circ\text{C}$, $I = 4\text{ M}$ (NaCl) and $[\text{NaGluc}]_{\text{T}} = 0.10\text{ M}$. The simulations were performed by using the $\log \beta_{\text{pqs}}$ stability products of the $\text{Ca}_p\text{Gluc}_r\text{H}_s^{(2p-r+s)+}$ complexes, the $\log K_{\text{sp}}$ solubility product of $\text{Ca}(\text{OH})_2$ and the corresponding ΔH and ΔS parameters given in *Table 15* and in Ref. [159].

Interestingly, the gluconate-containing Ca(II) complexes are formed to a high extent at $[\text{NaGluc}]_{\text{T}} = 0.1 \text{ M}$ even in the presence of a solubility-controlling solid phase (*Figure 54*). At $[\text{OH}^-] \approx 0.02 \text{ M}$, about 40% of $[\text{Ca}^{2+}]_{\text{T}}$ is present as $\text{Ca}_3\text{Gluc}_2(\text{OH})_4^0$, while the same fraction of $\text{Ca}_2\text{Gluc}_2(\text{OH})_4^{2-}$ is formed at $[\text{OH}^-] \approx 0.5 \text{ M}$. As the pH increases further, the $\text{Ca}(\text{OH})_2^0$ aqueous species becomes predominant.

Characterization of the solid phase forming at high temperature

As discussed above, the number of experimental points decreased to a large extent owing to the precipitate forming in the titrated solutions at $75 \text{ }^\circ\text{C}$. Although the explanation, that the K_{sp} of $\text{Ca}(\text{OH})_2$ of calcium hydroxide decreases with increasing temperature, seemed plausible, the fact that complexes with zero net charge tend to precipitate must have been considered.

First, XRD measurements were performed on the samples (*Figure 55*). Comparing the diffractograms of the sample with those of the reference materials, the lack of distinct reflections – which are typical of NaGluc, NaCl, $\text{Ca}(\text{OH})_2$ or CaCl_2 – indicated an amorphous structure, possibly indicating some kind of reaction between the metal and the ligand.

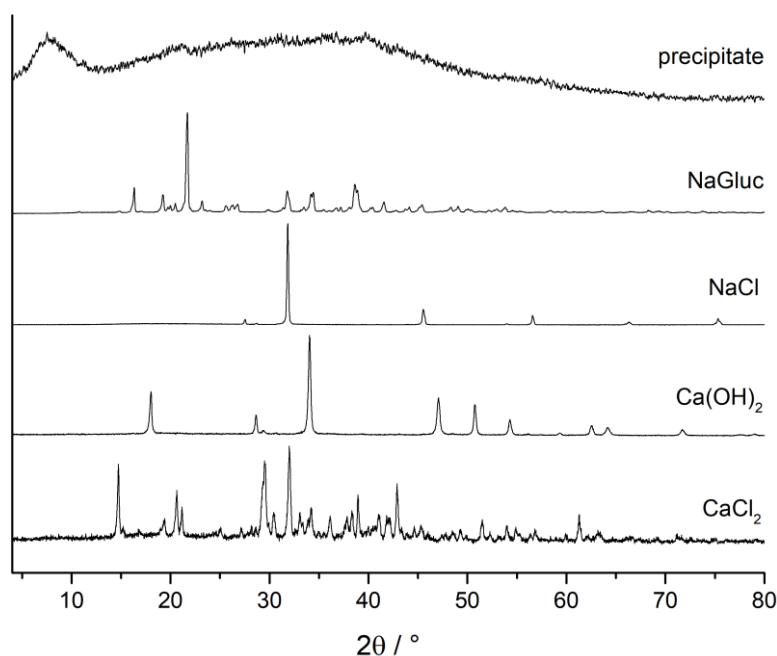


Figure 55 Diffractogram of the precipitate obtained from pH potentiometry (upper trace), in comparison with the solution-forming materials. The sample was prepared at $t = 75 \text{ }^\circ\text{C}$ and $I = 4 \text{ M}$ (NaCl) by titrating the solution containing $[\text{NaGluc}]_{\text{T},0} = 0.15 \text{ M}$ and $[\text{CaCl}_2]_{\text{T},0} = 0.10 \text{ M}$ with 1 M NaOH .

To verify this assumption, the FT-IR spectra of the precipitate and the Na-salt of the ligand were recorded (*Figure 56*). The comparison of the two spectra revealed that the amorphous

precipitate contained gluconate. The sharp O–H stretching vibrations (from 3250 cm^{-1} to 3500 cm^{-1}) of the plain ligand indicates that the coordination of the OH groups is weak. Regarding the precipitate, conversely, the broadened signal in the same region implies the coordination of OH groups. Such broadening was observed for the gluconate complexes of numerous divalent metal ions including Ca^{2+} [160,161]. Concerning the region of carbonyl vibrations of NaGluc (from 1350 cm^{-1} to 1650 cm^{-1}), the two peaks at 1633 cm^{-1} and 1597 cm^{-1} (presumably the two components of the asymmetric stretching vibrations of the COO^- group) shifted towards lower wavenumbers (to 1558 cm^{-1}) in the case of the Ca(II) complex. For Ca^{2+} -binding proteins, a shift of 10–25 cm^{-1} was attributed to the binding of Ca^{2+} [162]. In the present case, the shift is at least 40 cm^{-1} referring to strong metal ion coordination.

Furthermore, the difference between the peaks of the asymmetric and symmetric vibrations is an indicative of the probable coordination mode [163]. That is, the difference for NaGluc (200–235 cm^{-1}) refers to monodentate, whereas that for the Ca(II) complex (160 cm^{-1}) points to the bridging-type binding mode (each oxygen of the COO^- group is bound in a monodentate manner to a Ca^{2+} ion). Additionally, the signal with 1550 cm^{-1} has been attributed to the bridging-type coordination of the COO^- group in the stearate and oleate salts of calcium(II) [164].

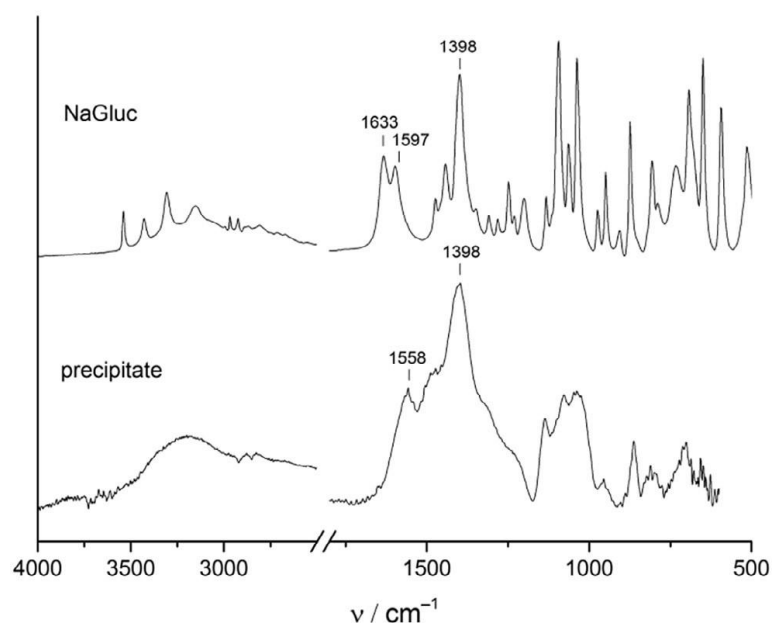


Figure 56 Infrared spectra of the precipitate obtained during the pH potentiometric titrations, in comparison with that of sodium gluconate (NaGluc). The sample was prepared at $t = 75\text{ }^{\circ}\text{C}$ and $I = 4\text{ M}$ (NaCl) by titrating the solution containing $[\text{NaGluc}]_{\text{T},0} = 0.15\text{ M}$ and $[\text{CaCl}_2]_{\text{T},0} = 0.10\text{ M}$ with 1 M NaOH. The positions of the symmetric (1398 cm^{-1}) and the asymmetric ($>1550\text{ cm}^{-1}$) stretching vibrations are indicated.

Finally, an attempt was made to derive the stoichiometry of the solid complex by using ICP-OES measurements. From the species distribution diagrams corresponding to 75 °C, the predominant complex in aqueous solution is the neutral $\text{Ca}_3\text{Gluc}_2\text{H}_4^0$, thus, this complex was expected to precipitate. From the ICP results and assuming that the remaining mass after subtracting the mass of Ca^{2+} is purely gluconate, the molar ratio of Ca^{2+} and Gluc^- was found to be approximately 3:2. For the trinuclear complex, two possible compositions with the same molar mass can be envisaged. In the first case, the formula of the species can be described as $\text{Ca}_3(\text{GlucH}_{-2})_2 \cdot 2\text{H}_2\text{O}(s)$, where the association of two double deprotonated gluconate and two water molecules takes place (beside calcium). Second, the combination of two single deprotonated ligands and two OH moieties, resulting in $\text{Ca}_3(\text{GlucH}_{-1})_2(\text{OH})_2(s)$, is also a plausible scenario. Using these two complex compositions, the aforementioned composition of the complex, the calculated mass of the sample from measured calcium(II) concentration agreed with the original mass of the sample within 1.1%. Overall, these measurements confirmed that the solid precipitate is the trinuclear complex, which lends credit to the proposed speciation model in the solution phase.

Conclusion

In this work, an extensive investigation was conducted on the complex formation reactions of calcium and aluminate with D-heptagluconate ions at high ionic strength and in strongly alkaline aqueous solutions. Furthermore, the temperature dependence of the interactions between Ca^{2+} and Gluc^- was studied to assess the speciation under conditions relevant to the Bayer process. Finally, the characterization of the structural and thermal properties of the solid phase forming in the $\text{Ca}^{2+} / \text{Al}(\text{OH})_4^- / \text{Hpgl}^-$ system was carried out employing a wide range of experimental methods.

In strongly alkaline solutions sugar carboxylates undergo deprotonation involving their alcoholic OH groups. However, it was found *via* ^{13}C NMR studies, that Gluc^- could undergo two consecutive deprotonation steps, yielding GlucH_{-1}^{2-} and GlucH_{-2}^{3-} particles. Although the formation of the latter was only around $\approx 30\%$, the existence of this species was proved by matrix-rank analysis as an independent method.

Upon the introduction of Ca^{2+} ions, Gluc^- and Hpgl^- form high stability polynuclear complexes in alkaline media. Slight changes in the speciation were found with the increasing ionic strength for both ligands: for Gluc^- the complex $\text{Ca}_2\text{Gluc}(\text{OH})_3^0$ was interchangeable with $\text{Ca}_2\text{Gluc}_2(\text{OH})_4^{2-}$, which yielded lower standard deviation on 4 M (NaCl) ionic strength. As for Hpgl^- , $\text{CaHpgl}(\text{OH})^0$ could not be fitted, instead it was replaced by the $\text{Ca}_3\text{Hpgl}_2(\text{OH})_3^+$. Therefore, the composition and stability products of polynuclear calcium complexes was found to be slightly dependent on the ionic strength, *i.e.*, it apparently facilitates the formation of charged species.

The interactions between aluminate and heptagluconate ions were studied in a broad pH range to get a sound understanding of the speciation of the system. Potentiometric titrations revealed the formation of several hitherto unknown species in the alkaline pH region, greatly extending the speciation models published earlier in the literature. The mononuclear 1:1 complex undergoes gradual protonation, while the species $\text{Al}(\text{OH})_2\text{Hpgl}^-$ could interact with additional two aluminate ions, forming complexes with 2:1 and even 3:1 composition. Polarimetry confirmed our calculated model and further broadened the speciation by the inclusion of $\text{Al}_3(\text{OH})_{13}\text{Hpgl}_2^{6-}$ and $\text{Al}_4(\text{OH})_{15}\text{Hpgl}_3^{6-}$ particles, both forming in the alkaline region.

To provide qualitative insights on the Al-binding sites of the ligand, ^1H and ^{13}C NMR experiments were conducted on pH = 4, 8 and 12. At pH = 4, the increase of ^1H signal FWHM

of C2-OH, C3-OH and C4-OH, as well as the drop of relative intensities of corresponding ^{13}C signals together with C5-OH outlined their vital role, as binding sites for aluminate coordination. Based on the spectra recorded at $\text{pH} = 8$, the species forming at neutral medium are ligand stabilized hydroxides. This proposition was supported by semi-quantitative solubility simulations, which showed, that in the pH range of 6 to 11 the total concentrations of Al^{3+} and OH^- ions exceeded the solubility product of $\text{Al}(\text{OH})_3(\text{s})$, yet no precipitation could be observed in the presence of heptagluconate ions. In alkaline solutions, the complexation proved to a slow process, thus being commensurate with the exchange rate of the free and bound ligand, which yielded numerous new peaks on the spectra. These signals could either belong to the coordination isomers of $\text{Al}(\text{OH})_4\text{Hpgl}^{2-}$ or the polynuclear $\text{Al}_4(\text{OH})_{15}\text{Hpgl}_3^{6-}$ complexes.

The calculated model was validated by freezing point depression (FPD) determinations and with ESI-MS experiments. FPD measurements indicated a large extent of association in solutions containing both aluminate and heptagluconate. Furthermore, the simulated $\Delta T_{f,\text{calc}}$ values, based on the speciation data, were in good agreement with the measured effect. ESI-MS studies confirmed the existence of the 2:1 species at $\text{pH} = 7$ and provided indirect information of its coordination mode as well.

The solid phases obtained from solutions containing Ca^{2+} , Al^{3+} and Hpgl^- ions, were characterized with various experimental methods. XRD and SEM-EDX measurements revealed, that these compounds have a low degree of crystallinity, homogeneous elemental distribution, and a significantly different morphology, than those of the commercially available Hpgl^- salts.

According to the results of UV-Vis and ICP-OES measurements, two types of complexes could be distinguished: $\text{CaAlHpgl}(\text{OH})_4^0$ along with $\text{Ca}_2\text{AlHpgl}_2(\text{OH})_5^0$ forms above $n_{\text{OH}}/n_{\text{Hpgl}} = 1.0$, while below the more uniform $\text{Ca}_3\text{Al}_2\text{Hpgl}_3(\text{OH})_9^0$ stoichiometry can be proposed. The latter strongly resembles to the composition of $\text{Ca}_3\text{Al}_2(\text{OH})_{12}$ (tricalcium aluminate, TCA), which explains the similar IR spectra published for the reaction of TCA with Gluc^- earlier. Regarding the binary complexes, the formation of $\text{Al}_3\text{Hpgl}(\text{OH})_8^0$ and various mixed Ca-containing binary complexes was invoked.

FT-IR and Raman spectroscopic measurements reinforced our assumption regarding the two different groups of complexes. Fourier self-deconvolution of the individual carboxylate bands of the complexes assumes different coordination to Ca^{2+} and Al^{3+} ions in the ternary and binary particles. Furthermore, the centrally symmetric arrangement of ligands around the metal ion was inferred from the positions of the fitted antisymmetric carboxylate stretching bands.

Based on the thermal analysis of the commercially available salts of heptagluconate along with the binary- and ternary complexes, the increased stability of the latter two was observed. This stability was the highest in case of ternary complexes, which was attributed to the simultaneous binding of both metal ions to the ligand(s).

Concerning the interactions of heptagluconate with Ca^{2+} and $\text{Al}(\text{OH})_4^-$ in strongly alkaline medium, the formation of ternary complexes was unambiguously detected by pH-potentiometry and polarimetry. It was found that ternary complexes typically start to form in the pH range of 8 to 14, while below pH = 8 the inclusion of binary complexes was adequate to describe the solution equilibria. Besides the various protonated forms of the $\text{CaAl}(\text{OH})_4\text{Hpgl}_2^-$ species, a plethora of other species with more complex compositions was detected with 1:2:2, 2:1:2, 2:2:2 and even 3:1:4 stoichiometries.

The ^1H and ^{13}C NMR spectra of heptagluconate in presence of Ca^{2+} and $\text{Al}(\text{OH})_4^-$ ions were also recorded in alkaline media. The rate of complex formation in the ternary solutions was found to be even slower, than that observed in case of the $\text{Al}(\text{OH})_4^- / \text{Hpgl}^-$ system, which yielded a plenty of distinct peaks on the spectra. According to the Ca^{2+} -dependent NMR series, at least three different ternary complexes could be inferred, which lined up well with the simulated distribution diagrams.

To approach industrially relevant conditions, the effect of elevated temperature and high ionic strength on the speciation was assessed for the $\text{Ca}^{2+} / \text{Gluc}^-$ system. It was found that the speciation is not significantly affected by the increasing temperature. Fitting the corresponding stability constants for each species using the van't Hoff equation, the ΔH and ΔS values for the individual complex forming reactions could be calculated. According to the calculated results, the formation of the CaGlucH_{-1}^0 is less endothermic than that of GlucH_{-1}^{2-} , which means that Gluc^- undergoes deprotonation more readily in the presence of Ca^{2+} ions.

Finally, the distribution of Ca^{2+} among the various aqueous species in gluconate and $\text{Ca}(\text{OH})_2(\text{s})$ containing solutions was extrapolated to $t = 100\text{ }^\circ\text{C}$, using the previously calculated thermodynamic constants.

Összefoglalás

Munkánk során a D-heptaglükonát ion kalcium és alumínát ionokkal való komplexképződési egyensúlyait tanulmányoztuk nagy ionerősségű erősen lúgos oldatokban. Megvizsgáltuk a Ca^{2+} és Gluc^- ionok közötti kölcsönhatások hőmérsékletfüggését, amely eredmények segítségével közelíteni tudtuk a részecskeeloszlást a Bayer folyamatra jellemző körülmények között. Az oldatfázis mellett a $\text{Ca}^{2+} / \text{Al}(\text{OH})_4^- / \text{Hpgl}^-$ rendszerben képződő szilárd fázis átfogó analízise is céljaink között szerepelt.

A cukorsavak alkoholos OH csoportjai erősen lúgos közegben hajlamosak a deprotonálódásra. Mindazonáltal, a Gluc^- ion esetében ^{13}C NMR mérések alapján megfigyelhető volt a ligandum két lépésben történő deprotonálódása, ezáltal a GlucH_1^{2-} és GlucH_2^{3-} részecskék képződése. Habár utóbbi részecske képződésének mértéke csak $\approx 30\%$ körüli volt, ugyanakkor a független mátrix-rang analízis bebizonyította a jelenlétét.

Ca^{2+} ionok hozzáadására lúgos közegben mind a Gluc^- , mind pedig a Hpgl^- esetében nagy stabilitású többmagvú komplexképződés figyelhető meg. Mindkét ligandum esetében a megnövelt ionerősség hatására kismértékű eltérést észleltünk a részecskeeloszlásban: a Gluc^- esetében a $\text{Ca}_2\text{Gluc}(\text{OH})_3^0$ összetételű részecske helyettesíthetőnek bizonyult a $\text{Ca}_2\text{Gluc}_2(\text{OH})_4^{2-}$ komplexszel, amely így kisebb illesztési hibát eredményezett 4 M (NaCl) közegben. A Hpgl^- esetében a $\text{CaHpgl}(\text{OH})^0$ részecske helyét a $\text{Ca}_3\text{Hpgl}_2(\text{OH})_3^+$ vette át, így megállapítottuk, hogy a többmagvú kalciumkomplexek stabilitása és képződése enyhén ionerősségfüggő, azaz a megnövelt ionerősség elősegíti a többmagvú, töltéssel bíró részecskék képződését.

Az alumínát és heptaglükonát ionok közötti kölcsönhatásokat széles (2–14) pH-tartományban tanulmányoztuk. A potenciometriás titrálások eredményei alapján számos lúgos közegben képződő, eddig ismeretlen oldatbeli részecske képződését detektáltuk, így árnyalva az e területen eddig közölt részecskeeloszlási modelleket. Az egymagvú, 1:1 összetételű komplex fokozatosan protonálódik, míg az $\text{Al}(\text{OH})_2\text{Hpgl}^-$ részecske további két alumínát ionnal is kölcsönhatást létesíthet, így 2:1 vagy akár 3:1 összetételű komplexek képződésére is lehetőség nyílik. A polarimetriás mérések megerősítették az általunk javasolt modellt, továbbá az $\text{Al}_3(\text{OH})_{13}\text{Hpgl}_2^{6-}$ és $\text{Al}_4(\text{OH})_{15}\text{Hpgl}_3^{6-}$ részecskék detektálásával tisztább képet szolgáltatott a lúgos közegben képződő részecskékről.

A ligandum kötőhelyeinek azonosítása céljából ^1H és ^{13}C NMR méréseket végeztünk pH = 4, 8 és 12 oldatokban. Savas közegben (pH = 4) a C2-OH, C3-OH és C4-OH protonjelek

kiszélesedése, valamint a megfelelő szénjelek és a C5-OH jel relatív intenzitásának csökkenése az aluminátionok koordinációja szempontjából kiemelt jelentőségű kötőhelyek jelenlétére utal. A pH = 8-on mért spektrumok ligandum-stabilizált összetett hidroxidok képződésére engednek következtetni. Ezt a félkvantitatív oldhatósági szimulációk is alátámasztják, melyek szerint a 6 és 11-es pH közötti tartományban a szabad Al^{3+} és OH^- ionok teljes koncentrációja meghaladja az $\text{Al}(\text{OH})_3(\text{s})$ oldhatósági szorzatát, csapadékképződés azonban nem volt észlelhető heptaglükonát ionok jelenlétében. Erősen lúgos (pH = 12) közegben a komplexképződés sebessége meglehetősen lassú, olyannyira, hogy összemérhetővé válik a szabad és kötött ligandum közötti cseresebességgel, ezáltal számos új csúcs megjelenését eredményezve a megfelelő NMR spektrumokon. Ezek az új csúcsok tartozhatnak mind az $\text{Al}(\text{OH})_4\text{Hpgl}^{2-}$ komplex koordinációs izomerjeihez, mind pedig a többmagvú $\text{Al}_4(\text{OH})_{15}\text{Hpgl}_3^{6-}$ részecskéhez is.

A számított modellt fagyáspontcsökkenés mérésekkel és ESI-MS kísérletekkel igazoltuk. Az aluminátot és ligandumot is tartalmazó oldatokban mért fagyáspontcsökkenés nagyfokú asszociációra utalt, továbbá a részecskeeloszlási adatok alapján számított $\Delta T_{f,calc}$ értékek is jól egyeztek a mért effektussal. Az ESI-MS mérések megerősítették a 2:1 összetételű részecske jelenlétét pH = 7-en, valamint közvetett információt szolgáltatottak a koordinációs módot illetően.

A Ca^{2+} -, Al^{3+} - és Hpgl⁻-tartalmú oldatokból kivált szilárd mintákat különféle analitikai és anyagtudományi módszerekkel tanulmányoztuk. A porröntgendiffrakciós (XRD) és elektronmikroszkópos (SEM-EDX) vizsgálatok alapján ezen anyagok alacsony kristályossági fokkal, homogén elemeloszlással és jelentősen eltérő morfológiával rendelkeznek, a kereskedelmi forgalomban is kapható Hpgl⁻-sókéhoz képest.

Az ICP-OES és UV-Vis mérések eredményei alapján két fajta komplexet különböztethettünk meg: Az $n_{\text{OH}}/n_{\text{Hpgl}} > 1.0$ arány mellett egyszerre képződő $\text{CaAlHpgl}(\text{OH})_4^0$ és $\text{Ca}_2\text{AlHpgl}_2(\text{OH})_5^0$ komplexeket, valamint a $n_{\text{OH}}/n_{\text{Hpgl}} < 1.0$ aránynál képződő, egységesebb sztöchiometriával rendelkező $\text{Ca}_3\text{Al}_2\text{Hpgl}_3(\text{OH})_9^0$ részecskét. Utóbbi összetétel nagymértékben hasonlít a $\text{Ca}_3\text{Al}_2(\text{OH})_{12}$ (trikalcium aluminát, TCA) szerkezetére, mely részben megmagyarázhatja a Gluc⁻ és TCA reakciójában keletkező anyag korábban közölt infravörös spektrumával való hasonlóságot. A biner komplexek esetében $\text{Al}_3\text{Hpgl}(\text{OH})_8^0$, valamint különféle Ca-tartalmú biner komplexek képződését feltételeztük.

Az FT-IR és Raman spektroszkópai mérések eredményei megerősítették a fenti két csoport létezésére tett feltevésünket. Az egyes komplexek karboxilát sávjainak Fourier-dekonvolúciója

alapján a biner és terner komplexek különbözőképpen koordinálódnak a Ca^{2+} illetve Al^{3+} ionokhoz. Továbbá az illesztett aszimmetrikus karboxilátrezgések helye alapján a ligandumok középpontos szimmetriában helyezkednek el a fémion körül.

A kereskedelmi forgalomban kaphatók heptaglikonát sók, valamint a Hpgl^- biner és terner komplexeinek termoanalitikai vizsgálata során utóbbi kettő jelentősen stabilisabbnak bizonyult. Ez a megnövekedett stabilitás a terner fémkomplexek esetében volt a legmagasabb, ami a két fém ligandum(ok) általi egyidejű megkötésének tulajdonítható.

A heptaglikonát Ca^{2+} és $\text{Al}(\text{OH})_4^-$ ionokkal való kölcsönhatását tekintve, a terner komplexek jelenléte lúgos közegben egyértelműen bizonyítható volt pH-potenciometriás és polarimetriás mérésekkel. Ezek a részecskék jellemzően a pH = 8 és 14 közötti tartományban képződtek, míg a pH < 8 tartományban az egyes oldatbeli biner fémkomplexek elegendőnek bizonyultak a rendszer oldategyensúlyainak korrekt leírásához. A $\text{CaAl}(\text{OH})_4\text{Hpgl}_2^-$ különböző protonáltsági fokú komplexei mellett egy sor bonyolultabb összetételű részecske is képződik 1:2:2, 2:1:2, 2:2:2, valamint 3:1:4 sztöchiometriával.

A heptaglikonát lúgos közegben, Ca^{2+} és $\text{Al}(\text{OH})_4^-$ ionok jelenlétében felvett ^1H és ^{13}C NMR spektrumai alapján a komplexképződési sebesség az $\text{Al}(\text{OH})_4^- / \text{Hpgl}^-$ rendszerben tapasztaltnál is lassabb, nagyszámú új csúcsot eredményezve az NMR spektrumokon. A kalcium-függő mérési sorozat esetében a csúcsok száma és helye alapján legalább 3 különböző fémkomplex képződése volt megfigyelhető, amely összhangban van a modell alapján azonos körülményekre szimulált részecskeeloszlással.

Végül a magas ionerősség és hőmérséklet speciációra gyakorolt hatását is megvizsgáltuk a már ismert $\text{Ca}^{2+} / \text{Gluc}^-$ modellrendszeren keresztül, mely során a részecskeeloszlás nem változott jelentősen. Az egyes oldatbeli részecskék különböző hőmérsékleteken meghatározott stabilitási állandói és a van't Hoff egyenlet segítségével kiszámítottuk az egyes reakciók ΔH és ΔS értékeit. Ezek szerint a CaGlucH_1^0 komplex képződése endotermebbnek bizonyult a GlucH_1^{2-} részecskéénél, mely értelemben a Gluc^- ion könnyebben deprotonálódik Ca^{2+} ionok jelenlétében. A korábban meghatározott termodinamikai állandók segítségével extrapolálni tudtuk a Ca^{2+} -tartalmú részecskék eloszlását $\text{Ca}(\text{OH})_2(\text{s})$ és Gluc^- -ot tartalmazó $t = 100^\circ\text{C}$ hőmérsékletű oldatokra.

References

1. Farber, S.J.; Schubert, M. The Binding of Cations by Chondroitin Sulfate. *J. Clin. Invest.* **1957**, *36*, 1715–1722, doi:10.1172/JCI103573.
2. Roberts, B.D.; Bailey, G.D.; Buess, C.M.; Carper, W.R. Purification and Characterization of Hepatic Porcine Gluconolactonase. *Biochem. Biophys. Res. Commun.* **1978**, *84*, 322–327.
3. Bailey, G.D.; Roberts, B.D.; Buess, C.M.; Carper, W.R. Purification and Partial Characterization of Beef Liver Gluconolactonase. *Arch. Biochem. Biophys.* **1979**, *192*, 482–488.
4. Gajda, T.; Gyurcsik, B.; Jakusch, T.; Burger, K.; Henry, B.; Delpuech, J.-J. Coordination Chemistry of Polyhydroxy Acids: Role of the Hydroxy Groups. *Inorganica Chim. Acta* **1998**, *275–276*, 130–140, doi:10.1016/S0020-1693(97)06108-2.
5. Ma, S.; Li, W.; Zhang, S.; Ge, D.; Yu, J.; Shen, X. Influence of Sodium Gluconate on the Performance and Hydration of Portland Cement. *Constr. Build. Mater.* **2015**, *91*, 138–144, doi:10.1016/j.conbuildmat.2015.05.068.
6. Ramachandran, S.; Fontanille, P.; Pandey, A.; Larroche, C. Gluconic Acid: Properties, Applications and Microbial Production. *Food Technol. Biotechnol.* **2006**, *44.2*, 11.
7. Whittington, B. The Chemistry of CaO and Ca (OH) 2 Relating to the Bayer Process. *Hydrometallurgy* **1996**, *43*, 13–35.
8. Rosenberg, S.P.; Wilson, D.J.; Heath, C.A. Some aspects of calcium chemistry in the Bayer process. In *Essential readings in light metals*; Springer, 2016; pp. 210–216.
9. Pullman, A., Goldblum, N., Eds.; *Metal-Ligand Interactions in Organic Chemistry and Biochemistry: Part I*; Jerusalem Symposia; Springer Netherlands, 1977; ISBN 978-90-277-0754-3.
10. Whitfield, D.M.; Stojkovski, S.; Sarkar, B. Metal Coordination to Carbohydrates. Structures and Function. *Coord. Chem. Rev.* **1993**, *122*, 171–225, doi:10.1016/0010-8545(93)80045-7.
11. Venema, F.; Peters, J.; Van Bekkum, H. Multinuclear-Magnetic-Resonance Study of the Coordination of Aluminium (III)-Aldarate Complexes with Calcium (II) in Aqueous Solution. *Recl. Trav. Chim. Pays-Bas* **1993**, *112*, 445–450.

12. Rai, D.; Hess, N.J.; Xia, Y.; Rao, L.; Cho, H.M.; Moore, R.C.; Van Loon, L.R. Comprehensive Thermodynamic Model Applicable to Highly Acidic to Basic Conditions for Isosaccharinate Reactions with Ca(II) and Np(IV). *J. Solut. Chem.* **2003**, *32*, 665–689, doi:10.1023/B:JOSL.0000002988.99769.cb.
13. Steve P., R.; Darrell J., W.; C. A., H. Improved Bayer Causticisation, IFI CLAIMS Patent Services, Patent Number: PCT/AU1999/000757, **1999**.
14. Venema, F. Coordination of Aluminium(III) with Hydroxycarboxylates in water, PhD Thesis, TU Delft: Delft, **1992**.
15. McDonough, W.F.; Sun, S.-S. The Composition of the Earth. *Chem. Geol.* **1995**, *120*, 223–253.
16. Clayton, D. *Handbook of Isotopes in the Cosmos: Hydrogen to Gallium*; Cambridge University Press, **2003**; Vol. 1; ISBN 0-521-53083-0.
17. Greenwood, N.N.; Earnshaw, A. *Chemistry of the Elements*; Elsevier, **2012**; ISBN 0-08-050109-5.
18. Donaldson, D.; Raahauge, B.E. *Alumina and Bauxite*; Essential Readings in Light Metals; Wiley; TMS: Hoboken, New Jersey, **2013**; Vol. vol 1.; ISBN 978-1-118-63664-0.
19. Atkins, P.R.; Bayliss, C.; Ward, S. Bauxite Mining Sustainably. In *Essential Readings in Light Metals*; John Wiley & Sons Inc.: Hoboken, New Jersey, **2013**; Vol. 1, p. 1169.
20. Habashi, F. Bayer's Process for Alumina Production: A Historical Perspective. *Bull Hist Chem* **1995**, *17*, 15.
21. Lever, G. Identification of Organics in Bayer Liquor. In *Light Metals*; **1978**; Vol. 2, pp. 71–83.
22. Szabo, Z.; Orban, M.; Perl, I. Some Fundamental Research for Alumina Industry In: *Fourth International Congress for the Study of Bauxites, Alumina and Aluminum*. Hungary.; **1978**; Vol. 1, pp. 422–436.
23. Yamada, K.; Harato, T.; Kato, H.; Watanabe, H. Oxidation of Organic-Substances in the Bayer Process.; In: *Journal of Metals*. 420 Commonwealth DR, Warrendale, PA 15086: Minerals Metals Materials Soc., **1980**. p. 23-23.
24. Roumeliotis, P.; Unger, K.; Kudermann, G.; Winkhaus, G. Applicatory Possibilities of HPLC in the Separation, Isolation, Identification and Quantitative Determination of

- Substances From Complex Mixtures--as Exemplified by Carboxylic Acids in Sodium Aluminate Leaching Solutions From the Bayer Process for Aluminum Oxide Recovery.(WAA Translation). *Chromatographia* **1982**, *15*, 30.
25. Power, G.; Loh, J.S.; Wajon, J.E.; Busetti, F.; Joll, C. A Review of the Determination of Organic Compounds in Bayer Process Liquors. *Anal. Chim. Acta* **2011**, *689*, 8–21.
 26. Fischer, R.; Kuzel, H.-J. Reinvestigation of the System C4A. NH₂O – C4A. Co₂. NH₂O. *Cem. Concr. Res.* **1982**, *12*, 517–526.
 27. Malts, N. Efficiency of Lime Use in Bayer Alumina Production. *Light Met.* **1992**, 1337–1342.
 28. Roach, G.I. The equilibrium approach to causticisation for optimising liquor causticity. In *Essential Readings in Light Metals*; Springer, **2016**; pp. 228–234.
 29. Wells, L.S. Reaction of water on calcium aluminates. In *Bureau of Standards Journal of Research*; US Government Printing Office, **1928**; Vol. 1, p. 951.
 30. Brownmiller, L.T.; Bogue, R.H. System CaO-Na₂O-Al₂O₃. In *Bureau of Standards Journal of Research*; National Bureau of Standards, **1932**; Vol. 8, p. 289.
 31. Wells, L.S.; Clarke, W.F.; McMurdie, H.F. Study of the System CaO~Al₂O₃~H₂O at Temperatures of 21 Degrees and 90 Degrees C. *J. Res. Natl. Bur. Stand.* **1943**, *30*, 367, doi:10.6028/jres.030.027.
 32. Pepler, R.B.; Wells, L.S. The System of Lime, Alumina, and Water from 50-Degrees to 250-Degrees C. *J. Res. Natl. Bur. Stand.* **1954**, *52*, 75, doi:10.6028/jres.052.013.
 33. Whittington, B.; Fallows, T.; Willing, M. Tricalcium Aluminate Hexahydrate (TCA) Filter Aid in the Bayer Industry: Factors Affecting TCA Preparation and Morphology. *Int. J. Miner. Process.* **1997**, *49*, 1–29.
 34. Terzis, A.; Filippakis, S.; Kuzel, H.-J.; Burzlaff, H. The Crystal Structure of CaAl(OH)₆Cl·2H₂O. *Z. Für Krist.-Cryst. Mater.* **1987**, *181*, 29–34.
 35. Whittington, B.; Cardile, C. The Chemistry of Tricalcium Aluminate Hexahydrate Relating to the Bayer Industry. *Int. J. Miner. Process.* **1996**, *48*, 21–38.
 36. Turriziani, R. The Calcium Aluminate Hydrates and Related Compounds. *Chem. Cem.* **1964**, *1*, 233–286.
 37. Furka, Á. Szerves Kémia; Nemzeti Tankönyvkiadó: Budapest, **1998**;

38. De Lederkremer, R.M.; Marino, C. Acids and Other Products of Oxidation of Sugars. *Adv. Carbohydr. Chem. Biochem.* **2003**, *58*, 199–306.
39. Antus, S.; Mátyus, P. *Szerves Kémia III.*; Nemzeti Tankönyvkiadó: Budapest, **2007**;
40. Isbell, H.S.; Frush, H.L. The Oxidation of Sugars. I. The Electrolytic Oxidation of Aldose Sugars in the Presence of a Bromide and Calcium Carbonate. *Bur Stand J Res* **1931**, *6*, 1145.
41. Isbell, H.; Frush, H.L.; Bates, F. Manufacture of Calcium Gluconate by Electrolytic Oxidation of Dextrose. *Ind. Eng. Chem.* **1932**, *24*, 375–378.
42. Pfizer, C. Improvements in or Relating to the Preparation of Metal Gluconates. *Br. Pat.* 786 **1957**, 288.
43. De Wilt, H.; Van der Baan, H. Part II. Oxidation of Glucose to K-Gluconate. Platinum-Catalyzed Oxidation with Oxygen in Aqueous Alkaline Solutions. *Ind. Eng. Chem. Prod. Res. Dev.* **1972**, *11*, 374–378.
44. Rinsant, D.; Chatel, G.; Jérôme, F. Efficient and Selective Oxidation of D-glucose into Gluconic Acid under Low-frequency Ultrasonic Irradiation. *Chem. Cat. Chem.* **2014**, *6*, 3355–3359.
45. Amaniampong, P.N.; Karam, A.; Trinh, Q.T.; Xu, K.; Hirao, H.; Jérôme, F.; Chatel, G. Selective and Catalyst-Free Oxidation of D-Glucose to D-Glucuronic Acid Induced by High-Frequency Ultrasound. *Sci. Rep.* **2017**, *7*, 1–8.
46. Rico-Rodríguez, F.; Villamiel, M.; Ruiz-Aceituno, L.; Serrato, J.C.; Montilla, A. Effect of the Lactose Source on the Ultrasound-Assisted Enzymatic Production of Galactooligosaccharides and Gluconic Acid. *Ultrason. Sonochem.* **2020**, *67*, 104945.
47. Vinke, P.; de Wit, D.; De Goede, A.; Van Bekkum, H. Noble metal catalyzed oxidation of carbohydrates and carbohydrate derivatives. In *Studies in Surface Science and Catalysis*; Elsevier, **1992**; Vol. 72, pp. 1–20 ISBN 0167-2991.
48. Comotti, M.; Pina, C.D.; Rossi, M. Mono- and Bimetallic Catalysts for Glucose Oxidation. *J. Mol. Catal. Chem.* **2006**, *251*, 89–92, doi:10.1016/j.molcata.2006.02.014.
49. Liang, X.; Liu, C.; Kuai, P. Selective Oxidation of Glucose to Gluconic Acid over Argon Plasma Reduced Pd/Al₂O₃. *Green Chem.* **2008**, *10*, 1318–1322, doi:10.1039/B804904A.

50. Solmi, S.; Morreale, C.; Ospitali, F.; Agnoli, S.; Cavani, F. Oxidation of D-Glucose to Glucaric Acid Using Au/C Catalysts. *Chem. Cat. Chem.* **2017**, *9*, 2797–2806.
51. Roukas, T. Citric and Gluconic Acid Production from Fig by *Aspergillus Niger* Using Solid-State Fermentation. *J. Ind. Microbiol. Biotechnol.* **2000**, *25*, 298–304, doi:10.1038/sj.jim.7000101.
52. Singh, O.V.; Jain, R.K.; Singh, R.P. Gluconic Acid Production under Varying Fermentation Conditions by *Aspergillus Niger*. *J. Chem. Technol. Biotechnol.* **2003**, *78*, 208–212, doi:10.1002/jctb.748.
53. Liu, J.-Z.; Weng, L.-P.; Zhang, Q.-L.; Xu, H.; Ji, L.-N. A Mathematical Model for Gluconic Acid Fermentation by *Aspergillus Niger*. *Biochem. Eng. J.* **2003**, *14*, 137–141, doi:10.1016/S1369-703X(02)00169-9.
54. Znad, H.; Markoš, J.; Baleš, V. Production of Gluconic Acid from Glucose by *Aspergillus Niger*: Growth and Non-Growth Conditions. *Process Biochem.* **2004**, *39*, 1341–1345, doi:10.1016/S0032-9592(03)00270-X.
55. Seiskari, P.; Linko, Y.-Y.; Linko, P. Continuous Production of Gluconic Acid by Immobilized *Gluconobacter Oxydans* Cell Bioreactor. *Appl. Microbiol. Biotechnol.* **1985**, *21*, 356–360, doi:10.1007/BF00249979.
56. Velizarov, S.; Beschkov, V. Production of Free Gluconic Acid by Cells of *Gluconobacter Oxydans*. *Biotechnol. Lett.* **1994**, *16*, 715–720, doi:10.1007/BF00136477.
57. Zhou, P.; Yao, R.; Zhang, H.; Bao, J. Unique Glucose Oxidation Catalysis of *Gluconobacter Oxydans* Constitutes an Efficient Cellulosic Gluconic Acid Fermentation Free of Inhibitory Compounds Disturbance. *Biotechnol. Bioeng.* **2019**, *116*, 2191–2199, doi:https://doi.org/10.1002/bit.27020.
58. Carey, F.A. *Organic Chemistry*; 6th Edition.; McGraw-Hill: New York, US, 2006; ISBN 0-07-111562-5.
59. Reusch, W. Virtual Textbook of Organic Chemistry; Available online: <https://www2.chemistry.msu.edu/faculty/reusch/VirtTxtJml/intro1.htm> (accessed on 25 January 2021).
60. Clayden, J.; Greeves, N.; Warren, S.; Wothers, P. *Organic Chemistry*; Oxford University Press: New York, US, **2001**; Vol. 1; ISBN 0 19 850346 6.

61. Perrin, D.D.; Dempsey, B.; Serjeant, E.P. *PK_a Prediction for Organic Acids and Bases*; Springer: London, UK, **1981**; Vol. 1;.
62. Roos, J.T.; Williams, D.R. Formation Constants for Citrate-, Folic Acid-, Gluconate- and Succinate-Proton-Manganese(II), and -Zinc(II) Systems: Relevance to Absorption of Dietary Manganese, Zinc and Iron. *J. Inorg. Nucl. Chem.* **1977**, *39*, 367–369.
63. Zhang, Z.; Gibson, P.; Clark, S.B.; Tian, G.; Zanonato, P.L.; Rao, L. Lactonization and Protonation of Gluconic Acid: A Thermodynamic and Kinetic Study by Potentiometry, NMR and ESI-MS. *J. Solut. Chem.* **2007**, *36*, 1187–1200, doi:10.1007/s10953-007-9182-x.
64. Pallagi, A.; Bajnóczi, É.G.; Canton, S.E.; Bolin, T.; Peintler, G.; Kutus, B.; Kele, Z.; Pálinkó, I.; Sipos, P. Multinuclear Complex Formation between Ca(II) and Gluconate Ions in Hyperalkaline Solutions. *Environ. Sci. Technol.* **2014**, *48*, 6604–6611, doi:10.1021/es501067w.
65. Coccioni, F.; Vicedomini, M. On the Dissociation of Gluconate Ions and Their Complex Formation with Lead (II) in Alkaline Solution. *J. Inorg. Nucl. Chem.* **1978**, *40*, 2106–2110.
66. Pallagi, A.; Csendes, Z.; Kutus, B.; Czeglédi, E.; Peintler, G.; Forgo, P.; Pálinkó, I.; Sipos, P. Multinuclear Complex Formation in Aqueous Solutions of Ca(II) and Heptagluconate Ions. *Dalton Trans.* **2013**, *42*, 8460, doi:10.1039/c3dt00099k.
67. Tilden, W.A.; Shenstone, W.A. II. On the Solubility of Calcium Sulphate in Water in the Presence of Chlorides. *Proc. R. Soc. Lond.* **1885**, *38*, 331–336.
68. Shenstone, W.; Cundall, J.T. XL. The Influence of Temperature on the Composition and Solubility of Hydrated Calcium Sulphate and of Calcium Hydroxide. *J. Chem. Soc. Trans.* **1888**, *53*, 544–550.
69. Kolthoff, I. Die Dissoziationskonstante Der Erdalkalihydroxyde. *Recl. Trav. Chim. Pays-Bas* **1923**, *42*, 973–979.
70. Johnston, J.; Grove, C. The Solubility of Calcium Hydroxide in Aqueous Salt Solutions. *J. Am. Chem. Soc.* **1931**, *53*, 3976–3991.
71. Yeatts, L.B.; Marshall, W.L. Aqueous Systems at High Temperature. XVIII. Activity Coefficient Behavior of Calcium Hydroxide in Aqueous Sodium Nitrate to the Critical Temperature of Water. *J. Phys. Chem.* **1967**, *71*, 2641–2650.

72. Sipos, P.; May, P.M.; Hefter, G.T. Carbonate Removal from Concentrated Hydroxide Solutions. *The Analyst* **2000**, *125*, 955–958, doi:10.1039/a910335j.
73. Shannon, R.T.; Prewitt, C.T. Effective Ionic Radii in Oxides and Fluorides. *Acta Crystallogr. B* **1969**, *25*, 925–946.
74. Shannon, R.D. Revised Effective Ionic Radii and Systematic Studies of Interatomic Distances in Halides and Chalcogenides. *Acta Crystallogr. A* **1976**, *32*, 751–767.
75. Brown, P. L., Ekberg, C. *Hydrolysis of metal ions*. John Wiley & Sons, **2016**.
76. Bates, R.; Bower, V.; Canham, R.; Prue, J. The Dissociation Constant of CaOH^+ from 0 to 40 C. *Trans. Faraday Soc.* **1959**, *55*, 2062–2068.
77. Gimblett, F.; Monk, C. Emf Studies of Electrolytic Dissociation. Part 7. Some Alkali and Alkaline Earth Metal Hydroxides in Water. *Trans. Faraday Soc.* **1954**, *50*, 965–972.
78. Bell, R.; Prue, J. Reaction-Kinetic Investigations of the Incomplete Dissociation of Salts. Part I. The Decomposition of Diacetone Alcohol in Solutions of Metallic Hydroxides. *J. Chem. Soc. Resumed* **1949**, 362–369.
79. Bell, R.; Waind, G. Reaction-Kinetic Investigations of the Incomplete Dissociation of Salts. Part II. The Hydrolysis of Carbethoxymethyltriethylammonium Iodide and of Ethyl Acetate by Solutions of Metal Hydroxides. *J. Chem. Soc. Resumed* **1950**, 1979–1983.
80. Kilde, G. Ein Verfahren zur Bestimmung der Calciumionenkonzentration und Ihre Anwendung zur Bestimmung der Dissoziation des Calciumhydroxyds. *Z. Für Anorg. Allg. Chem.* **1934**, *218*, 113–128.
81. Davies, C.W. The Extent of Dissociation of Salts in Water. Part VI. Some Calcium Salts of Organic Acids. *J. Chem. Soc. Resumed* **1938**, 277–281.
82. Bell, R.; George, J. The Incomplete Dissociation of Some Thallous and Calcium Salts at Different Temperatures. *Trans. Faraday Soc.* **1953**, *49*, 619–627.
83. Davies, C.; Hoyle, B. The Interaction of Calcium Ions with Some Phosphate and Citrate Buffers. *J. Chem. Soc. Resumed* **1953**, 4134–4136.
84. Hopkins Jr, H.P.; Wulff, C.A. The Solution Thermochemistry of Polyvalent Electrolytes. I. Calcium Hydroxide. *J. Phys. Chem.* **1965**, *69*, 6–8.
85. Langmuir, D. Stability of Calcite Based on Aqueous Solubility Measurements. *Geochim. Cosmochim. Acta* **1968**, *32*, 835–851.

86. Lito, M.G.H.; Camões, M.F.G.; Covington, A.K. Equilibrium in Saturated $\text{Ca}(\text{OH})_2$ Solutions: Parameters and Dissociation Constants. *J. Solut. Chem.* **1998**, *27*, 925–933.
87. Pokrovsky, O.; Mielczarski, J.; Barres, O.; Schott, J. Surface Speciation Models of Calcite and Dolomite/Aqueous Solution Interfaces and Their Spectroscopic Evaluation. *Langmuir* **2000**, *16*, 2677–2688.
88. Reardon, E.; Fagan, R. The Calcite/Portlandite Phase Boundary: Enhanced Calcite Solubility at High pH. *Appl. Geochem.* **2000**, *15*, 327–335.
89. Granholm, K.; Ek, P.; Sokalski, T.; Harju, L.; Bobacka, J.; Ivaska, A. Determination of Calcium with Ion-Selective Electrode in Black Liquor from a Kraft Pulping Process. *Electroanal. Int. J. Devoted Fundam. Pract. Asp. Electroanal.* **2009**, *21*, 2014–2021.
90. Yuan, T.; Wang, J.; Li, Z. Measurement and Modelling of Solubility for Calcium Sulfate Dihydrate and Calcium Hydroxide in NaOH/KOH Solutions. *Fluid Ph. Equilibria* **2010**, *297*, 129–137, doi:10.1016/j.fluid.2010.06.012.
91. Williams, T.R. Handbook of Analytical Chemistry (Meites, Louis). *J. Chem. Educ.* **1963**, *40*, 560, doi:10.1021/ed040p560.1.
92. Huntz, A.M. In Equilibres Acido-Basiques, pH: Cours et Exercices; Comprendre et appliquer; Masson et Cie: Paris, **1975**;
93. Pallagi, A.; Tasi, Á.; Gácsi, A.; Csáti, M.; Pálinkó, I.; Peintler, G.; Sipos, P. The Solubility of $\text{Ca}(\text{OH})_2$ in Extremely Concentrated NaOH Solutions at 25°C. *Cent. Eur. J. Chem.* **2012**, *10*, 332–337.
94. Malinin, S.D.; Kurosavskaya, N.A. Experimental Study of the Solubility of Fluorite (CaF_2) in Aqueous Solutions of Hydrogen Chloride-Sodium Chloride under the Temperature 25 to 90 C. *Geokhimiya* **1979**, *5*, 693–703.
95. Kutus, B.; Gácsi, A.; Pallagi, A.; Pálinkó, I.; Peintler, G.; Sipos, P. A Comprehensive Study on the Dominant Formation of the Dissolved $\text{Ca}(\text{OH})_2(\text{aq})$ in Strongly Alkaline Solutions Saturated by Ca(II). *RSC Adv.* **2016**, *6*, 45231–45240.
96. Gyurcsik, B.; Nagy, L. Metal Complexes of Carbohydrates and Their Derivatives: Coordination Equilibrium and Structure. *Coord Chem Rev* **2000**, *203*, 81–149.
97. Kutus, B.; Dudás, C.; Orbán, E.; Lupan, A.; Attia, A.A.A.; Pálinkó, I.; Sipos, P.; Peintler, G. Magnesium(II) D-Gluconate Complexes Relevant to Radioactive Waste Disposals:

- Metal-Ion-Induced Ligand Deprotonation or Ligand-Promoted Metal-Ion Hydrolysis? *Inorg. Chem.* **2019**, *58*, 6832–6844, doi:10.1021/acs.inorgchem.9b00289.
98. Mehlretter, C.L.; Alexander, B.H.; Rist, C.E. Sequestration by Sugar Acids. *Ind. Eng. Chem.* **1953**, *45*, 2782–2784, doi:10.1021/ie50528a060.
99. van Duin, M.; Peters, J.A.; Kieboom, A.P.G.; van Bekkum, H. Synergic Coordination of Calcium in Borate-Polyhydroxycarboxylate Systems. *Carbohydr. Res.* **1987**, *162*, 65–78, doi:10.1016/0008-6215(87)80201-X.
100. Sipes, G. E. Structure and stability constants of boron, calcium, and magnesium gluconate chelates from optical rotation and computer analysis. University of Illinois at Urbana-Champaign, **1969**.
101. Kutus, B.; Gaona, X.; Pallagi, A.; Pálinkó, I.; Altmaier, M.; Sipos, P. Recent Advances in the Aqueous Chemistry of the Calcium(II)-Gluconate System – Equilibria, Structure and Composition of the Complexes Forming in Neutral and in Alkaline Solutions. *Coord. Chem. Rev.* **2020**, *417*, 213337, doi:10.1016/j.ccr.2020.213337.
102. Wesolowski, D.J. Aluminum Speciation and Equilibria in Aqueous Solution: I. The Solubility of Gibbsite in the System Na-K-Cl-OH-Al (OH)₄ from 0 to 100 C. *Geochim. Cosmochim. Acta* **1992**, *56*, 1065–1091.
103. Apps, J.; Neil, J. Correlation of the Solubilities of Aluminum Hydroxides and Oxyhydroxides in Alkaline Solutions with the Thermodynamic Properties of Al(OH)₄⁻, California Digital Library, University of California, **1989**.
104. Apps, J.A.; Neil, J.M. Correlation of the Solubilities of Aluminum Hydroxides and Oxyhydroxides in Alkaline Solutions with the Thermodynamic Properties of Al(OH)₄⁻, California Digital Library, University of California, **1990**.
105. Robie, R.A.; Hemingway, B.S. Heat Capacities of Kaolinite from 7 to 380 K and of DMSO-Intercalated Kaolinite from 20 to 310 K. The Entropy of Kaolinite Al₂Si₂O₅(OH)₄. *Clays Clay Miner.* **1991**, *39*, 362–368.
106. Aluminium, Gallium, Indium and Thallium. In *Hydrolysis of Metal Ions*; Brown, P.L., Ekberg, C., Eds.; Wiley-VCH Verlag GmbH & Co. KGaA: Weinheim, Germany, **2016**; pp. 757–834 ISBN 978-3-527-65618-9.
107. Sipos, P. The Structure of Al(III) in Strongly Alkaline Aluminate Solutions – A Review. *J. Mol. Liq.* **2009**, *146*, 1–14, doi:10.1016/j.molliq.2009.01.015.

108. O'reilly, D. NMR Chemical Shifts of Aluminum: Experimental Data and Variational Calculation. *J. Chem. Phys.* **1960**, *32*, 1007–1012.
109. Lanaspèze, P.; Eyraud, C. Structure et Evolution des Solutions d Aluminate de Sodium. *Bull. Société Chim. Fr.* **1960**, 313–321.
110. Haraguchi, H.; Fujiwara, S. Aluminum Complexes in Solution as Studied by Aluminum-27. Nuclear Magnetic Resonance. *J. Phys. Chem.* **1969**, *73*, 3467–3473.
111. Moolenaar, R.J.; Evans, J.C.; McKeever, L. Structure of the Aluminate Ion in Solutions at High pH. *J. Phys. Chem.* **1970**, *74*, 3629–3636.
112. Akitt, J.; Gessner, W.; Weinberger, M. High-field Aluminium-27 Nuclear Magnetic Resonance Investigations of Sodium Aluminate Solutions. *Magn. Reson. Chem.* **1988**, *26*, 1047–1050.
113. Buvari-Barcza, A.; Rózsahégyi, M.; Barcza, L. Hydrogen Bonded Associates in the Bayer Process (in Concentrated Aluminate Lyes): The Mechanism of Gibbsite Nucleation. *J. Mater. Chem.* **1998**, *8*, 451–455.
114. Gale, J.D.; Rohl, A.L.; Watling, H.R.; Parkinson, G.M. Theoretical Investigation of the Nature of Aluminum-Containing Species Present in Alkaline Solution. *J. Phys. Chem. B* **1998**, *102*, 10372–10382.
115. Swaddle, T.W.; Rosenqvist, J.; Yu, P.; Bylaska, E.; Phillips, B.L.; Casey, W.H. Kinetic Evidence for Five-Coordination in AlOH^{2+} (aq) Ion. *Science* **2005**, *308*, 1450–1453.
116. Akitt, J.; Gessner, W. Aluminium-27 Nuclear Magnetic Resonance Investigations of Highly Alkaline Aluminate Solutions. *J. Chem. Soc. Dalton Trans.* **1984**, 147–148.
117. Watling, H.; Fleming, S.; Bronswijk, W.; Rohl, A. Ionic Structure in Caustic Aluminate Solutions and the Precipitation of Gibbsite. *J. Chem. Soc. Dalton Trans.* **1998**, 3911–3918.
118. Wajand, J.; Szabo, Z.; Ruff, I.; Burger, K. Determination of the Dimerization Constant of Aluminate Ion in Alkaline Sodium Aluminate Solutions. *Magy. Kem. Folyoirat* **1980**, *86*, 339–345.
119. Barcza, L.; Pálfalvi-Rózsahégyi, M. The Aluminate Lye as a System of Equilibria. *Mater. Chem. Phys.* **1989**, *21*, 345–356.
120. Carreira, L.; Maroni, V.; Swaine Jr, J.; Plumb, R. Raman and Infrared Spectra and Structures of the Aluminate Ions. *J. Chem. Phys.* **1966**, *45*, 2216–2220.

121. Konenkova, T.Y. Potentiometric Investigation of Composition of Hydroxo Complexes of Aluminum in Alkaline-solutions. *J. Appl. Chem. USSR* **1976**, *49*, 2214–2217.
122. Watling, H. Spectroscopy of Concentrated Sodium Aluminate Solutions. *Appl. Spectrosc.* **1998**, *52*, 250–258.
123. Motekaitis, R.J.; Martell, A.E. Complexes of Aluminum(III) with Hydroxy Carboxylic Acids. *Inorg. Chem.* **1984**, *23*, 18–23, doi:10.1021/ic00169a006.
124. Escandar, G.M.; Olivieri, A.C.; González-Sierra, M.; Frutos, A.A.; Sala, L.F. Complexation of Aluminium(III), Gallium(III) and Indium(III) Ions with D-Gluconic and Lactobionic Acids. A Potentiometric and Nuclear Magnetic Resonance Spectroscopic Study. *J. Chem. Soc. Dalton Trans.* **1995**, 799–804.
125. Lakatos, A.; Kiss, T.; Bertani, R.; Venzo, A.; Di Marco, V.B. Complexes of Al(III) with d-Gluconic Acid. *Polyhedron* **2008**, *27*, 118–124.
126. Pallagi, A.; Tasi, Á.G.; Peintler, G.; Forgo, P.; Pálinkó, I.; Sipos, P. Complexation of Al(III) with Gluconate in Alkaline to Hyperalkaline Solutions: Formation, Stability and Structure. *Dalton Trans.* **2013**, *42*, 13470, doi:10.1039/c3dt51401c.
127. Sipos, P.; Capewell, S.G.; May, P.M.; Hefter, G.; Laurenczy, G.; Lukács, F.; Roulet, R. Spectroscopic Studies of the Chemical Speciation in Concentrated Alkaline Aluminate Solutions. *J. Chem. Soc. Dalton Trans.* **1998**, 3007–3012, doi:10.1039/a805271i.
128. Kron, I.; Marshall, S.; May, P.; Hefter, G.; Königsberger, E. The Ionic Product of Water in Highly Concentrated Aqueous Electrolyte Solutions. *Monatshefte Für Chemie/Chemical Mon.* **1995**, *126*, 819–837.
129. Sipos, P.; Schibeci, M.; Peintler, G.; May, P.M.; Hefter, G. Chemical Speciation in Concentrated Alkaline Aluminate Solutions in Sodium, Potassium and Caesium Media. Interpretation of the Unusual Variations of the Observed Hydroxide Activity. *Dalton Trans.* **2006**, 1858, doi:10.1039/b513357b.
130. Peintler, G.; Kormányos, B.; Gyurcsik, B. PHCal, Version 1.32 a-20070323. *Univ. Szeged Szeged Hung.* **2007**.
131. Buckó, Á.; Kutus, B.; Peintler, G.; Pálinkó, I.; Sipos, P. Temperature Dependence of the Acid–Base and Ca²⁺-Complexation Equilibria of d-Gluconate in Hyperalkaline Aqueous Solutions. *Polyhedron* **2019**, *158*, 117–124, doi:10.1016/j.poly.2018.10.034.

132. Irving, H.; Miles, M.; Pettit, L. A Study of Some Problems in Determining the Stoichiometric Proton Dissociation Constants of Complexes by Potentiometric Titrations Using a Glass Electrode. *Anal. Chim. Acta* **1967**, *38*, 475–488.
133. *MassLynx v4.2*; Waters Corp.: Milford MA, US, 2019;
134. Zékány, L.; Nagypál, I.; Peintler, G. PSEQUAD for Chemical Equilibria. *Tech. Softw. Distrib. Baltim. MD* **1991**.
135. Puigdomenech, I. MEDUSA: Make Equilibrium Diagrams Using Sophisticated Algorithms. *Window Program Stockh. Vers* **2001**, *21*.
136. *Thermo Scientific™ GRAMS/AI™*; Thermo Electron Corporation, 2004;
137. Buckó, Á.; Kutus, B.; Peintler, G.; Kele, Z.; Pálinkó, I.; Sipos, P. Stability and Structural Aspects of Complexes Forming between Aluminum (III) and D-Heptagluconate in Acidic to Strongly Alkaline Media: An Unexpected Diversity. *J. Mol. Liq.* **2020**, 113645.
138. Escandar, G. M.; Sala, L. F.; Sierra, M. G. Complexes of Cobalt(II) and Nickel(II) with D-aldonic and D-alduronic acids in aqueous solution. *Polyhedron*, **1994**, *13.1*: 143-150.
139. Escandar, G.M.; Sala, L.F. Complexes of Cu(II) with D -Aldonic and D -Alduronic Acids in Aqueous Solution. *Can. J. Chem.* **1992**, *70*, 2053–2057, doi:10.1139/v92-259.
140. Peintler, G.; Nagypal, I.; Jancso, A.; Epstein, I.R.; Kustin, K. Extracting Experimental Information from Large Matrixes. A New Algorithm for the Application of Matrix Rank Analysis. *J. Phys. Chem. A* **1997**, *101*, 8013–8020.
141. Kutus, B.; Dudás, C.; Peintler, G.; Pálinkó, I.; Sipos, P. Configuration-Dependent Complex Formation between Ca(II) and Sugar Carboxylate Ligands in Alkaline Medium: Comparison of L-Gulonate with D-Gluconate and D-Heptagluconate. *Carbohydr. Res.* **2018**, *460*, 34–40, doi:10.1016/j.carres.2018.01.012.
142. Kutus, B.; Buckó, Á.; Peintler, G.; Pálinkó, I.; Sipos, P. Calcium Complexation and Acid–Base Properties of L -Gulonate, a Diastereomer of D -Gluconate. *Dalton Trans.* **2016**, *45*, 18281–18291, doi:10.1039/C6DT03907C.
143. Rendleman Jr, J. Complexes of alkali metals and alkaline-earth metals with carbohydrates. In *Advances in carbohydrate chemistry*; Elsevier, **1967**; Vol. 21, pp. 209–271 ISBN 0096-5332.

144. Kutus, B.; Ozsvár, D.; Varga, N.; Pálinkó, I.; Sipos, P. ML and ML₂ Complex Formation between Ca(II) and D-Glucose Derivatives in Aqueous Solutions. *Dalton Trans.* **2017**, *46*, 1065–1074, doi:10.1039/C6DT04356A.
145. Best, W.M.; Harrowfield, J.M.; Shand, T.M.; Stick, R.V. Aluminum(III) Coordination to Hydroxy Carboxylates: The Influence of Hydroxy Substituents Enabling Tridentate Binding. *Aust. J. Chem.* **1994**, *47*, 2023–2031.
146. Baes, C.; Mesmer, R. The Hydrolysis of Cations. John Wiley & Sons, New York, London, Sydney, Toronto 1976. 489 Seiten, Preis:£ 18.60. *Berichte Bunsenges Für Phys Chem* **1977**, *81*, 245–246, doi:10.1002/bbpc.19770810252.
147. Green, D.W.; Southard, M.Z. *Perry's Chemical Engineers' Handbook*; McGraw-Hill Education, 2019; ISBN 0-07-183408-7.
148. Rossiter, D.S.; Fawell, P.D.; Ilievski, D.; Parkinson, G.M. Investigation of the Unseeded Nucleation of Gibbsite, Al(OH)₃, from Synthetic Bayer Liquors. *J. Cryst. Growth* **1998**, *191*, 525–536, doi:10.1016/S0022-0248(98)00110-9.
149. Beckham, K.; Clarke, P.; Cornell, R. Inhibition of Gibbsite Crystallization: Adsorption of the Gluconate Ion.; 2005; pp. 108–111.
150. Sipos, P. The Structure of Al(III) in Strongly Alkaline Aluminate Solutions – A Review. *J. Mol. Liq.* **2009**, *146*, 1–14.
151. Kim, C.-E.; Lee, S.-H. Effect of Sodium Gluconate on the Hydration of Tricalcium Aluminate(II) Early Hydration Behavior. *J. Korean Ceram. Soc.* **1986**, *23*, 1–6.
152. Kim, C.-E.; Lee, S.-H.; Lee, S.-K. Complex Formation between 3CaO·Al₂O₃ and Sodium Gluconate. *J. Korean Ceram. Soc.* **1990**, *27*, 883–890.
153. Nakamoto, K. Infrared and Raman Spectra of Inorganic and Coordination Compounds. *Handb. Vib. Spectrosc.* **2006**.
154. Papageorgiou, S.K.; Kouvelos, E.P.; Favvas, E.P.; Sapalidis, A.A.; Romanos, G.E.; Katsaros, F.K. Metal–Carboxylate Interactions in Metal–Alginate Complexes Studied with FTIR Spectroscopy. *Carbohydr. Res.* **2010**, *345*, 469–473.
155. Yang, W.; Kim, Y.; Liu, P.K.T.; Sahimi, M.; Tsotsis, T.T. A Study by in Situ Techniques of the Thermal Evolution of the Structure of a Mg–Al–CO₃ Layered Double Hydroxide. *Chem. Eng. Sci.* **2002**, *57*, 2945–2953, doi:10.1016/S0009-2509(02)00185-9.

156. Frost, R.L.; Palmer, S.J.; Theiss, F. Synthesis and Raman Spectroscopic Characterisation of Hydrotalcites Based on the Formula $\text{Ca}_6\text{Al}_2(\text{CO}_3)(\text{OH})_{16} \cdot 4\text{H}_2\text{O}$. *J. Raman Spectrosc.* **2011**, *42*, 1163–1167.
157. Crea, F.; Stefano, C.D.; Gianguzza, A.; Piazzese, D.; Sammartano, S. Protonation of Carbonate in Aqueous Tetraalkylammonium Salts at 25°C. *Talanta* **2006**, *68*, 1102–1112, doi:10.1016/j.talanta.2005.07.025.
158. The, P.J.; Sivakumar, T.J. The effect of impurities on calcium in Bayer liquor. In *Essential Readings in Light Metals*; Springer, **1985**; pp. 209–222.
159. Bube, C.; Metz, V.; Bohnert, E.; Garbev, K.; Schild, D.; Kienzler, B. Long-Term Cement Corrosion in Chloride-Rich Solutions Relevant to Radioactive Waste Disposal in Rock Salt–Leaching Experiments and Thermodynamic Simulations. *Phys. Chem. Earth Parts ABC* **2013**, *64*, 87–94.
160. Tajmir-Riahi, H.A. Carbohydrate Metal Ion Complexes. Interaction of D -Glucono-1,5-Lactone with Zn(II), Cd(II), and Hg(II) Ions in the Solid and Aqueous Solution, Studied by ^{13}C -NMR, FT-IR, and X-Ray Powder Diffraction Measurements. *Can. J. Chem.* **1989**, *67*, 651–654, doi:10.1139/v89-098.
161. Tajmir-Riahi, H. A. Carbohydrate complexes with alkaline earth metal ions. Interaction of D-glucono-1, 5-lactone with the Mg (II), Ca (II), Sr (II), and Ba (II) cations in the crystalline solid and aqueous Solution. *J. Inorg. Biochem.*, **1990**, *39*.1: 33-41.
162. Nara, M.; Tanokura, M. Infrared Spectroscopic Study of the Metal-Coordination Structures of Calcium-Binding Proteins. *Biochem. Biophys. Res. Commun.* **2008**, *369*, 225–239.
163. Deacon, G.; Phillips, R. Relationships between the Carbon-Oxygen Stretching Frequencies of Carboxylato Complexes and the Type of Carboxylate Coordination. *Coord. Chem. Rev.* **1980**, *33*, 227–250.
164. Lu, Y.; Miller, J.D. Carboxyl Stretching Vibrations of Spontaneously Adsorbed and LB-Transferred Calcium Carboxylates as Determined by FTIR Internal Reflection Spectroscopy. *J. Colloid Interface Sci.* **2002**, *256*, 41–52.

Acknowledgement

First of all, I would like to express my gratitude to my supervisors Prof. Pál Sipos and Prof. István Pálinkó for welcoming me into their research group. Without their wisdom, continuous guidance and financial support, this work could not have been completed.

Furthermore, I would like to extend my gratefulness to Dr. Gábor Peintler, who devoted countless hours of his time helping me resolve my experimental and computational issues, as well as teaching me, that persistence is one of the largest virtues of a scientist.

Many thanks to my postdoc-in-charge and dear friend, Dr. Bence Kutus for his patience, instructions and for teaching me literally everything what I know about coordination chemistry. His scientific attitude and unique personality made him the best co-researcher I could ever wish for!

The indispensable help of Dr. Ottó Berkesi and Dr. Zoltán Kele in the evaluation of Vibrational and Mass spectra is highly appreciated.

My special thanks go to my friends and colleagues in the Material and Solution Structure Research group, who made my graduate and postgraduate years in the university special. Moreover, a big thank you goes to Dr. Márton Szabados and Dr. Zsolt Kása for helping me with their expertise in solid-state chemistry, as well as for Ilona Halasiné Varga for her professional help in the labwork.

Last, but not least, I am incredibly grateful to my family and my fiancée, Nelli Suba, for their endless love and encouragement; finishing my degree and completing this work would not have been possible without their support.